Improving Buckling Behavior of Steel Members using Unbonded Carbon Fiber Reinforced Polymer (CFRP) Laminates

(非接着CFRPを用いた鋼部材の座屈性状改善に関する研究)

July, 2021

Doctor of Philosophy (Engineering)

Fengky Satria Yoresta
フエンキ サトリア ヨレスタ

Toyohashi University of Technology

ABSTRACT

A Carbon Fiber Reinforced Polymer (CFRP) laminates has been increasingly favored as a material for strengthening steel structures replacing conventional methods of bolting or welding additional steel plates. The CFRP is chosen as it offers several advantages such as high strength-to-weight ratio, excellent fatigue behavior, resistance to corrosion (excellent durability), light weight, and ease of handling and installation. In recent decades, many research programs on strengthening steel structures with CFRP have been conducted. However, the main focus of the previous researches has been limited to strengthening with an adhesive-bonding technique. This research program investigates a new and promising method of strengthening steel using unbonded CFRP laminates which is manufactured through a process of Vacuum-assisted Resin Transfer Molding (VaRTM). The main advantage of this strengthening method is that steel surface treatments are completely no longer needed. This method of strengthening does not rely on the bond strength between steel and CFRP because these two materials are separated by an unbonded layer. The CFRP is expected to contribute only through its flexural rigidity because elastic modulus of carbon fiber is much higher than steel. The proposed unbonded CFRP strengthening is intended to be used for improving buckling performance of axial compression steel members.

The first experiment was conducted to axial compression steel bars with a diameter of 32 mm. A total of eight specimens were prepared consisting of six strengthened specimens and two control specimens. The CFRP requirements for strengthening were derived through analytical models. Three conditions considered included stiffness, strength, and circumferential strength. The unbonded CFRP was applied to only a part of length of the steel bar and positioned at center. Variation of specimens was made for buckling length, CFRP length, and number of CFRP layers. However, the number of specimens prepared was limited as it was a preliminary investigation. The test results showed that the proposed unbonded CFRP strengthening succeeded to increase the buckling capacity of the steel bars. The strengthening effect can even reach almost 50%. Besides that, the CFRP suffered no damage at all. Buckling curvature of the specimen changed from plastic hinge at middle height of specimen to plastic hinge at around the end of CFRP.

A method of equivalent slenderness ratio was then proposed to determine a design (recommendation) strength of the unbonded CFRP strengthened specimens. The effectiveness of this method was confronted against the performed experimental results and the results of numerical simulations developed for 30 strengthened models. It was clear that the proposed method of equivalent slenderness ratio provides very good results and can be used to determine the recommended strength of axial compression steel bars strengthened with unbonded CFRP laminates.

The next experiment was carried out to angle steel. This program aimed to explore the potential use of the proposed unbonded CFRP to strengthen a real or large-scale steel member. Angle steel is chosen because it is very popular for lateral resisting element in steel buildings. Thus, it is very prone to buckling failure. The strengthening scheme was still same with that applied to the steel bars where CFRP was applied to cover the entire steel surface along the strengthening area (angle steel fully-jacketed cross section). Besides that, the CFRP was also installed at middle span of the specimen through the VaRTM process. A total of twelve specimens, including two control un-strengthened angle steels, were prepared and tested. They were allowed to buckle in their weak axis only. The specimens were divided into two different groups based on the specimen length, i.e., 1618 and 1218 mm. In the first group, in addition to bare steel, three specimens were strengthened with 1000 mm length CFRP, and the other three were strengthened with only 500 mm length CFRP. However, in Group 2, with also one control un-strengthened angle steel, the other four specimens were strengthened with the same CFRP length, namely, 500 mm. It could be confirmed that the CFRP created from the VaRTM process in this study has higher fiber content, at approximately 60%. This described the advantage of VaRTM over hand layup process which is commonly used in adhesive bonding strengthening techniques. The test results showed that the buckling performance of the angle steel can be well improved. Load-bearing capacity of the angle steel can be increased by 8.5%-54.3%. The increase in load-bearing capacity occurred as increasing number of CFRP layers and CFRP length. However, for strengthening with the same number of layers and CFRP length, a greater capacity increase was attained in specimens with smaller angle steel slenderness ratios. Validation of the effectiveness of the equivalent slenderness ratio method in determining strength recommendation of the angle steel strengthened with unbonded CFRP showed that this method gives better results. The safety factor fell within the

range of 1.14-1.34 with coefficient variations of 2.2%, 0.6%, and 5.2% depending on strengthening variations.

The final investigation also involved angle steel with the same properties but its strengthening scheme is slightly different from the previous research. The unbonded CFRP was only applied to both legs of the angle steel (angle steel partially-jacketed cross section). This experimental program was conducted to explore another alternative strengthening scheme that allows reduction in amount of CFRP usage. The test results also showed that the proposed unbonded CFRP strengthening can improve the buckling performance of angle steel. The buckling capacity of angle steel could be increased by up to about 69%.

In conclusion, the investigation results presented in this dissertation clearly prove that the proposed unbonded CFRP strengthening method can be used for improving buckling behavior of axial compression steel members. However, there are some topics that have not been explored within this study and the author has identified them as recommendations for future research.

ACKNOWLEDGMENTS

All praises to Allah and His blessing for the completion of this doctoral thesis. And my greatest gratitude to the holy Prophet Muhammad (Peace be upon him) whose way of life has been a truly guidance for me.

First and foremost, I would like to sincerely acknowledge my supervisor, Assoc. Prof. Yukihiro Matsumoto, for his invaluable guidance and support during the research program. Assoc. Prof. Yukihiro Matsumoto has been an excellent supervisor and a role model for me throughout my study. My special thanks to the members of my doctoral thesis committee, Prof. Taiki Saito, Prof. Shoji Nakazawa, and Assoc. Prof. Tomoya Matsui, for their helpful suggestions and comments.

I also would like to thank Toyohashi University of Technology for allowing me to complete my study with the donation of Amano Institute of Technology (AMANO scholarship).

Finally, my deepest gratitude goes to my beloved wife, Qorina Novitri, for her excellent support and patience during the completion of my doctoral study. I extend my gratefulness to my parents for all their prayers on my best wishes. I hereby dedicate this doctoral thesis to them.

May Allah shower the above cited personalities with success and honor in their life.

TABLE OF CONTENTS

LIST OF TABLES

LIST OF FIGURES

CHAPTER 1
INTRODUCTION

1.1 Background

Nowadays, the use of Carbon Fiber Reinforced Polymer (CFRP) for repairing and/or strengthening steel structures has been being increasingly developed by adhesively-bonding technique, which in some literatures is also termed as "externally-bonded" or "bonded". In this method of strengthening, the CFRP laminates are attached onto steel surface using adhesive materials. Steel surface treatments, for example hand grinding, grit blasting, and/or sand blasting are much needed prior to bonding of the CFRP, to roughen the steel surface in order to obtain a good bond (both chemical and mechanical bonding) between the CFRP and steel. The bonding strength becomes a key point and of critical importance to the performance of the structures (Teng et al., 2012; Yu et al., 2012).

The effectiveness of this strengthening method in enhancing and/or improving performance of steel structures has been proven by many researchers in many research programs. However, this strengthening method has several disadvantages. First, it is a common to use CFRP plates. This type of CFRP can only be applied to flat surfaces. It is difficult to be bonded to steel which surface is not smooth enough or to steel member with an irregular shape. Second, the installation process of CFRP is usually carried out by hand-layup technique so that the CFRP-to-steel bond strength produced will much affected by skill of workers who work on it. The hand layup process has also a higher risk of possibility of entrapped air inside the composite. In addition, if the CFRP itself is also molded by hand-layup process of carbon fiber sheets, the quality of the CFRP produced will greatly vary (not uniform) as well as difficult to control. Third, adhesively-bonded strengthening requires steel surface treatment such as sand blasting, hand grinding, or grit blasting prior to CFRP application. This is not a simple task as it difficult to do (on-site) to steel members in existing building structures, and it gets worse if chemical or electrochemical treatments are also applied. Moreover, the bond strength of CFRP-to-steel is also greatly influenced by quality of the steel surface resulted from treatment by workers. It is also difficult to control because of different skill of workers. A necessity on the surface treatment leads to longer time for CFRP

installation and thus increases construction costs. Fourth, the bond strength of CFRP-to-steel is prone to performance degradation because of environmental exposures. The most influential conditions are temperature, moisture, and ultraviolet exposure (Nguyen et al., 2011; Li et al., 2016; Al-Shawaf and Zhao, 2013; and Nguyen et al., 2012). If the CFRP must be replaced, a new another higher cost must be spent and it will be unwise solution.

As an alternative to the adhesively bonded CFRP, a free-bond CFRP laminates (unbonded CFRP) strengthening method is proposed in this work. The method does not rely on the bond strength between steel and CFRP because indeed these two materials are not bonded together. The CFRP and steel are separated by a layer so that no stress transfer is expected from steel to CFRP which is a key point in the adhesively-bonded strengthening method. The CFRP is expected to contribute only through its flexural rigidity. Several advantages of this strengthening method are, namely: 1) the CFRP can be used for a longer period of time because it does not depend on the bond strength between CFRP and steel, as in the bonding method, which its performance can be decreased because of inevitable environmental exposures; 2) steel surface treatments are completely no longer needed. It leads to CFRP installation time shorter and saving labor as well as construction costs; and 3) the CFRP is created through a Vacuum-assisted Resin Transfer Molding (VaRTM) process which has not been widely used before in CFRP/steel strengthening application. The VaRTM process is able to produce a higher and stable quality of laminates as compared to hand-layup process (Uddin et al., 2004).

1.2 Research Objectives

The general purpose of this research is to investigate a new and promising method of strengthening steel structures using unbonded CFRP laminates which is fabricated by an advantageous VaRTM process. This method of strengthening does not require any steel surface treatments, so that easy to apply on-site for existing building. In particular, this research investigates experimentally and numerically the use of unbonded CFRP strengthening method for enhancing buckling performance of axial compression steel members. Analytical studies are also carried out to develop models for CFRP requirements and for compressive strength design of the strengthened members. Another goal of this work is to contribute for scientific development in civil and/or structural engineering field by providing innovation through the findings of this research.

1.3 Structure of the Report

This dissertation consists of six chapters. A brief description of each chapter is as follows:

Chapter 1: Introduction. This chapter provides a background of the research program. It also highlights the objectives of the current study. An introduction to other chapters is presented in the last part of this chapter.

Chapter 2: Literature Review. This chapter presents a review of literatures related to strengthening steel with CFRP materials. The review is divided into several parts: strengthening of short steel columns, long steel columns and steel braces strengthening, strengthening of flexural members, and shear, tensile, and torsion strengthening of steel members. It is also reviewed the factors influencing the bonding performance between steel and CFRP material.

Chapter 3: Axial Compression Steel Bars. This chapter describes the experimental and numerical works that focus on strengthening compression steel bars against buckling by using a proposed method of unbonded CFRP laminates. Detail of specimens, the CFRP preparation by VaRTM process, material used, test setups, instrumentations, and also test results are described. The requirements of CFRP for strengthening are derived through analytical models. A method of equivalent slenderness ratio is further introduced for strength design for strengthened compression member and validated with the numerical and experimental test results.

Chapter 4: Angle Steel Fully-Jacketed Cross Section. The applicability of the proposed unbonded CFRP method for strengthening axial compression steel member is presented in this chapter through strengthening of large-scale angle steel members. Detail of specimens, preparation of the CFRP laminates by VaRTM process, material used, test setups, instrumentations, and test results are described. The requirements for CFRP derived in chapter 3 are used in the design stage. The experimental results are used to validate the equivalent slenderness ratio method described in chapter 3. In addition, a procedure to predict the post-buckling curve for the strengthened steel member is also proposed in this chapter.

Chapter 5: Angle Steel Partially-Jacketed Cross Section. This chapter presents the application of unbonded CFRP strengthening for large-scale angle steel members with

different scheme to study whether it is also effective in improving buckling performance of the angle steel and thereby reducing the amount of CFRP usage. Detail of specimens, preparation of CFRP by VaRTM process, material used, test setups, instrumentations, and test results are described.

Chapter 6: Summary and Conclusions. This chapter provides a brief summary of the research program as well as conclusions that can be drawn. Recommendations are also included at the end of this chapter for future research of CFRP/steel strengthening system.

CHAPTER 2
LITERATURE REVIEW

2.1 Introduction

Following its successful application to the concrete structures, in recent years, the use of CFRP for strengthening steel structures has also begun to show a growth trend replacing conventional methods of bolting or welding additional steel plates. The CFRP is preferred as it has excellent properties, namely: light weight, high strength-to-weight ratio, excellent fatigue and corrosion resistance, and easy to handle and process. This chapter describes available literatures on the use of CFRP material for strengthening steel structures. In the first part, the applications of CFRP for strengthening short steel column are examined through several experimental research programs. It is followed by a summary of studies for long steel column in which capacity improvement becomes the most concern within investigations. Studies that investigated flexural strengthening of the steel members using CFRP are also summarized in the next section. Afterwards, research programs available for shear, tensile, and torsion strengthening using CFRP are examined in one combined section. Because steel strengthening using CFRP is mostly accomplished by bonding technique, the last section of this chapter focuses on the CFRP-to-steel bonding characteristics and environmental conditions affecting.

2.2 Strengthening Short Steel Columns using CFRP

The potential use of CFRP for strengthening short steel columns was conducted by Shaat and Fam (2006). A total of twenty-seven square hollow structural section (HSS) column specimens (89 mm × 89 mm × 3.2 mm, slenderness ratio = 5, and yield strength = 380 MPa) were prepared to study the effect of CFRP sheet orientation in the longitudinal and transverse directions. The application of CFRP was preceded by sand blasted surface treatment of steel to remove any rust. Then, the steel surface was cleaned with acetone and also coated with a layer of resin. After CFRP was applied, the specimens were cured for at least 6 days before being tested. The compression test results found that the maximum strength gain achieved was 18%. Transverse CFRP layers were effective in confining local buckling.

Bambach et al. (2009) also conducted compression test on short square hollow sections (SHS) strengthened with CFRP. The SHS specimens were produced by spot-welding. This investigation was an extension of their previous study on commercially produced SHS strengthened with CFRP in same manner (Bambach and Elchalakani, 2007). There were two different fiber layouts of the CFRP investigated (Figure 2.1): 1) one layer lay transversely with one layer longitudinally (1T1L), and 2) two layers transversely with two layers longitudinally (2T2L). The CFRP for strengthening was bonded directly to the steel using epoxy: Araldite 420 for the commercially produced SHS and Mbrace Part A and B saturant for the spot-welded SHS. However, prior to bonding the CFRP, the surface of the SHS was roughened by hand grinding (for commercially produced SHS) or sand blasting (for spot-welded SHS), and cleaned with acetone. The results of the experimental test shows that application of CFRP can increase the axial capacity of steel section by up to 2 times compared to control un-strengthened steel section.

Haedir and Zhao (2011) studied the compressive behavior of circular steel tubular short columns strengthened using bonded CFRP sheets. The concentric loading test was undertaken to totally ten specimens, which four columns were bare steel and six were strengthened with CFRP sheets in various configurations (hoop and longitudinal). In this study, unidirectional high-strength carbon fibre sheets (MBrace CF 130) were used. However, prior to implementing the CFRP, the surface of the steel columns was ground with an abrasive disc and then solvent cleaned to promote good adhesion between steel and CFRP. The strengthened column specimens were cured for two weeks before testing. It was concluded from the experimental results that a combination of hoop and longitudinal CFRP can promote the attainment of the yield capacity of the bare column. The axial strength of the columns was increased with higher amount of CFRP.

Sundarraja et al. (2014) investigated the CFRP for strengthening HSS columns (91.5 mm×91.5 mm×3.6 mm) in different scheme. Eighteen of twenty-one specimens (length = 600 mm) were strengthened with transversely direction bonded CFRP having a constant width of 50 mm wrapped with the spacing of 20 mm and 30 mm (Figure 2.2). Sand blasting was conducted for surface preparation of steel before attaching the CFRP. After this treatment the steel surface was cleaned with acetone to remove any dust. All the test specimens including control un-strengthened columns were tested in compression testing machine having capacity of 2000 kN. Based on the experimental results, it can be concluded that the external bonding of CFRP can effectively reduce

the axial shortening of specimens by providing confinement against the elastic deformation. The existence of CFRP also delayed local buckling of the steel tube.

Ghaemdoust et al. (2016) performed experimental test to study the effect of using CFRP sheets for strengthening short SHS steel columns which have initial horizontal or vertical deficiencies. One control un-strengthened column and twelve specimens with different dimension of deficiencies were prepared. Unidirectional high-strength carbon fiber (SikaWrap-230C) was used for CFRP. The investigation was performed for two different fiber layouts of CFRP: one layer being placed transversely with one layer longitudinally. Eight of thirteen specimens were externally bonded with CFRP sheets using epoxy Sikadur-330. To obtain a good bonding between steel tube and CFRP, before strengthening, surfaces of the specimens were blasted by the rough sand to make the surfaces clean and rough. Then, the steel surfaces were cleaned by acetone. The carbon fiber was bond onto steel surface by using epoxy Sikadur-330. It was confirmed from the experimental test that the application of CFRP could significantly recover the specimens strength-lost due to deficiency, increase the load-bearing capacity, and delay the local buckling.

Almost similar to the research conducted by Ghaemdoust et al. (2016), Karimian et al. (2017) performed laboratory test to examine the structural behaviors and impact of CFRP on strengthening steel circular hollow section (CHS) short columns. The columns also had initial horizontal or vertical deficiencies (Figure 2.3). A total of eight steel CHS columns specimens were tested including one control specimen (without deficiency). The CFRP (SikaWrap®-230 C) with 238.000 MPa of elastic modulus were used to be bonded to steel surface as strengthening materials. The steel surfaces were sandblasted before attaching the CFRP sheets. After the external surfaces of steel were covered using adhesive, the CFRP sheets were bonded by four layers. The first and third layers were installed in transverse direction while the second and fourth layers in longitudinal direction. All specimens were then tested in axial compression. The test results reveal that capacity reduction of the deficient columns could be compensated by the presence of four CFRP layers used. The CFRP also delayed the local buckling in the columns, leading to increase bearing capacity.

Chen et al. (2018) investigated the effect of using CFRP sheets on the behavior of lateral impact-damaged steel short columns. A total of thirty-three columns including sixteen circular and eighteen square columns were tested. All the columns had 350 mm height. The outer diameter and wall thickness of circular short steel columns were 165

mm and 3.5 mm, respectively, and the section width and wall thickness of square short steel columns were 120 mm and 4.0 mm, respectively. The specimens were damaged first by means of impact test before strengthened using CFRP. The CFRP sheets were attached to the surface of specimens after it was cleaned from oil, grease and dirt. The material used to attach the CFRP sheets was epoxy resin. All the columns specimens were tested under compression load. The experimental test results concluded that the bearing strength of column specimens can be improved by wrapping the CFRP sheets. Moreover, the strength improve on circular columns were better compared to that of square columns.

Abu-sena et al. (2019) conducted experimental test on twenty short square and rectangular hollow sections (SHS and RHS with total length of 700 mm) steel columns. The columns were divided into fully strengthened and partially strengthened specimens. The partially strengthened specimens were using CFRP strips of single layers and CFRP strips with two layers. The strips were 100 mm wide and placed for every 50 mm space. In all the studied columns, the CFRPs were applied in transverse direction only. A unidirectional carbon fiber fabric SikaWrap-300c was used for CFRP. This carbon fiber had thickness of 0.17 mm, elastic modulus of 230 GPa, and tensile strength of 4 GPa. The CFRP was bonded to steel surface using Sikadur-330. All the columns were tested under axial compression load with small increments. It could be concluded from the test results that, in fully strengthened specimens, the CFRP effectively delayed the local buckling. However, for partially strengthened specimens, failure could be found at the non-strengthened zones between CFRP strips. The gain in ultimate capacity for SHS and RHS specimens were 19.1-34.5% and 18-41.3%, respectively.

2.3 Long Steel Columns and Steel Braces Strengthened with CFRP

Shaat and Fam (2009) strengthened slender steel columns using high-modulus (313 GPa) CFRP plates. Eighteen slender hollow structural section square column specimens (44 mm×44 mm×3.2 mm), were prepared and concentrically tested to failure. Slenderness ratios of the columns were 46, 70, and 93. All the strengthened specimens the same CFRP retrofitting scheme. The CFRP used was unidirectional pultruded plates which had 50 mm wide and 1.4 mm thick. An epoxy resin, Sikadur-30, was used to bond the CFRP plates to steel surface. Prior to bonding, the outer surface of the columns was sandblasted to remove rust and also to roughen the steel surface for its better interlock with the adhesive. The results of the experimental test

showed the effectiveness of the CFRP strengthening system in increasing axial strength of the columns. The axial load capacity of the tested columns was increased by 6, 35, and 71% for columns with slenderness ratios 46, 70, and 93, respectively. Moreover, the axial stiffness of the columns was also increased, namely 10, 16, and 17% for columns with slenderness ratios 46, 70, and 93, respectively.

Tamai et al. (2012) demonstrated the use of CFRP to enhance the capacity of angle steel, 50 mm×50 mm×4 mm, as shown in Figure 2.4a. The CFRP was bonded to the outer surface of the angle steel (Figure 2.4b). Two types of CFRP plates used were high tenacity type carbon fiber and middle modulus type carbon fiber. Both of them had a same thickness, namely 2 mm. The surface of angle steels was prepared using a grinding machine and then polished with glass paper (#100) before CFRP were applied using epoxy resin. A total of twelve specimens were tested in compression with varied lengths of 800 mm, 1000 mm, 1170 mm, 1300 mm, 1500 mm, and 1600 mm. The test results showed an increasing in load carrying capacity of the angle steel. Enhancing in specimen's flexural rigidity could also be confirmed but not for axial stiffness.

Haydaroglu and Celik (2012) conducted test to investigate the effectiveness of using CFRP sheets in delaying local buckling of HSS steel brace having dimension of 70mm×70 mm×3 mm. Their experiment involved 3 large-scale specimens: one control specimen and two specimens with CFRP strengthening. In all strengthened braces, position of CFRP was at mid-span. The two strengthened braces had a length of CFRP 450 mm and 900 mm, respectively. Before the CFRP was bonded to steel, the surfaces of the brace were cleaned and prepared by grit blasting. The CFRP were then partially bonded (wrapped) to the brace. The cyclic test was performed to specimens according to ATC-24 protocol. The results had not shown significant contribution of CFRP used because number of specimens used was limited. However, if all of their experimental results are evaluated and compared, the CFRP strengthening showed effective way to prevent local buckling at mid-span of the brace.

Gao et al. (2013) studied the effects of bonded CFRP strengthening on overall buckling behavior of circular tubular steel braces (88.9 mm × 4 mm). A total of five specimens were prepared and tested (Figure 2.5a). Length of the braces was 2.4 m (slenderness ratio 80). The application of CFRP was preceded by sandblasting on steel surface to remove any rust. Then, the steel surface was cleaned with acetone. High-modulus carbon fiber sheets were used for strengthening. It was bonded to the steel braces in the longitudinal direction. Before the application of CFRP, one layer of glass

fiber was installed directly on the steel surface to prevent galvanic corrosion between carbon fibers and steel. Based on the experimental results, it could be concluded that longitudinal bonded CFRP sheets were effective in increasing the axial strength and stiffness of the slender braces. The increasing ranged between 28–124% and 25–105% for the axial strength and stiffness respectively (Figure 2.5b and 2.5c).

Ritchie et al. (2015) performed an axial compression test of twelve 2.6 m long S-sections (S75 × 8) steel columns of 197 slenderness ratio to examine the effect of CFRP strengthening. Totally 12 steel columns were prepared. The columns were tested under pin-ended conditions and allowed to buckle around their weak axes only. In this experimental test, there were four affected parameters investigated, i.e., level of initial out-of-straightness, CFRP modulus, CFRP reinforcement ratio, and length of CFRP plate. The CFRP plates used were ultrahigh modulus of 430 GPa, high modulus of 212 GPa, and standard modulus of 168 GPa. The strengthening system was performed by bonding the CFRP plates to the outer surface of the two flanges of the S-section using epoxy resin (Figure 2.6). For this purpose, the steel surfaces were first sandblasted and then cleaned with acetone to remove any dust. They confirmed from the test results that the axial strength increase ranged between 11% and 29%. In general, this increment occurred as increasing of the first three parameter mentioned before. It is clear that the column peak load related consistently with global buckling failure.

Keykha et al. (2015) presented a result of their study on the partially and fully strengthening of hollow steel columns using CFRP. The column specimens were cut from 6 m length SHS steel (40 mm×40 mm×2 mm) into 3 m length. Total specimens tested were 6 columns: five strengthened and one control un-strengthened specimens. The strengthened columns had a same number of CFRP layer (2 plies) but varied in CFRP coverage (20%, 30%, 40%, 50%, and 100% of column length). To achieve good bonding between CFRP and steel, the columns surface were blasted by a coarse sand to remove rust and to make the surface rough. After that, the treated surface was cleaned by acetone. The carbon fiber was bonded to outer surface of the columns using epoxy resin. It was concluded from the test that maximum bearing capacity of columns was directly affected by percentage of CFRP coverage. It was also clear that column with 100% CFRP coverage has the highest gain in load bearing capacity.

Kumar and Senthil (2016) used CFRP to strengthen CHS steel having slenderness ratio of 30, 35, and 40 and diameter-to-thickness ratio of 16.55. The experimental tests were carried out on a total of 54 specimens under axial static and axial cyclic loading.

The CFRP strengthening schemes were one layer of longitudinal and transverse directions and two layers of longitudinal and transverse direction. A unidirectional CFRP was used in their study. Before the CFRP was bonded to steel using epoxy resin, surface of the CHS steel were made rough by sandblasting and then wiped with acetone. Several conclusions could be drawn from their study were the static and axial cyclic compressive strength of both strengthened and un-strengthened CHSs decreased as increasing slenderness ratio. The presence of CFRP enhanced axial capacity of the CHS by up to 39.47% for static axial loading and 41.02% for axial cyclic loading.

Sayed-ahmed et al. (2018) investigated the efficiency of CFRP strengthening to enhance the buckling behavior of steel columns. Thirty HSS (48 mm×48 mm×2 mm) column specimens were prepared and then eccentrically loaded until failure. The load eccentricity was varied, namely 25, 50, and 100 mm measured from centroidal axes of the specimens (Figure 2.7a). Besides eccentricity, the effective buckling lengths of the columns were also varied to be 1260 mm, 1850 mm, and 2440 mm. The CFRP laminate was bonded onto two opposite sides of the column's section using adhesive (Figure 2.7b). Before it was done, the outer surface were firstly sandblasted to roughen and to remove the rust and any mill scale. And then, the surface was cleaned using air nozzle and then mopped with acetone. It had been found from the test results that the gain in axial load capacity of the CFRP-strengthened columns ranged between 40 and 107%. The column with medium slenderness ratio provided the maximum increase in the loading capacity. It could be also observed that debonding of CFRP laminates occurs in the strengthened specimen.

Shadan and Kabir (2018) conducted axial compression test on SHS steel braces strengthened with CFRP. The three influence parameters evaluated were slenderness ratio, number of CFRP layers, and length of CFRP. The SHS brace used (90 mm×90 mm×4 mm) was non-compacted cross section based on AISC 341-10. The CFRP was bonded to the steel brace in transverse direction only. For this purpose, the steel surface were scrubbed from primary rusts using a wire brush drill and then polished with an abrasive disk. Afterwards, the steel surface was cleaned again by using acetone. The specimens were tested after being cured for 14 days at temperatures around 18°C. The investigation results showed this strengthening technique was effective in postponing local buckling of the SHS brace. The local buckling in brace having larger slenderness ratios could be prevented only with lower percentage of FRP coverage.

2.4 Flexural Strengthening of Steel Members using CFRP

Flexural behavior of a rolled steel beams strengthened using partial-length CFRP plates was studied by Lenwari et al. (2005). A total of seven W100×17.2 steel beam specimens having span length of 1.80 m were prepared. The length of CFRP was varied to be 0.50, 0.65, and 1.20 m. The CFRP plates were bonded to the bottom flange of the beam using epoxy adhesive while the top flange was welded with steel plates (thickness = 12.2 mm) to prevent compressive yielding. Prior to bonding of CFRP, the surface of steel was sandblasted until it reached white metal condition. Then, the treated surface was cleaned again using isopropyl alcohol. All the beam specimens were tested in four-point loading. Their test results concluded that the CFRP plates bonded to the beams significantly increased the beams strength and extended the range of elastic region of the beams. It was also confirmed that failure load increased as increasing CFRP length.

Colombi and Poggi (2006a) strengthened H-shaped steel beams (HEA 140) using pultruded CFRP strips. The CFRP strips were adhesively bonded (using epoxy resin) to the bottom flanges of the steel beam specimens 1 and 3, while a less viscous epoxy was used for bonding the strips to the tension flange of the beam specimen 2. Number of CFRP layers for the beam specimen 1, 2, and 3 were 1, 1, and 2 layers, respectively. The surface of the steel beam where the CFRP strips would be bonded were treated first by using abrasive disk and then degreased by a xylene based solvent. After the CFRP strips were applied, the specimens were cured for two weeks before being tested. The experimental test was performed in three point bending. It was concluded from the test results that the bonded CFRP strips were very promising in improving performance of the steel beams. The load-carrying capacity could be increased by 9.2, 10.5 and 23.31% for beam specimens 1, 2, and 3, respectively (at mid-span deflection level of 20 mm).

Haedir et al. (2009) studied the potential of CFRP for strengthening CHS steel beams under pure bending. They prepared eighteen specimens for the test which were divided into three series based on their cross-sectional sizes. The steel beam specimens varied in nominal diameters (33.8-88.9 mm), nominal thicknesses (2.7-3.2 mm), and effective length-to-diameter ratios (4-12). Moreover, the orientation of fiber for CFRP was also made in combination of hoop and longitudinal. For CFRP application, the beams surface was treated using an abrasive disk and then cleaned with a solvent-based cloth. The pure bending test results proved that the use of CFRP had a huge potential in enhancing strength, stiffness and ductility of CHS steel beams. Strength increases of the beams were greatly affected by the amount and orientation of carbon fiber.

Hmidan et al. (2011) discussed the results of experimental work on the damaged steel beams repaired by CFRP. The beams were hot-rolled steel sections (W100 × 19). Total of six beams were loaded in four-point bending with loading span and constant moment zone of 1882 mm and 444 mm, respectively (Figure 2.8). The damaged of the beams was represented by notching located in both sides of the tension flange (with initial crack in web). There were three different notch depths (a_0) investigated, namely: 10.6 cm, 31.8 mm, and 53.0 mm. Prior to CFRP application, tension flange of the beam was grit blasted to obtain a rough surface of steel. After grit blasting, steel surface was cleaned using air compressor and acetone. Through this investigation, it was revealed that the presence of CFRP was able to stabilize the crack mouth opening displacement of the beams until significant debonding occurs. The CFRP is more effective when the level of damage increases.

Narmashiri et al. (2012) studied the effects of applying CFRP with different bond lengths on flexural behavior of steel I-beams. One control non-strengthened specimen and five strengthened steel beams (yield stress = 250 MPa, tensile strength = 370 MPa) were prepared. CFRP bond lengths selected were 600 mm, 1000 mm, 1500 mm, 1700 mm, and 1800 mm. Steel surface preparation before bonding CFRP was sandblasting. After sandblasting process, CFRP plates were bonded to bottom flange of the beams and cured until the adhesive material had been completely hardened (about one week). In this experiment, only one type of CFRP was used. All specimens were tested in four-point bending (Figure 2.9). The experimental results proved that the performances of steel I-beams were depending on the CFRP bond length. Applying longer CFRP caused higher load bearing capacity. It could also significantly decrease strain on adhesive.

Chen et al. (2015) tested RHS steel beams (100 mm×50 mm×6 mm) with various depths of initial crack (3, 6, and 30 mm). The total specimens tested were eight beams including three control specimens and five beams strengthened with CFRP plates. Three of the five strengthened beams utilized CFRP plates without prestressing while another two were bonded with prestressed CFRP plates. For CFRP installation, they grounded bottom surfaces of the beam using abrasive disk to remove rust. The treated surfaces were then cleaned with acetone to remove dust. After this process, the CFRP plates were bonded onto steel and then cured for more than one week. All specimens were tested to failure under three-point loading (Figure 2.10). The experimental results concluded that ultimate loads of the cracked beams could be increased by using CFRP plate. This strengthening technique could significantly reduce deformation of the beams.

Altaee et al. (2017) focused on the application of CFRP to strengthen steel beams having web openings. Their laboratory test consisted of four beams (305 mm×102 mm×25 mm) with 3 m clear span. One specimen served as control beam without web openings whereas another three had rectangular web openings located in different positions (Figure 2.11). The unstrengthenend versions of the three beams were modeled using finite element software (Abaqus) for comparison purpose. CFRP was bonded to steel surface to strengthen the beams. To obtain a good bond, the steel surface was first treated by mechanical grinding to remove the weak oxide layer. Then, it was cleaned using acetone to remove grease or oil. All the beams were tested in six point bending. Based on their investigation, they revealed that CFRP was effective for enhancing strength and stiffness of the steel beams. A greater load capacity could be achieved between 5 and 20% after CFRP application.

Siwowski and Siwowska (2018) conducted test to study the flexural behavior of steel I-beams strengthened with CFRP plates. They applied two different schemes of strengthening, namely: adhesively-bonded passive CFRP plates and adhesively-bonded prestressed or active CFRP plates (Figure 2.12). Steel beams had 4.80 m span length and tested in four point bending. A total of ten beam specimens were tested, consisting of one control reference beam and nine strengthened beams. The strengthened beams were divided into three groups depending on the CFRP used (two different modulus of elasticity) and strengthening method (active or passive). Their investigation concluded that the bonded CFRP plates only increase the elastic stiffness of the strengthened steel beams less than 5%. However, it was effective in increasing the yield and ultimate flexure capacity of the strengthened beams (10-20% and 10%, respectively).

Peiris and Harik (2021) strengthened steel wide flange beams (W10 × 22) using Ultra-High Modulus (UHM) CFRP strip panels (Figure 2.13). In addition to one control beam, one strengthened beam was prepared with a continuous UHM CFRP laminate and the two remaining beams with the UHM CFRP strip panels. Prior to application of CFRP, the beams were grit blasted to promote bonding. The treated surfaces were cleaned again using a solvent. The beams were flexural tested in four-point bending with a constant moment region of 762 mm. The test result showed that the UHM CFRP strip panels could increase the loading capacity of the beams at which yielding initiates. The failure loads for the beams strengthened with UHM CFRP laminate and 10 mm and 5 mm wide CFRP strips were respectively 39%, 27%, and 26% larger than the load initiating yield in the un-strengthened beam.

2.5 Shear, Tensile, and Torsion Strengthening of Steel Members with CFRP

Hatami et al. (2012) used CFRP to strengthen steel shear walls and then studied its behavior. Through experimental and numerical studies, they evaluated the effects of fiber content/angle and panel width on the properties of the walls. There were two types of specimens prepared: a steel shear wall without CFRP and a shear wall strengthened with CFRP. In the strengthened shear wall, both surfaces of the steel were roughened by sand blasting before application of CFRP layers. The CFRP were glued to the steel surface using epoxy resin. Their investigation results concluded that the higher width of shear walls results in higher stiffness, shear capacity and energy absorption values. The energy absorption, stiffness, over-strength and capacity also increased as higher fiber contents, but ductility values decreased.

Poul et al. (2016) performed shear loading test on thin steel plates strengthened by CFRP. The plates (thickness of 1 mm) were strengthened by CFRP with different numbers of layers and orientations. They prepared four specimens in this investigation: one was control un-strengthened specimen and another three were strengthened with CFRP as shown in Figure 2.14 (the fiber orientations were 0^o, 45^o, -45^o, and 90^o). The CFRP sheets were applied after steel surfaces were treated by sand blasting. The CFRP were carefully bonded to steel plates using epoxy adhesive and cured for two weeks. The experiment was conducted under cyclic quasi-static loading along diagonal axes of specimen. The results showed that CFRP was effective in enhancing behavior of the plates. Yield strength, ultimate strength, and secant stiffness could be significantly increased. Additional of two layers of CFRP also had an effect on increasing ultimate strength, but not for stiffness and energy absorption.

Kazem et al. (2018) conducted experimental study to examine the use of small-diameter CFRP strands for shear strengthening of steel plates. The aim was to increase the shear capacity of steel plates subjected to pure shear stresses. Total of specimens prepared were nine square steel plates having dimension 915 mm× 915 mm and 5 mm thick. The steel plates were prepared by sandblasted and cleaned before applying CFRP strands using epoxy adhesive. The CFRP were bonded to steel with orientation of 45^o, 90^o, and $\pm 45^o$ relative to the applied load. Each side of the plate had one or two layers of CFRP strands. Based on the experimental findings, it was concluded that the small-diameter CFRP strands provided an excellent strengthening system for increasing the shear capacity of the steel plates. Their proposed strengthening system eliminated the typical debonding failure commonly observed by CFRP laminates.

Colombi and Poggi (2006b) studied the effectiveness of the use of CFRP plates to strengthen tensile steel members. They considered three types of reinforcements, i.e, double side reinforcements of continuous steel plates, double lap joints, and also bolted joints (as shown in Figure 2.15). The average value of elastic tensile modulus of CFRP obtained from coupon test was 197000 MPa. Two different epoxy resins were used for bonding the CFRP onto steel plates (Sikadur-30 and Sikadur-330). The steel plates were treated first by an abrasive disk and then cleaned using acetone to achieve a rough and clean surface of steel. All specimens were tested under uniaxial tensile static load. A constant rate of control displacement equals to 0.008 mm/s. Experimental results revealed that the use of Sikadur-30 and Sikadur-330 respectively produced a ductile and a brittle behavior of specimens. The failure mode found in all cases was interfacial failure at the steel–adhesive interface.

Lu et al. (2015) evaluated the use of CFRP for strengthening steel plates against tensile load. The involved parameters were number of CFRP layers (from one to four), strengthening schemes (single-sided and double-sided bonding), and temperatures (ranging from 25 to 120 ^{o}C). The CFRP was adhesively-bonded to steel through hand lay-up technique. The surfaces of steel plates were roughened with fine emery paper and then cleaned with ethanol before applying epoxy resin. The CFRP was placed upon the steel plates while applying pressure to ooze out voids and excess resin. Tensile test was carried out with loading speed of 1 mm/min through a universal testing machine. It was confirmed from the test that number of CFRP layers and strengthening schemes did not has significant effect on failure modes of specimens. The bonding CFRP increased the ultimate load significantly. However, it was also observed that the ultimate load was significantly decreased as temperature increased.

Wang et al. (2016) strengthened the open hole and bolted steel plates using CFRP strips to investigate its tensile behavior. A total of thirty-nine specimens (Figure 2.16) were prepared with different combination of washer length and/or number of CFRP layers. To apply the CFRP, surface of the steel plates for strengthening was grounded using sandpaper by hand to remove roughs. Then, the surface was cleaned from grease and rust by using acetone. The prepared specimens were cured for two weeks before being tested. The experimental tensile test was carried out using a 100 kN capacity of universal testing machine. It was found from the test that tensile strength of the specimens could be enhanced by increasing the number of CFRP layers and further moderately improved with the bolted washer clamp-up.

Chahkand et al. (2013) investigated the use of CFRP for torsional strengthening of SHS steel. The SHS specimen had a length of 1400 mm with the test region length of 1160 mm. Two specimens were prepared as control specimens and four specimens were strengthened using CFRP with different strengthening configurations. For the first type of strengthening, the SHS steel wrapped with five layers of CFRP vertically with respect to the longitudinal axis of the specimen. In second type, the wrapping using two layers of CFRP reverse-spirally. In the third type, there was a combination of three layers of CFRP reverse-spirally and one layer of CFRP spirally wrap. And for the last, a combination of two layers of CFRP spirally and two layers of CFRP reverse-spirally wrap was used. Surface preparation on steel using grinding and cleaning with acetone were completed before bonding the CFRP. The pure torsion test results concluded that torsional strength of the SHS steel was increased due to the presence of CFRP. The best strengthening scheme for the greater torque capacity was spirally wrap configuration.

Sharrock et al. (2015) also performed experimental test to investigate the torsional behavior of CFRP-strengthened SHS steel (100 × 100 mm). The test program involved SHS steel with three different depth-to-thickness ratios (D/t), i.e., 16.67, 33.33, and 50. The steel surfaces were prepared by sand blasting for bonding CFRP. Its process was carried out using 30-60 sand (0.6 mm to 0.25 mm grain size) at a pressure of 0.8 MPa. Afterwards, the surface was cleaned using isopropanol for impurities removing. All specimens were wrapped (bonding) with four layers CFRP at the inclined angle of 45^{o}. The experimental results showed that the increase in maximum torsional capacity was related to values of depth-to-thickness ratios (D/t). It was clear that the larger ratio had a greater increase.

The experimental test of using CFRP for torsional strengthening CHS steel was presented by Wu et al. (2018). They prepared five different types of CHS with three different diameters and three wall thicknesses. The CFRP strengthening scheme was also made into five types with the fibers aligned in different angles. In this study, they used unidirectional carbon fiber fabric and epoxy (Araldite 420) for CFRP materials. Sand blasting and then cleaning using isopropanol was selected for surface preparation on CHS steel before applying CFRP. Their experimental test results revealed that the torsional strengthening performance was affected by geometry of the CHS (diameter and wall thickness) and CFRP strengthening schemes (wrapping angle and wrapping sequence). It was clear that the most effective CFRP strengthening scheme was 45^{o} "spiral" directions against the longitudinal axis of the CHS specimens.

2.6 Factors Influencing CFRP/steel Adhesively-Bonded

An experimental research to examine the mechanical behavior of steel/CFRP adhesively-bonded double strap joints at elevated temperatures was conducted by Nguyen et al. (2011). A series of strap joints were prepared to be tested in tension at temperatures between 20^{o}C and 60^{o}C. In this experiment, they used carbon fiber having nominal elastic modulus and tensile strength of 240 GPa and 3800 MPa, respectively. Araldite 420 was selected as epoxy adhesive. It had nominal tensile strength and tensile modulus of 32 MPa and 1900 MPa, respectively. The glass transition temperature T_g was 42^{o}C. Sand blasting was applied to surfaces of the steel plates (180 mm length, 50 mm width and 5 mm thickness) and then cleaned with acetone before the joints were formed using a wet lay-up method. Results of their experiment showed decreasing in the joint stiffness as temperature increased: 20% reduction at the T_g, 50% at 10^{o}C above T_g, and 80% at 20^{o}C above T_g. The joint strength also decreased with temperature: about 15%, 50% and 80% when temperatures reached T_g, 10^{o}C above T_g, and 20^{o}C above T_g, respectively.

Li et al. (2016) also studied the effect temperature on the bond behavior between CFRP and steel. Slightly different with Nguyen et al. (2011), they examined the bond behavior for temperatures between 27^{o}C and 120^{o}C. A total of 21 double strap joints were tested to failure. CFRP sheets were bonded to steel surface using epoxy adhesive after treatment was applied. The steel plate was roughened by emery wheel and cleaned using acetone to remove grease or rust. The CFRP used was a unidirectional material Glass transition temperature T_g of the epoxy adhesive was 50^{o}C. Their experimental study found that initial stiffness and ultimate load of the specimens tend to decrease due to thermal exposure, especially at temperatures above T_g. Failure mode of specimens changed from debonding along steel-adhesive to debonding along CFRP-adhesive.

Al-Shawaf and Zhao (2013) evaluated the effect of subzero temperatures (20, 0, -20, and -40^{o}C) on the bond strength between CFRP and steel. They prepared CFRP/steel double strap joint specimens for tensile test in this work. The CFRP laminates was obtained through wet lay-up process using a normal modulus unidirectional carbon fiber sheets (E = 240 GPa) and three different epoxy resins (Araldite 420, MBrace Saturant, and Sikadur-30). In the process, the bond-lap areas of steel plates were treated by mechanical roughening (using power cutting-disc) via a $\pm$ 45^{o} perpendicular shallow scratching for a good bonding. The experimental results indicated that there was no bond strength reduction occurred at the down of temperatures to -40^{o}C for the specimens with

Araldite 420 and Sikadur-30. The bond strength reduced about 40% for specimens using MBrace Saturant when the temperature dropped from 20 to -40^{o}C.

Agarwal et al. (2014) investigated the long term durability of the bond strength between CFRP and steel under freeze thaw cycles. They prepared a total of 48 single lap shear specimens to be tested in tension. Two different adhesives, Sikadur-330 and Sikadur-30, were used for CFRP installation. Prior to CFRP application, the surface of the steel plates was prepared. It was hand grounded using sand paper and then cleaned with acetone to make it clean from grease and rust. Their experimental results concluded that the bond strength of the joint specimens was decreased. After exposures to 40 freeze thaw cycles, the bond strength of the steel-CFRP joints using Sikadur-330 adhesive decreased about 28% and the joints using Sikadur-30 decreased about 18%.

Zhao et al. (2014) reported findings of the research conducted by Nguyen et al. (2012) in investigating the effect of ultraviolet (UV) exposures on the CFRP/steel double strap joints behavior. A unidirectional high tensile strength carbon fiber sheets was used in this study and Araldite 420 for epoxy adhesive. The two steel plates were sand blasted and cleaned with acetone before epoxy and carbon fiber were applied. The steel/CFRP double strap joints were exposed to a UV irradiation setting of 1.26 W/m^2/nm at 340 nm for 124, 248, and 372 h on every surface. The maximum value of 744 h (2 surface × 372 h) equals to one year UV outdoor dose of 250 MJ/m^2 in Victoria, Australia. The tensile test results of the joints showed decreasing in capacity with exposure time. The significant decrease occurred in the first 124 hours (each surface). The maximum decrease in strength was 18.7% after 372 h exposures (each surface).

The effect of combination of steel surface treatments and used adhesives on the CFRP/steel bonding performance was evaluated by Fernando et al. (2013). The surface treatments including solvent cleaning, hand grinding after solvent cleaning, and grit blasting after solvent cleaning and the adhesive material used was Sika and Araldite. The experimental program consisted of butt-joint tensile tests and single-lap shear tests. Each of the tests has a total of 60 specimens. The test results showed that steel surface treatments selected could affect the bonding performance between CFRP and steel. They concluded that adhesion failure between steel and adhesive (a failure which much more likely occurred) could be avoided if a suitable adhesive was applied together with grit blasting treatment. A grit-blasting provided a significant higher adhesion strengths compared to the solvent cleaning and the hand grinding after solvent cleaning.

2.7 Summary

A summary of the current research on strengthening steel structures using CFRP is summarized within this chapter. All of the research focuses on strengthening by adhesively-bonding technique, where CFRP is directly stuck onto steel surface using adhesive material. The effectiveness of this strengthening technique has been proven through experimental program conducted to short and long steel columns, steel braces, flexural members, and shear, tensile, and torsion steel members. A crucial issue regarding durability of the bond strength between CFRP and steel makes research also lead to find out this phenomenon and investigates any factors influenced. Although various studies have been described in this chapter, research on strengthening steel using CFRP is still limited and requires much innovation so that CFRP can be effectively utilized in a real construction.

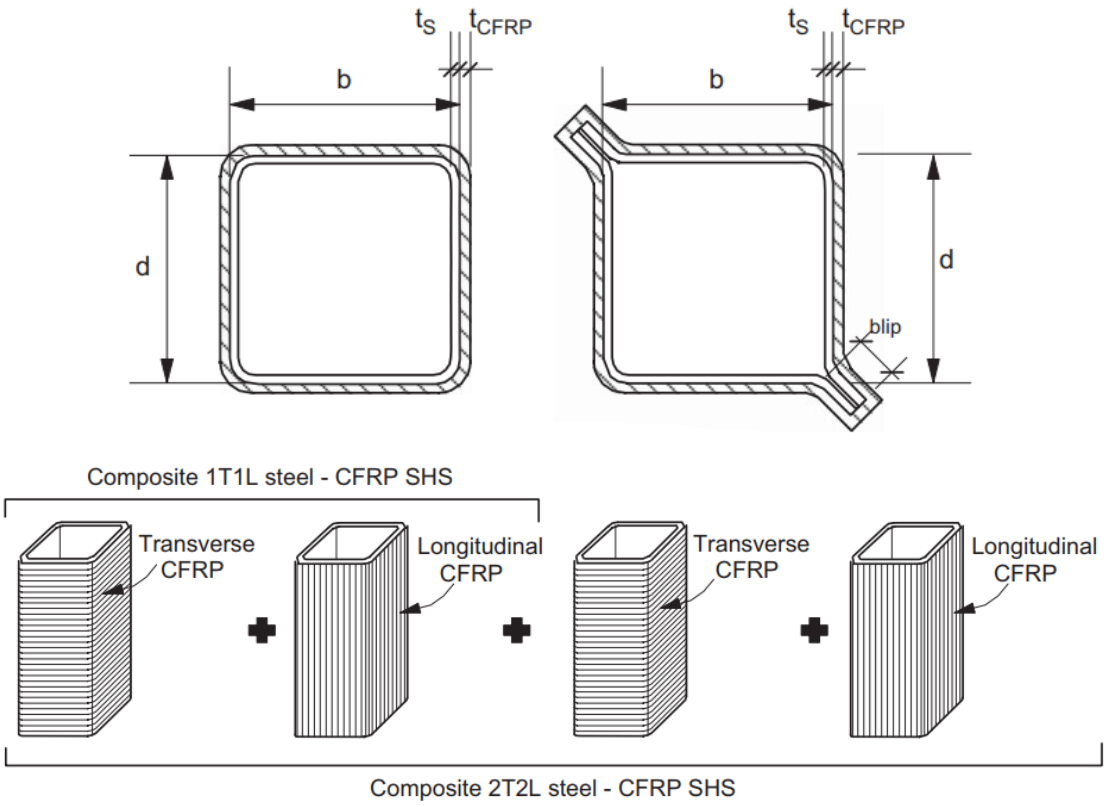

Figure 2.1 SHS specimens and layouts of fiber (Bambach, et al., 2009)

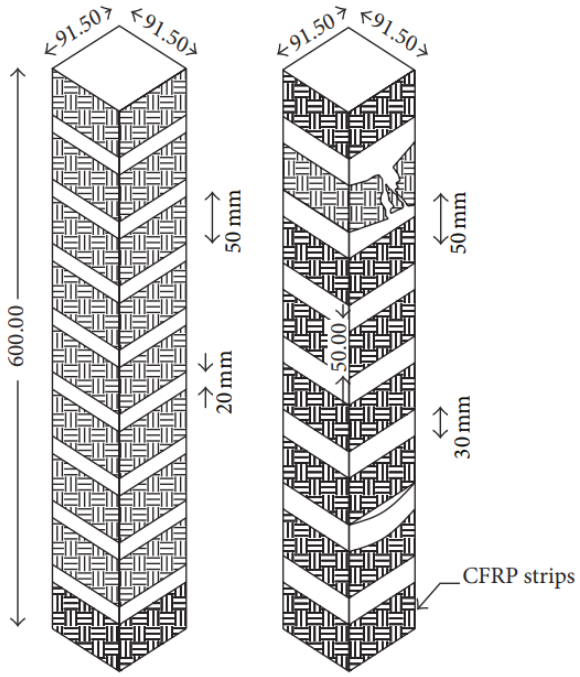

Figure 2.2 CFRP wrapping scheme (Sundarraja et al., 2014)

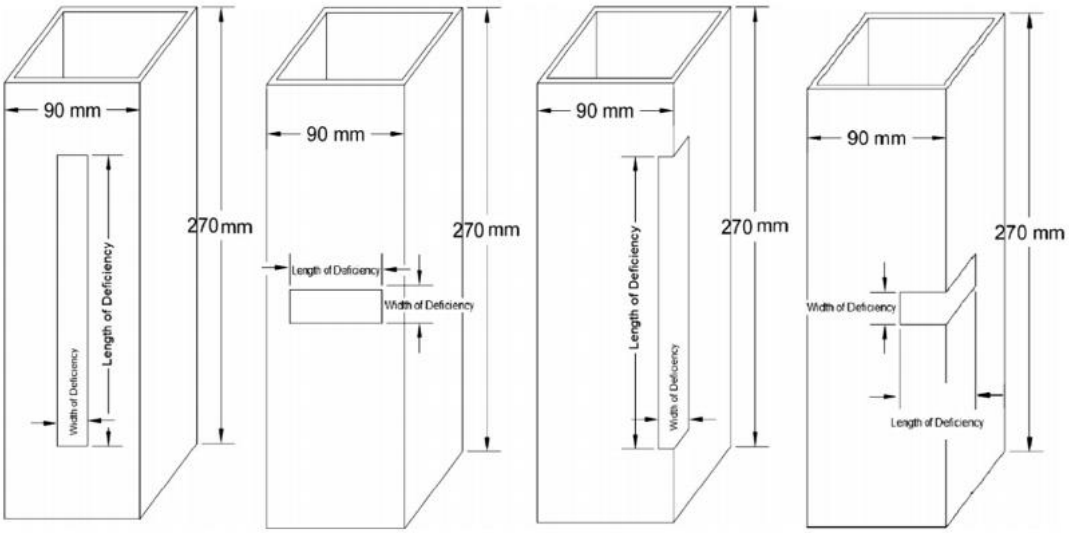

Figure 2.3 Deficiency patterns on specimens (Ghaemdoust et al., 2016)

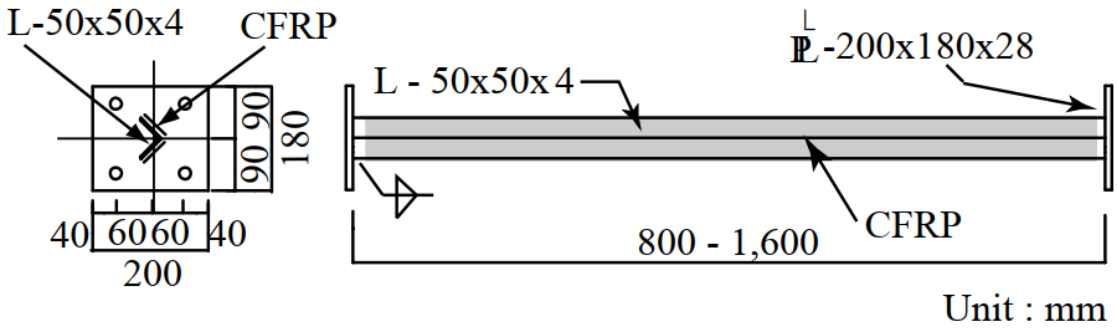

(a) test specimen

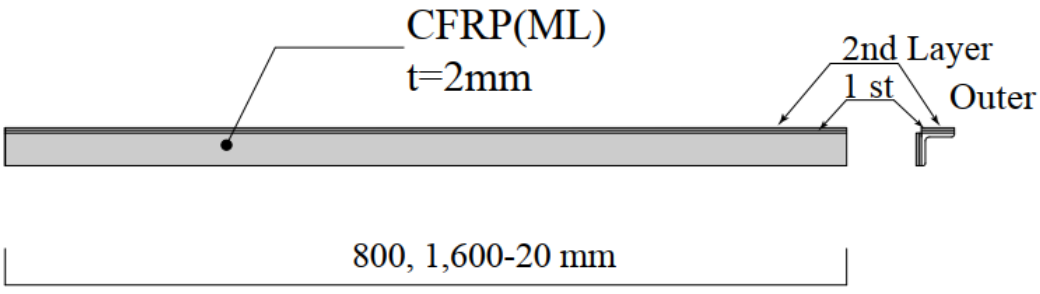

(b) strengthening scheme

Figure 2.4 Angle steel strengthened with bonded CFRP (Tamai et al., 2012)

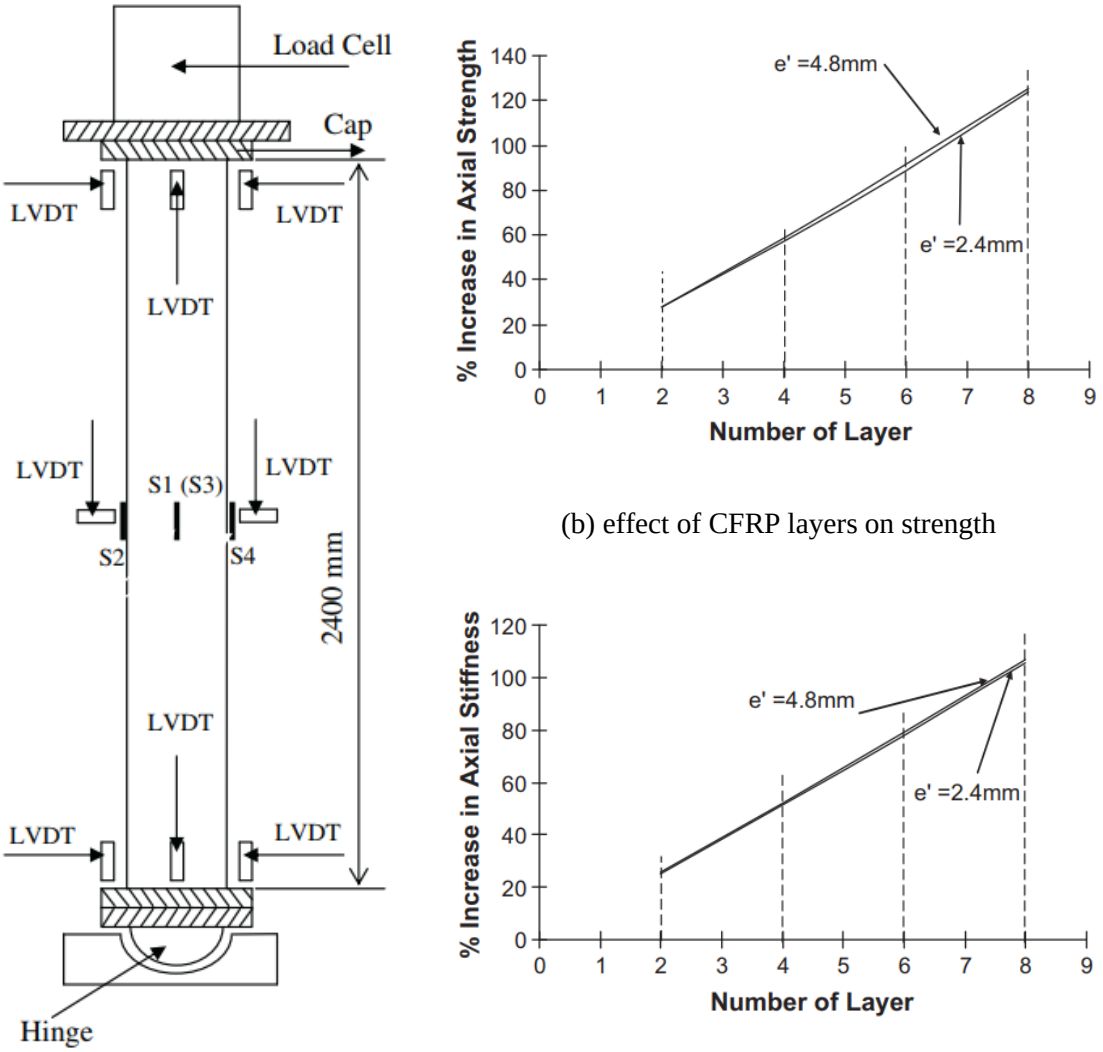

(a) test setup

(b) effect of CFRP layers on strength

(c) effect of CFRP layers on axial stiffness

Figure 2.5 Compression test of circular tubular steel brace (Gao et al., 2013)

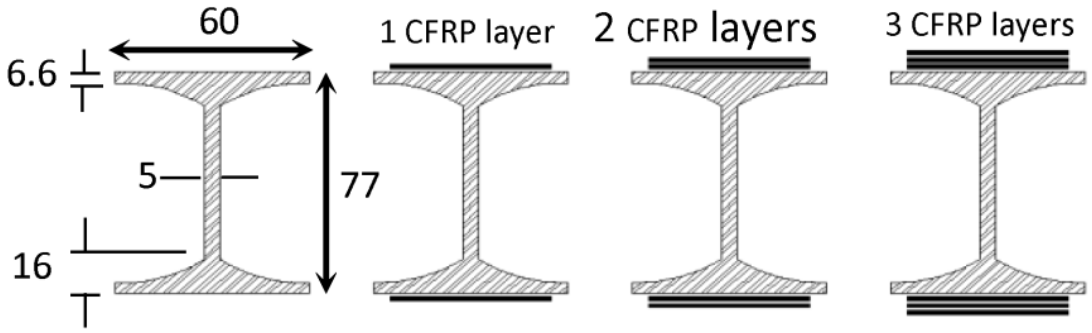

Figure 2.6 Specimen cross-section configurations – unit in mm (Ritchie et al., 2015)

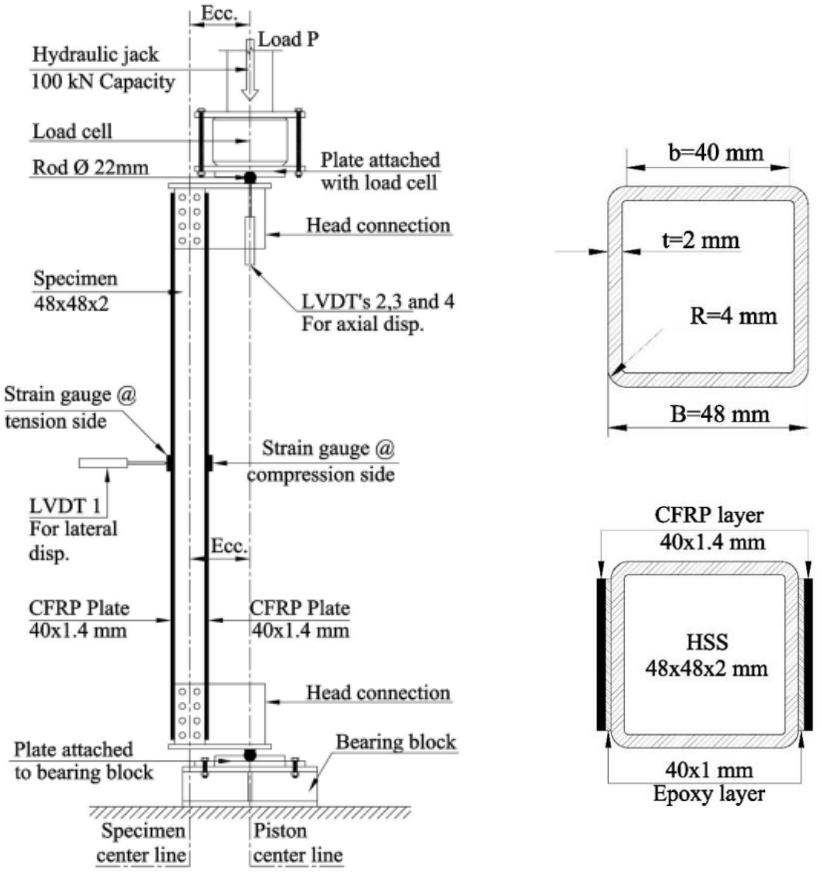

(a) eccentric loading test setup (b) strengthening scheme

Figure 2.7 Test setup and strengthening scheme (Sayed-ahmed et al., 2018)

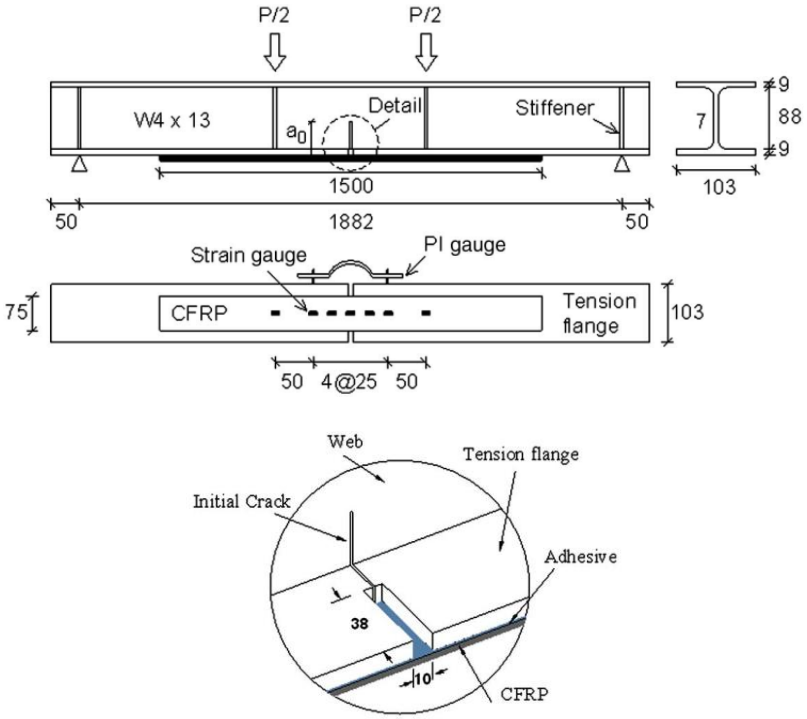

Figure 2.8 Damaged condition and test setup (Hmidan et al., 2011)

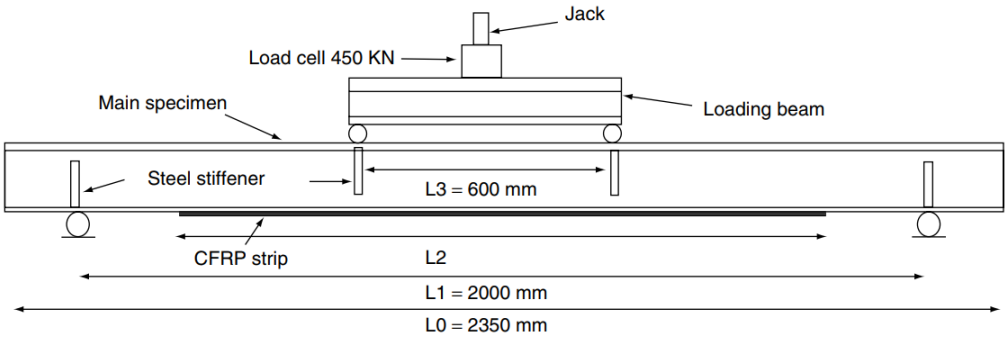

Figure 2.9 CFRP strip position and test setup (Narmashiri et al., 2012)

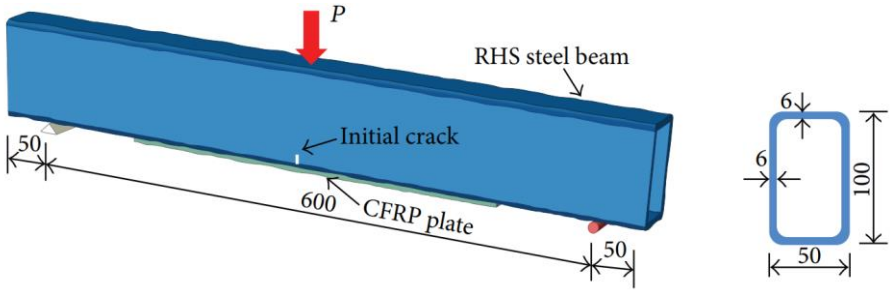

Figure 2.10 Bending test for CFRP-strengthened RHS steel beams (Chen et al., 2015)

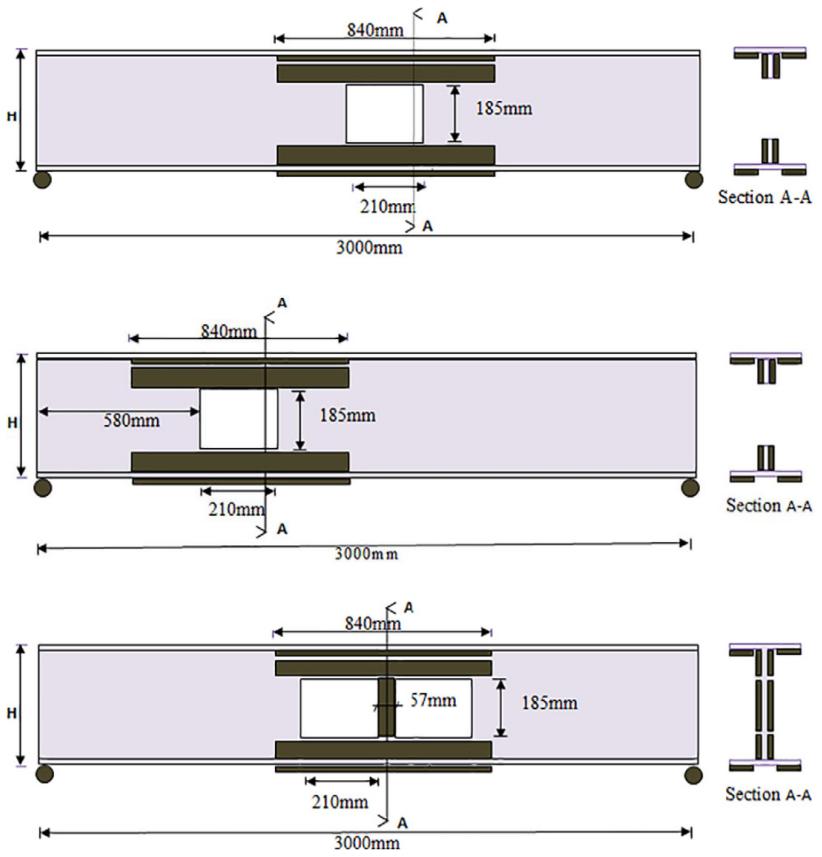

Figure 2.11 Location of web openings (Altaee et al., 2017)

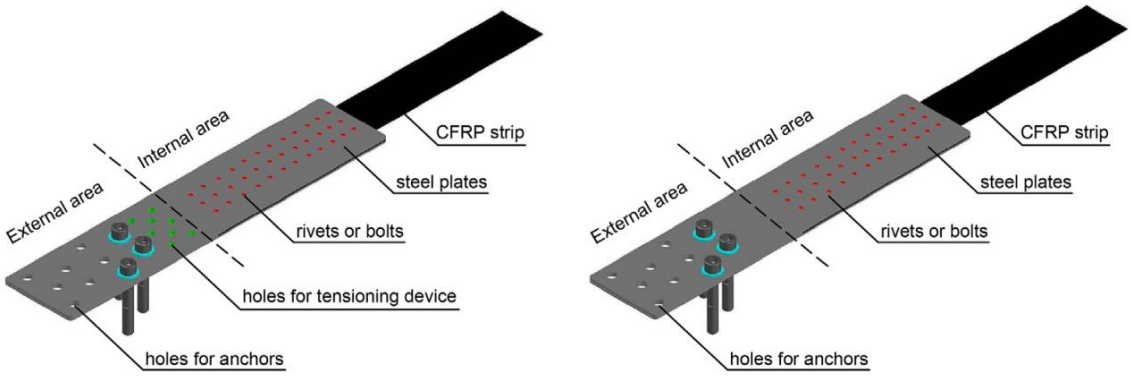

active strengthening passive strengthening

Figure 2.12 Active and passive CFRP strengthening (Siwowski and Siwowska, 2018)

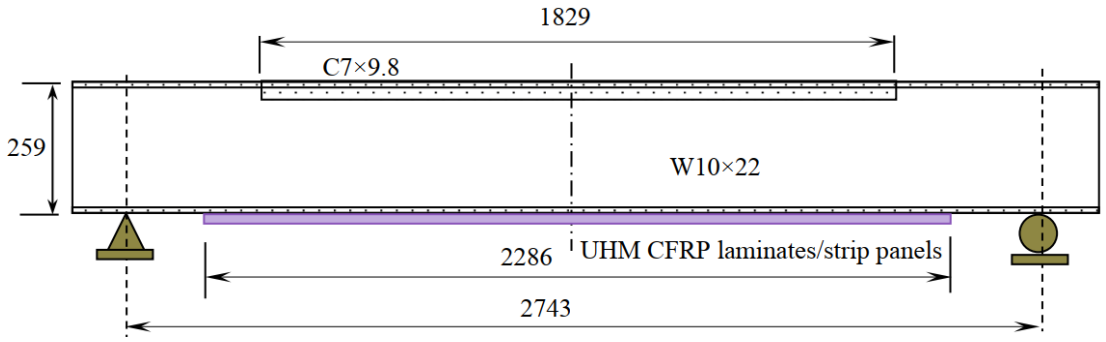

Figure 2.13 Steel beam with UHM CFRP strengthening (Peiris and Harik, 2021)

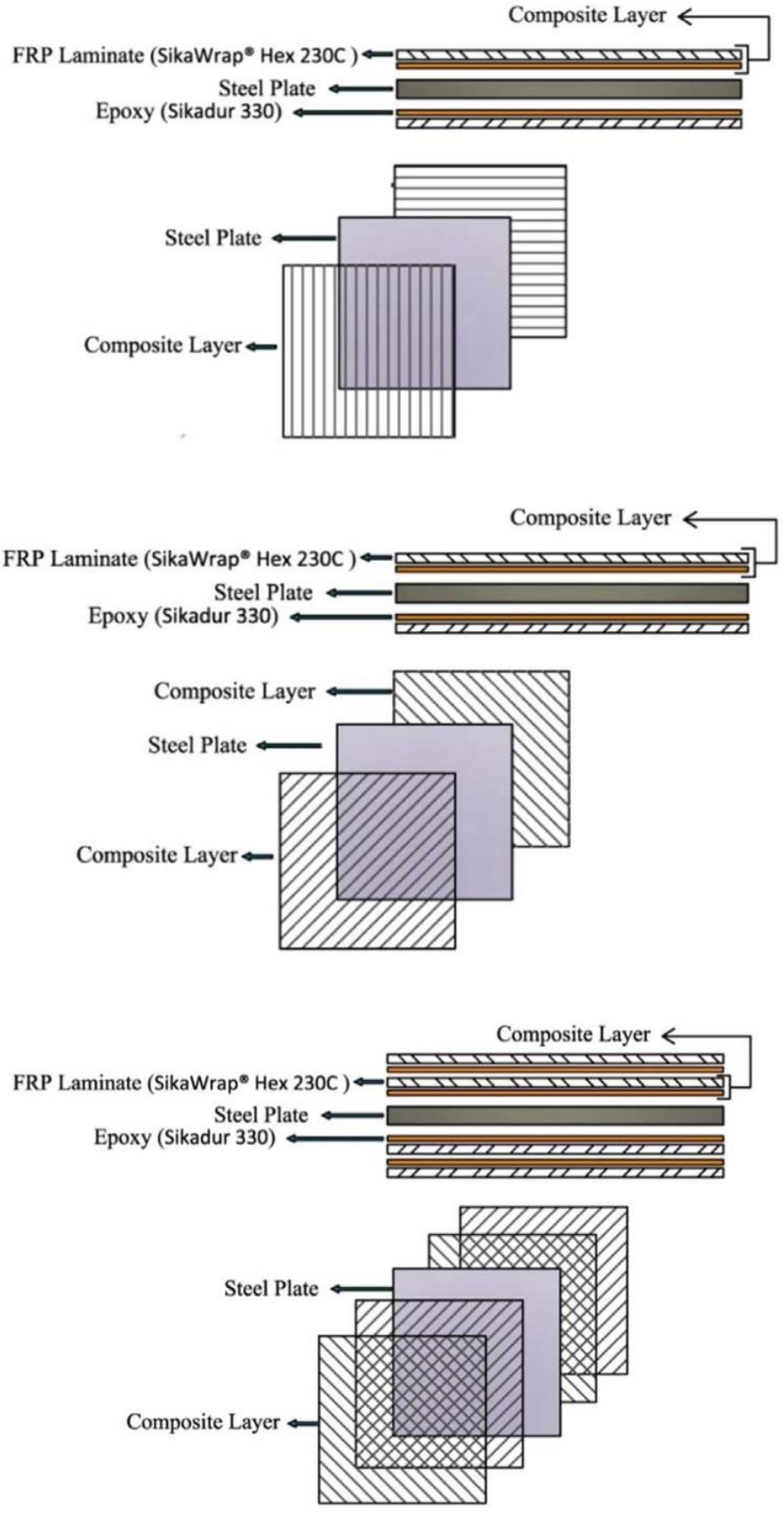

Figure 2.14 Shear strengthening scheme of steel plate using CFRP (Poul et al., 2016)

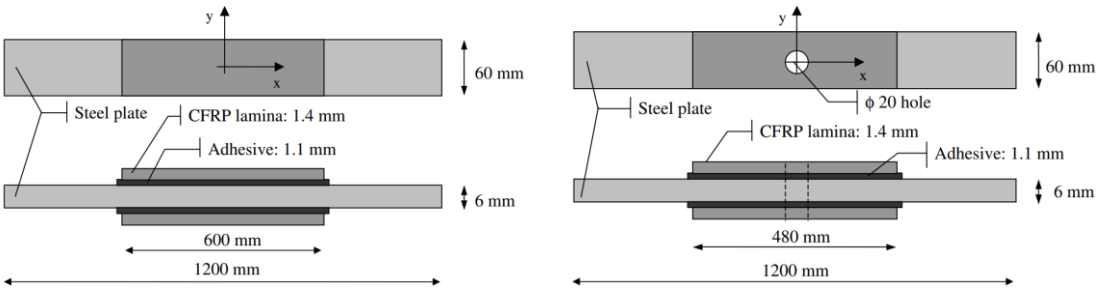

Double side reinforcement

Drilled double side reinforcement

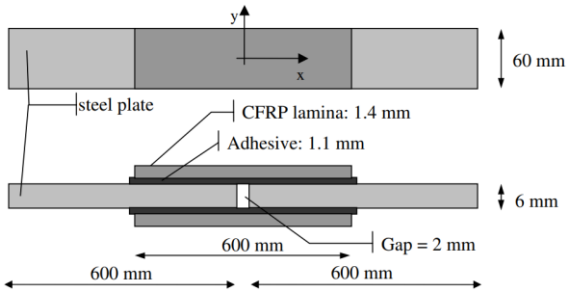

Double lap joints reinforcement

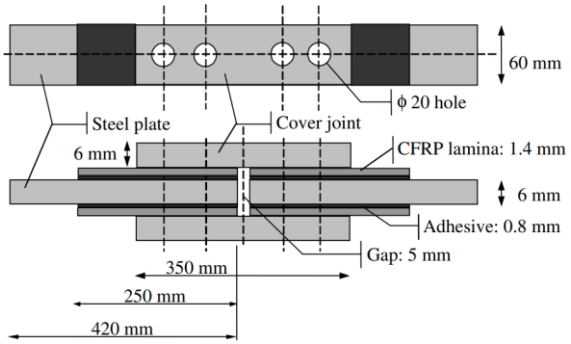

Bolted joints reinforcement

Figure 2.15 Type and configuration of specimens (Colombi and Poggi, 2006)

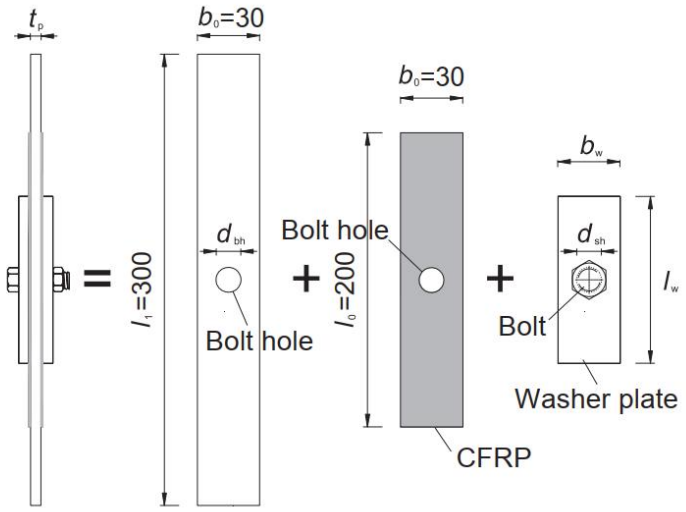

Figure 2.16 Configuration of tensile test specimens (Wang et al., 2016)

CHAPTER 3
AXIAL COMPRESSION STEEL BARS

3.1 Introduction

This chapter demonstrates the ability of the proposed unbonded CFRP strengthening method in enhancing buckling performance of steel bars. Steel bar is selected for initial investigation purpose. Mechanical model for the CFRP requirements is firstly developed at the beginning of this chapter. Several specimen parameters are then determined for the experimental program. Analytical models are also developed to represent the specimens as well as determining strength recommendation of the strengthened members. In addition to experimental study, finite element analysis is performed to validate the analytical model developed and to identify the influential experimental parameters. The experiences gained from this chapter become reference for next experiments on unbonded CFRP strengthened angle steel which are discussed in next chapters.

3.2 Analytical Modeling for Restrainer

3.2.1 Stiffness

Figure 3.1 shows the structural model used in this study. The member is partially stiffened with CFRP lamination at the middle of span and it is assumed to be fully straight without initial deflection caused by e.g. initial core buckling, imperfection of restrainer, and/or eccentricity of axial loads. The unbonded condition is represented by space (δ_0) between steel and stiffener (CFRP). Both ends of the member are considered free for boundary conditions.

Considering the model in Figures 3.1a and 3.1b, when the compressive load P is increasingly applied to the member, the load then introduces bending moment at the end of restrainer $M_1 = P\delta_1$ and bending moment at the middle of member $M_2 = \{P(\delta_0+\delta_1+\delta_2) - (Q/2)(L_2/2)\}$ (see Figure 3.1c). In order to allow hinge occurs at non-restrained portion of the steel, the moment in this part should be larger than that in the restrained portion ($M_1 > M_2$). Therefore,

$$P\left(\delta_0 + \delta_2\right) < \frac{1}{4}QL_2 \qquad \ldots (1)$$

where δ_1 and δ_2 are deformation of steel and CFRP, respectively; Q is lateral thrust generated when a contact occurs between the steel core and stiffener; and L_2 is length of stiffener. The value of Q is determined by considering the stiffener as a simple beam in three point bending state:

$$Q = \frac{\delta_2}{\frac{{L_2}^3}{48E_{CF}I_{CF}} + \frac{L_2}{2G_{CF}A_{CF}}} \quad \ldots (2)$$

where E_{CF} and G_{CF} are elastic modulus and shear modulus of CFRP, respectively; I_{CF} and A_{CF} are moment inertia and sectional area of CFRP, respectively. Shear modulus and elastic modulus of CFRP are determined by using Eq. (3) and (4) (Hiroshi, 2009) since the CFRP adopted in this study is a cross-ply laminate. The term of h in these equations denotes thickness of CFRP lamination, and the A_{ij} are components of extensional stiffness matrix determined from Classical Lamination Theory (CLT) (Jones, 1999).

$$E_{CF} = \frac{1}{h}\frac{A_{11}A_{22}A_{66} + 2A_{12}A_{26}A_{16} - A_{22}A_{16}^2 - A_{12}^2A_{66} - A_{11}A_{26}^2}{A_{22}A_{66} - A_{26}^2} \quad \ldots (3)$$

$$G_{CF} = \frac{1}{h}\frac{A_{11}A_{22}A_{66} + 2A_{12}A_{26}A_{16} - A_{22}A_{16}^2 - A_{12}^2A_{66} - A_{11}A_{26}^2}{A_{11}A_{22} - A_{12}^2} \quad \ldots (4)$$

Substituting Eq. (2) into (1) and simplifying the resulting equation, the stiffness requirement of stiffener can then be expressed as in Eq. (5).

$$P\left(1 + \frac{\delta_0}{\delta_2}\right) < \left(\frac{{L_2}^2}{12E_{CF}I_{CF}} + \frac{2}{G_{CF}A_{CF}}\right)^{-1} \quad \ldots (5)$$

Assuming that compressive load P is equal to design load for axial compression steel member specified by AIJ recommendation (AIJ 2005), the designed CFRP should satisfy the expression in Eq. (6) where f_{sc} and A_S are allowable compressive stress (for sustained load) and sectional area of steel member, respectively.

$$1.5 f_{sc}A_S\left(1 + \frac{\delta_0}{\delta_2}\right) < \left(\frac{{L_2}^2}{12E_{CF}I_{CF}} + \frac{2}{G_{CF}A_{CF}}\right)^{-1} \quad \ldots (6)$$

3.2.2 Strength

As in Figure 3.1c, due to force Q, the failure of CFRP should be considered either in shear or bending. The design capacity of CFRP used for restrainer ($Q_{CF,ul}$) should be the minimum value from these two cases as in Eq. (7). The ultimate design force in case of shear failure ($Q_{CF,ul,LT}$) depends on its shear cross-sectional area and it is determined by Eq. (8) where $f_{CF,ul,LT}$ is shear strength of CFRP. Meanwhile, the ultimate force for bending $Q_{CF,ul,L}$ is determined by Eq. (9) where Z_{CF} and $f_{CF,ul,L}$ are section modulus and axial strength of CFRP, respectively.

$$Q_{CF,ul} = \min\ (Q_{CF,ul,L}, Q_{CF,ul,LT}) \quad \ldots (7)$$

$$Q_{CF,ul,LT} = f_{CF,ul,LT}\ A_{CF} \quad \ldots (8)$$

$$Q_{CF,ul,L} = \frac{4 f_{CF,ul,L}\ Z_{CF}}{L_2} \quad \ldots (9)$$

Substituting Eq. (7) into Eqs. (1) and (2) and then combining these two resulting equations, the out-of-plane deformation capacity of CFRP ($\delta_{2,CF,ul}$) is introduced and the expression for strength requirement of CFRP is then proposed as in Eq. (10).

$$1.5 f_{sc} A_S \left(\delta_0 + \delta_{2,CF,ul}\right) < \frac{1}{4} Q_{CF,ul} L_2 \quad \ldots (10)$$

3.2.3 Circumferential strength

As shown in Figure 3.1d, the member need to be able to resist the force $Q/2$ acting on that location where the plastic hinge emerge in order to avoid failure on the edge of stiffener. Since the member is consisted of two components (CFRP and steel), only a part of the force is then assumed and considered to be supported by CFRP. The portion of the force for CFRP Q_{CF} will depend on thickness of this material (t_{CF}) as a forming part of the outer diameter of the member's cross-section and be calculated as $Q_{CF} = \{(Q/2) \times (0.5D/t_{CF})\}$. The value of $Q/2$ in this expression should be substituted by $Q_{CF,ul}$ which is determined from Eq. (7) since this step constitutes inseparable process from previous design stages (stiffness and strength). In addition to this, it is also assumed that the area of CFRP for bearing force Q_{CF} is only in range of 90^o of the cross-section and along half of outer diameter ($0.5D$) in longitudinal direction of the member. This assumption will let to form a triangular shape (red-color, as shown in Figure 3.2) and thus produce an assumed equivalent internal pressure on CFRP due to

Q_{CF}. By involving all assumptions above, CFRP is designed to be appropriate in circumferential strength ($f_{CF,ul,T}$) by following Eq. (11).

$$f_{CF,ul,T} > \frac{Q_{CF,ul}}{\frac{1}{2}\times\frac{\pi D}{4}\times\frac{D}{2}}\times\frac{0.5D}{t_{CF}} = \frac{8Q_{CF,ul}}{\pi t_{CF} D} \quad \ldots (11)$$

3.3 Experimental program

3.3.1 General Description of the Test Specimens

This experimental program consisted of compressive testing eight specimens under concentric loading. The specimens are divided into two main groups based on slenderness ratio, namely 70 and 95. These two slenderness ratios are below the critical limit (Λ) of 101.39 specified by the code (AIJ 2005) for long member. Each group has one bare steel serving as control unstrengthened specimen (denoted by "NS" in specimen name). The length of CFRP is designed to be 260 and 340 mm for specimens in Group 1 (slenderness ratio = 70) and 360 and 460 mm for specimens in Group 2 (slenderness ratio = 95). The number of carbon fiber (CF) layers is also varied to be 26, 27, 28, and 30 plies. The CFRP is positioned at the middle of span of all strengthened specimens. Table 3.1 summarizes details of the specimens used in this study where the first column shows the specimen ID. The outline of tested specimen is shown in Figure 3.3.

3.3.2 Material Properties

Round steel bar Grade G3101 SS400 (JIS Standard) is used in this experiment. The steel bar is 32 mm in diameter. Yield stress, modulus of elasticity, elongation, and also ultimate strength of the steel are directly obtained from manufacturer. Table 3.2 shows the material properties and specifications of steel bar used in this study.

The steel bar is strengthened by using commercially available bi-directional high strength cloth carbon fiber ([0/90^o] fiber orientation angle) (Figure 3.4). The carbon fiber is produced in Japan by Toray Industries, Inc. and termed as BT70-20. Shaped like sheet, this material is easy to handle as well as impregnate resin. The properties of this material are also obtained from manufacturer as shown in Table 3.3.

The epoxy resin E205 produced by Konishi Co.,Ltd. (Osaka, Japan) is adopted to form the CFRP laminates covering the steel bar. However, it is not intended to be used to bond CFRP laminates onto steel surface since these two materials will be separated

by a peel ply. This epoxy resin is ultra-low viscosity, high strength, and excellent durability. Based on manufacturer technical data sheet, the properties of this material are shown in Table 3.4.

3.3.3 Specimen Preparation

All strengthened specimens in this study are prepared by applying unbonded CFRP wrapping, where the CFRP is not adhesively patched onto steel surface. The CFRP is fabricated by an established process, Vacuum-assisted Resin Transfer Molding (VaRTM) (Uddin et al., 2004; Abusera et al., 2019; and Yalcinkaya et al., 2017) which has been widely used in aeronautical, marine, and automotive applications. VaRTM is preferred since it has many advantages, such as faster workmanship, easy to mold for any kind of shapes, environmentally safer, and ideal for producing large structures. VaRTM also creates a final product of laminates that are high fiber content and more stable in mechanical characteristics (consistent in quality). As result, significant cost reduction and savings in time, material and labor can be achieved (Uddin et al., 2004). And then, the most important for currently experimental program is that, VaRTM process is able to yields much thinner laminates and thus a zero clearance between CFRP and steel for stable behavior of the strengthened members.

The preparation of specimens is begun with cutting the steel bar into the designated length (Figure 3.5a). Both ends of the cut steel are deliberately formed like a knife blade to achieve free end rotation during compression test. After the surface of steel is cleaned using acetone to remove any remaining dust particles, the steel bar is then directly covered by a layer of peel ply to ensure there is no bond between steel and CFRP laminates (unbonded strengthening). The peel ply is applied without preceded by any steel surface treatments, such as sand blasting, hand grinding, grit blasting, etc. The carbon fiber sheets that have been cut into the required length are then wrapped around the bar following the peel ply until reaching the designated number of laminations. The fiber sheets are installed to steel bar so that 0^o fiber orientation angle is in longitudinal direction of the steel bar while the 90^o is in transverse direction. Afterwards, another peel ply, infusion mesh (resin media), infusion spiral tube, a bagging film (with firmly gum tape connection), and PVC hose (for resin feed line) are installed sequentially before conducting resin impregnation by way of suction using a vacuum pump (Figure 3.5b). The ultimate pressure of the pump utilized is 6.7×10^{-1} Pa (ULVAC Model GLD-202BB). Once the vacuuming process is complete, the specimens are then cured for a

minimum of one week before being tested (Figure 3.5c). The detail of molding cross section is shown in Figure 3.6.

3.3.4 Test Setup and Instrumentation

All cured and control specimens are monotonically tested in a 2000 kN Maekawa compression testing machine, shown in Figure 3.7. A load cell built-in within the testing machine is used to measure the applied load. The load is applied at a constant rate and is continued up to buckling of each specimen. Slightly concave bearings are used at both end of specimen to ensure the specimen remains on its position during the test. Six transducers are mounted around the specimens to measure a reliable out-of-plane displacement. The longitudinal strain in specimens is measured by strain gauges attached directly to the CFRP and steel in several locations. Each location possessives strain gauges in two opposite sides of specimens (see Figure 3.8).

3.4 Experimental Results

Maximum axial loads (P_{max}) of the members and strengthening effect (η) of application of unbonded CFRP in all strengthened specimens obtained from the experimental investigation are presented in Table 3.5. The strengthening effect is calculated by comparing the difference of maximum axial load of members (with and without CFRP strengthening) and the maximum load of appropriate control specimen (NS56BL or NS76BL). The table also lists the maximum loads in normalized form by the yield capacity of the steel bar. It is clearly shown in Table 3.5 that all members fail before yielding of steel, and unbonded CFRP gives positive strengthening effect. The highest increase of maximum load is attained in member BL76F46 which is 49.9% of strengthening effect, while the lowest increase is found in BL56F26-2 with only 6.3% strengthening effect. Other than that, variation in increasing load capacity of members can also be confirmed. A comparison is made by ignoring the difference of the number of carbon fiber layer used which is very small. The first two strengthened members in Group 1 (BL56F26-1 and BL56F26-2) have a same CFRP strengthening length (260 mm), but these two members have a quite large difference in strengthening effect that is more than two times. The same case is also found for the next two specimens in this group (BL56F34-1 and BL56F34-2). With CFRP strengthening length of 340 mm, these two members have nearly two times difference in CFRP strengthening effect.

Generally comparing members with shorter and longer CFRP strengthening length, the increase of axial load capacity tends to occur as increasing length of CFRP.

As in Group 1 (buckling length 560 mm), the members with CFRP strengthening length 340 mm have larger load capacity (even though not significant) compared to members with 260 mm CFRP strengthening length. The same case is also performed by two members in Group 2 (buckling length 760 mm). However, something different appears when comparing members in these two Groups. The larger CFRP strengthening length members (BL76F46 and BL76F36) possessive axial load capacity almost similar or even smaller than that of all strengthened members in Group 1 (relatively shorter in CFRP length). This indicates that the member's axial load capacity is strongly governed by length of remaining steel part (CFRP unstrengthen ed part of steel) as long as CFRP is designed to satisfy strength and stiffness requirements.

Figures 3.9a and 3.9b present the relationships between the applied axial load and the resulting mid-height lateral displacement of the tested members. A very small lateral displacement occurs before reaching maximum load. But, after maximum load, flexural buckling causes excessive lateral deflection and it continues occurring for given loads.

Figures 3.10 and 3.11 present the modes of failure for the tested members in Group 1 and 2 respectively; and its summary is showed in Table 3.5. A failure due to the classical global buckling of the both-end-pinned column is experienced by control unstrengthened specimens in both groups, as shown in Figures 3.10a and 3.11a. Compared with control specimens, the deformed shape of all CFRP-strengthened specimens is quite different. A change in curvature appears on steel at the edge of CFRP. This can be viewed as a result of change in stiffness of the members between unstrengthened and strengthened part of the steel bar. However, it is confirmed that there is no failure encountered in CFRP material during the test. Figures 3.10(b-c) and 3.11(b-c) show the failure mode of the tested CFRP strengthened members having slenderness ratio of 70 and 95, respectively.

The load versus longitudinal strain responses at the edge of CFRP and at mid-height of the members for all strengthened specimens is shown in Figures 3.12 and 3.13, respectively. Due to the existence of unbonded material (peel ply) covering the steel bar prior to CFRP, which separates these two materials, the axial force acting on the steel should not be transferred to the CFRP. The normal stress in the CFRP laminates must be zero until buckling occurs. However, thoroughly strains examination on the surface of CFRP reveals that the CFRP is not completely free from sustaining axial load. It is found that the strains at both sides of CFRP are under compression

before the ultimate load is reached. But, after buckling, the strains on one side revert to tension while another side develops higher compressive strains.

Comparing with elastic strain value theoretically calculated by assuming all member components are steel, the CFRP is also indicated to behave as a fully composite with the steel bar. However, this only happens until up to about early half stage of loading as quite clearly shown in Figure 3.13, where the CFRP strain curves coincide with the curve of theoretical elastic strain (fully composite). Beyond this stage, the strain value on CFRP tends to remain constant or does not change much until buckling occurs, although slightly different behavior in specimen BL76F36 is also confirmed (Figure 3.12e). In specimen BL56F26-2 and BL56F34-2, the compressive strains of CFRP around 0.55×10^{-3} and 0.65×10^{-3} are respectively observed at mid-height of the members shortly before buckling. These values are 4.36% and 5.16% of the ultimate tensile strain of carbon fiber used. Furthermore, a slightly higher strain of 5.55% can then be obtained in both specimen BL56F26-1 and BL56F34-1; and the highest, not less than 6.75% of the ultimate tensile strain of the carbon fiber, is found to be experienced by CFRP laminates in all specimens in Group 2 (BL76F36 and BL76F46).

3.5 Strength Evaluation Procedure

In this section, a method for determining allowable compressive stress for CFRP strengthened members is introduced by using equivalent slenderness ratios. The slenderness ratios are obtained based on the value of critical stress (Euler stress) of two structural models. The first model considers that there is no bond at all between CFRP and steel (completely unbonded), so that the axial compressive load is only supported by steel and no stress transfer between these two materials until buckling occurs. The stress value of this model will be the minimum; therefore, it is then appointed to be a lower limit (Low). Next, the second structural model assumes that CFRP material behaves as a composite with steel bar. The axial load is not only carried by steel but also CFRP. Stress transfer perfectly occurs between these two materials. The process of stress calculation for this model is conducted by converting CFRP into steel with a certain moment of inertia (I_{eq}). Therefore, this model will be more like a stepped column and provide the maximum value of stress, so it becomes an upper limit (Up).

Figure 3.14 shows step by step in determining equivalent slenderness ratios of the CFRP strengthened members for obtaining recommended allowable compressive stress.

As on the picture, an unstrengthened member with a certain slenderness ratio (λ) has an Euler stress value (point A). Due to the presence of CFRP laminates, Euler stress then increases to point B, as shown in Figure 3.14a. By placing this increased stress value on the Euler curve (point C), an equivalent slenderness ratio (λ_{eq}) can be obtained by using the equation of elastic critical buckling stress (Figure 3.14b). Afterwards, allowable compressive stress is then determined based on provisions used (Figure 3.14c).

Two structural models used in this study, as previously mentioned, are shown in Figure 3.15. It is modeled as a half structure for each because of symmetrical. Lengths of unstrengthened and strengthened part, in these both half structure models, are denoted by L_1 and L_2 respectively. In model 2 (M2), where CFRP behaves as a composite with steel, the member is divided into two steel elements with different stiffness (Figure 3.15b). Element 2, that is a combination of steel bar and CFRP converted steel, has a higher stiffness (EI_T) than that of element 1 (EI). Unlike model 2, the member in model 1 (M1) is divided into three elements including CFRP for element 3 (Figure 3.15a). The CFRP sustains bending moment independently and it will not bend as long as its flexural stiffness is higher than moment acting on steel. By applying all boundary conditions, the elastic stiffness matrix (K_E) and geometric matrix (K_G) for M1 and M2 are established as in Eq. (12) to Eq. (15).

Setting up the determinant of stiffness matrix for each model to zero, $|K_E + K_G| = 0$, gives the critical buckling load for each of them. The Euler stress is then calculated for section area of steel bar A_S. The value of Euler stress, corresponding equivalent slenderness ratios, and the allowable compressive stress recommended for all CFRP strengthened members are then presented in Table 3.6. Furthermore, the maximum stresses obtained from experimental investigation are plotted in Figure 3.16 together with allowable stress curve of three established provisions.

$$K_{E.M1} = \begin{bmatrix} 12k_1 & 6k_1L_1 & -12k_1 & 6k_1L_1 & 0 \\ 6k_1L_1 & 4k_1L_1^2 & -6k_1L_1 & 2k_1L_1^2 & 0 \\ -12k_1 & -6k_1L_1 & 12k_1+12k_2+12k_{CF} & -6k_1L_1+6k_2L_2 & 6k_{CF}L_2 \\ 6k_1L_1 & 2k_1L_1^2 & -6k_1L_1+6k_2L_2 & 4k_1L_1^2+4k_2L_2^2 & 0 \\ 0 & 0 & 6k_{CF}L_2 & 0 & 4k_{CF}L_2^2 \end{bmatrix} \quad \ldots(12)$$

$$K_{E.M2}=\begin{bmatrix} 12k_1 & 6k_1L_1 & -12k_1 & 6k_1L_1 \\ 6k_1L_1 & 4k_1L_1^{\,2} & -6k_1L_1 & 2k_1L_1^{\,2} \\ -12k_1 & -6k_1L_1 & 12k_1+12k_T & -6k_1L_1+6k_TL_2 \\ 6k_1L_1 & 2k_1L_1^{\,2} & -6k_1L_1+6k_TL_2 & 4k_1L_1^{\,2}+4k_TL_2^{\,2} \end{bmatrix} \quad \ldots(13)$$

$$K_{G.M1}=-P\begin{bmatrix} \frac{6}{5L_1} & \frac{1}{10} & \frac{-6}{5L_1} & \frac{1}{10} & 0 \\ \frac{1}{10} & \frac{2}{15}L_1 & \frac{-1}{10} & \frac{-1}{30}L_1 & 0 \\ \frac{-6}{5L_1} & \frac{-1}{10} & \frac{6}{5L_1}+\frac{6}{5L_2} & 0 & 0 \\ \frac{1}{10} & \frac{-1}{30}L_1 & 0 & \frac{2}{15}L_1+\frac{2}{15}L_2 & 0 \\ 0 & 0 & 0 & 0 & 0 \end{bmatrix} \quad \ldots(14)$$

$$K_{G.M2}=-P\begin{bmatrix} \frac{6}{5L_1} & \frac{1}{10} & \frac{-6}{5L_1} & \frac{1}{10} \\ \frac{1}{10} & \frac{2}{15}L_1 & \frac{-1}{10} & \frac{-1}{30}L_1 \\ \frac{-6}{5L_1} & \frac{-1}{10} & \frac{6}{5L_1}+\frac{6}{5L_2} & 0 \\ \frac{1}{10} & \frac{-1}{30}L_1 & 0 & \frac{2}{15}L_1+\frac{2}{15}L_2 \end{bmatrix} \quad \ldots(15)$$

where :

$$k_1=\frac{EI}{L_1^{\,3}} \quad \ldots(16)$$

$$k_2=\frac{EI}{L_2^{\,3}} \quad \ldots(17)$$

$$k_{CF}=\frac{E_{CF}I_{CF}}{L_2^{\,3}} \quad \ldots(18)$$

$$k_T=\frac{EI_T}{L_2^{\,3}} \quad \ldots(19)$$

$$I_T=I+\left(\frac{E_{CF}}{E}\right)I_{CF} \quad \ldots(20)$$

As can be seen in Figure 3.16, experimental maximum stress of all strengthened members are plotted for the lower to upper limit of recommended allowable compressive stress corresponded to equivalent slenderness ratio. For making clear the process, specimen BL76F46 is chosen for illustration. Once compressive testing is conducted to the member without application of CFRP laminates, it gives actual maximum stress of 192.7 MPa (control specimen), as shown in point A in Figure 3.16. But this value increases to be 288.5 Mpa (point B), exceeding the member's Euler buckling stress of 224.2 MPa, when CFRP is applied for covering the steel bar. For this case, it will be still wasteful to recommend an equivalent member (with smaller equivalent slenderness ratio) which has Euler stress smaller than that maximum stress (288.5 MPa). Moreover, it will be unsafe to recommend a member with a much smaller slenderness ratio so that the allowable compressive stress exceeds the actual maximum stress. Therefore, this value is then plotted within the range of lower and upper limit of allowable compressive stress recommended (point C) which is obtained from equivalent slenderness ratio method described in Figure 3.14.

Based on Table 3.6 and Figure 3.16, it is clear that maximum stress of all CFRP strengthened members obtained from experiment lies between recommended allowable compressive stress and Euler buckling stress for both lower and upper limit. It is verified by three different provisions: AIJ 2005, CAN/CSA S16-09, and ANSI/AISC 360-16. One interesting to note is that the maximum stress of member BL76F36 is very close to the recommended allowable compressive stress of ANSI/AISC 360-16 for upper limit, which is only 5.21 MPa (2.2%) different. The lower stress of this specimen is thought to be caused by higher imperfection (even though it is not measured in this study). It is proven by its load-lateral displacement response in Figure 3.9b which is curved from beginning. Nevertheless, the maximum stress of member BL76F36 is still within the range of its recommended allowable stresses.

3.6 Finite Element Simulations

3.6.1 Description of Model

A three-dimensional (3D) finite element model is developed to predict the behavior of the pinned-ends axial compression steel members partially strengthened with unbonded CFRP laminates. The results obtained from finite element analysis are compared with experimental work for verification purposes. After correctness of the proposed model is verified, a numerical parametric study is conducted for varied

unbonded CFRP strengthening schemes. A commercial finite element (FE) package, LUSAS Version 14.7, is used for this implementation. The matrix of experimental specimens to be verified and designation for the finite element models used in the current study are shown in Table 3.7. The suffix "FE" is utilized in labeling the finite element models to distinguish them from the experimental specimens.

Two symmetrical planes have been identified for along and across the geometric model. This condition allows the finite element model in the current study to be developed in one quarter where the specimen is reduced to only half the width and half the length, respectively. This is an effort that is intended to get the advantage of symmetric properties of specimens in terms of geometry, material properties, loading, and also boundary conditions. Moreover, building a quarter model of the structure can also reduce the total number of elements and thus shorten the computational time significantly. Figure 3.17 shows the geometrical features of the quarter FE model developed.

3.6.2 Meshing and Elements

Modeling the finite element model involves creating two parts: steel and CFRP. All the parts are modeled by using four-noded solid continuum elements (TH4). The thickness and length of the CFRP are respectively assigned to be same with the measured values obtained from the experiment, as given in Table 3.7. An irregular mesh type with a relatively fine mesh density is applied for both CFRP and steel. However, in order to get good results but also not to spend too much time on analysis, numerical simulations are firstly conducted to the bare steel (control unstrengthened specimen, NS56BL) by applying three different element sizes, as shown in Figure 3.18a. Mesh 1 has 25,195 elements, mesh 2 has 43,245 elements, and mesh 3 has 92,042 elements. Then, an identical result on the load-lateral displacement behavior can be confirmed from Figure 3.18b. As such, mesh 1 with 25,195 elements is used for all analyses in this study, as its computer run-time will be much smaller than that of the other larger mesh elements.

3.6.3 Material Properties

A bilinear stress–strain behavior is used to take into account the non-linearity (plasticity) of steel (see Figure 3.19). Here, the isotropic hardening rule and Von Mises yield criterion are adopted. The yield strength, modulus of elasticity, and ultimate tensile strength are the same as those used in experiment (328 MPa, 205 GPa, and 459

MPa, respectively). The tangent modulus after the initial yielding of steel (E_t) is assumed to be 1% of its elastic modulus (0.01E), and the Poisson's ratio is taken to be equal to 0.3.

In this study, CFRP is considered to act as a stiffener that solely sustains bending about the longitudinal axes due to the buckling of the structure. Besides that, it is made from carbon fiber layers having balanced fiber orientations in the lamination stack-up sequence (Figure 3.20) so that it falls within the category of quasi-isotropic laminates. The many layers of carbon fiber utilized also make it become thicker in size. These conditions make the elastic properties not be defined for each direction separately. The CFRP is assumed to behave as an elastic isotropic material. This is also the reason behind choosing the solid element for its modeling, as previously mentioned. The elastic modulus of CFRP is strongly dependent on the fiber volume contents (V_f) and determined by applying the Classical Laminated Theory once the actual thickness of the CFRP in the strengthened members had been obtained after the demolding process in the experiment. The elastic modulus value (E_{CFRP}) and Poisson's ratios (v) of the CFRP used in the current finite element analysis are given in Table 3.7, which are calculated based on the assumption that the elastic modulus and Poisson's ratio of epoxy resin used are 4 GPa and 0.3, respectively.

3.6.4 Support Conditions

As previously mentioned, the FE model is developed in one-quarter of the specimen because of the double symmetry of the members. To reach this goal in length, the bottom end of the member is kept restrained for translation in the z-direction only. Meanwhile, the other end is kept restrained for the x and y-direction translation to allow loading the application along the length of the member (z-direction). Then, to achieve symmetric width, all the nodes along the longitudinal symmetry plane are kept restrained in the y-direction. This led to allowing out-of-plane buckling deformation occurring in the x-direction only, as desired (see Figure 3.17b).

3.6.5 Unbonded Condition

A very small gap of 1/1000 mm with no-friction slidelines application on both the CFRP and steel surface is defined to establish an unbonded condition between these two materials (Figure 3.17a). This assumption was applied since small strain values are experimentally observed at CFRP before buckling occurred (i.e., below the ultimate loads), and it is relatively constant until reaching the ultimate load.

3.6.6 Load Application and Model Validation

The load is assigned at position 1% of the steel diameter (0.01D) in the positive direction of the x-axis. This assumed value is determined after several numerical trials for representing unmeasured imperfections in all the real specimens in experimental works, which is usually due to the different values in the initial straightness, inevitable misalignment within the test setup, or a combination of these factors. The load P is applied as a distributed pressure over the length of the knife edge (Figure 3.17), which corresponds to the load application in laboratory tests. In analysis, the arc-length control method (Crisfield, 1981) is used to control the load application. This is a better choice for buckling problems, as it prevents instability (divergence) in non-linear iterative processes, even if the slope is zero (or negative) (El-Kholi et al., 2019). A convergence can be achieved for near-limit points because the load level is not constant during increments.

The accuracy of the finite element model is verified by comparing with the experimental results. Table 3.8 shows comparison of load-carrying capacity between FE analysis and the experimental test. Furthermore, Figures 3.21 to 3.23 shows the load versus lateral mid-height deflection response of specimens from the experimental measurements and finite element prediction. It is clear from Table 3.8 and Figures 3.21 to 3.23 that a good agreement between the experimental and numerical results can be confirmed. The difference of load-carrying capacity is confirmed to be less than 10%. The variation of differences is most likely due to the application of the same imperfection for all specimens. For further validation, the failure modes of the FE models are also compared with those obtained from the experiment. The buckled shapes of each model predicted by finite element analysis including strain contours in the longitudinal (z) direction (at 20 mm lateral displacement of mid-height) and the typical failure mode of steel members having strengthening lengths of 260 mm (BL56F26) and 340 mm (BL56F34) are shown in Figures 3.24 to 3.26. It is clear from the figures that control specimen undergoes a change in curvature at middle height and all strengthened specimen experiences it around the edge of the CFRP, which is similar to buckling failure modes observed in the tests. Thus, it is concluded that the proposed FE models are valid and can be reliably used as a numerical tool to predict the axial compression response of steel members strengthened with unbonded CFRP laminates.

3.6.7 Parametric Study

A parametric study is carried out by creating 33 models with the same material properties and cross-sectional dimension of steel as those used in the experimental works. The models are developed based on the stiffening design requirements to investigate the effect of some influential parameters, namely: (1) the number of CFRP layers, (2) the length of the CFRP, (3) the slenderness ratio, and (4) the elastic modulus of the CFRP, on the buckling behavior and ultimate strength of axial compression of a steel member strengthened with fully cross-sectional-jacketed unbonded CFRP.

Excluding the control specimen, the following labeling system was built to facilitate identification of the models. The first number indicates the slenderness ratio of the initial steel member (bare steel, namely 120, 100, and 70), while the second number represents the length of CFRP strengthening (385, 480, and 625). The combination 'number–letter' following these two numbers is used for identifying the number of CFRP layers involved. Then, the last term (E1 and E2) indicates the values of elastic modulus of the CFRP, which correspond to the assumed fiber volume content (50% and 55%) used herein, i.e., 62.63 GPa and 68.72 GPa, respectively. For instance, 120-385-20L-E2 identifies a specimen model that has a slenderness ratio of 120, strengthened with 20 layers of CFRP of 385 mm length, which have an elastic modulus of 68.72 GPa. For control specimens, labeling only uses the word "control" followed by the slenderness ratio—for example, bare steel with a slenderness ratio of 100: "Control-100". It should be noted that the use of 50% and 55% fiber content are based on the experimental findings for the estimation of the lowest and highest value of fiber content in CFRP resulting from the VaRTM molding process.

The results obtained from the finite element simulation, including the maximum loads and lateral displacement at mid-height at maximum loads, are summarized in Table 3.9. The table also presents the percentage increases in maximum loads as well as decreases in lateral displacements at maximum loads over the unstrengthened model. The load versus lateral displacement responses of all specimens are shown in Figure 3.27. Figure 3.28 presents a summary of the parametric study, which shows the effect of each parameter investigated on the percentage increases of compression strength and decreases in lateral displacements at maximum loads.

The effect of the number of CFRP layers on the increase of compressive strength and lateral displacement reduction of members can be seen in Figure 3.28 (a,c, and e) and Figure 3.28 (b, d, and f), respectively. Moreover, it is also demonstrated by all the

graphs in Figure 3.27. It is clear from Figures 3.27 and Figure 3.28 (a, c, and e) that the compressive strength increases along with the increasing number of CFRP layers, but the rate is not linear. The increase in compressive strength tends to be constant when the steel member is strengthened with an increasing number of CFRP layers. For steel with a slenderness ratio of 120, this trend begins when 50 CFRP layers are used. Yet, the trend occurs earlier (smaller number of CFRP layers) as the slenderness ratio decreases (see Figure 3.28c). Comparing with the specimens model with a slenderness ratio of 100, for example, where the strength increase tends to be constant in the use of 40 layers of CFRP, the rate of increase in strength for the specimens model with a slenderness ratio of 70 has flattened in the use of only 20 CFRP layers. In line with the increasing strength, Figure 3.28 (b, d, and f) shows that such a non-linear trend also occurs in the rate of lateral displacement reduction. Based on these conditions, the authors believe that there is a certain number of CFRP layers (optimum layers) where the axial compression strength begins not to increase significantly, and the optimum layers will greatly depend on the dimensional parameters of the steel and the length of the CFRP.

The slenderness ratio also highly affects the compressive strength increase of the members. The strength gain increases as the slenderness ratio is increased. This becomes very clear when a large number of CFRP layers are used. For example, for the use of 10-layer CFRP, the increase in compressive strength for members with slenderness ratios of 70 and 120 are only 6.25% and 11.4%, respectively (5.15% difference). However, when the layers are increased to 80, the strength gains of the members increase to be 13.7% and 68.4%, respectively (54.70% difference). However, as an increasing number of CFRP layers is used, a trend of the constant rate in strength increase can be observed, especially for members with smaller slenderness ratio. Figure 3.28c summarizes the effect of slenderness ratios on the strength increase of members.

The effects of CFRP length on increase of ultimate load and lateral displacement reduction of the members can be seen in Figure 3.27 (a, c, and e), which are then summarized in Figure 3.28 (a and b). It is clear from Figure 3.28a that the compressive strength increases along with the increasing CFRP length. This finding is in line with experimental results. The difference of strength increases also becomes greater as the number of CFRP layers increased. The members with CFRP lengths of 385 mm and 625 mm are examples. Regarding the use of 10-layer CFRP, the strength increases of the members are 11.4% and 17.3% (5.90% difference), respectively. However, when

the layers are increased to 80, the increase in strength changed to 68.4% and 112.7%, respectively (44.30% difference). The increase in lateral displacement reduction also occurs as the CFRP layers increased, but the difference between using smaller and greater number layers of CFRP is not large, as shown in Figure 3.28b (8.44% and 20.40% difference for using 10 and 80 CFRP layers, respectively). All of the above can be understood as results of decreasing the remaining length of the unstrengthened part of the steel while the CFRP are still within the required flexural rigidity for strengthening.

The difference in the elastic modulus of CFRP is closely related to the fiber volume content (V_f) and CFRP thickness. Theoretically, CFRP with a higher fiber volume content will have a lower thickness but higher elastic modulus. Conversely, CFRP with a smaller elastic modulus will have a higher thickness. The elastic modulus and thickness of CFRP will determine its flexural rigidity and contribution effect on strengthening the steel members. Figure 3.28 (e and f) respectively demonstrate the effect of the elastic modulus of the CFRP ($E1$ = 62.63 GPa and $E2$ = 68.72 GPa) on the increase of compressive strength and lateral displacement reduction of steel members. It is confirmed that there is a very small increase in the strength gain and displacement reductions of steel members due to the decrease of CFRP's elastic modulus from 68.72 to 62.63 GPa.

3.6.8 Strength Evaluation

In this section, the method of equivalent slenderness ratio is used for determining recommended allowable stress of the strengthened members. The maximum stresses of all strengthened steel members obtained from finite element analysis are summarized in Table 3.10 and then plotted together with an allowable stress curve as well as Euler curve, as shown in Figure 3.29. The stresses are plotted within the range of the lower and upper limit of its recommended allowable compressive stress. It is clear from Figure 3.29 and Table 3.10 that the stresses lay between the allowable stress curve and Euler buckling curve with a reduction factor calculated to be mostly less than 1. It is indicated that the equivalent slenderness ratio can be used in determining design values of the axial compression steel members that are strengthened with unbonded CFRP laminates.

3.7 Summary and Conclusions

A research program was carried out to investigate the potential of unbonded CFRP for strengthening axial compression steel members against buckling. As for initial investigation, steel bars with slenderness ratio of 70 and 95 (diameter 32 mm) were used. Specimens were strengthened with unbonded CFRP at middle of span. The requirements of CFRP were derived through analytical model for stiffness, strength, and circumferential strength. Based on the investigation results, the followings can be drawn:

1. The proposed unbonded CFRP strengthening could successfully increase load-carrying capacity of the steel bars.
2. It was confirmed that CFRP has no damages and change of buckling curvature appears in steel around the edge of CFRP due to change in stiffness between unstrengthened and strengthened part of the steel bars.
3. The finite element model developed provided good correspond to experimental results so that it can be used for parametric study.
4. The equivalent slenderness ratio method could be used for determining strength recommendation for the unbonded CFRP strengthened steel bars.

Table 3.1 Specimen details

Specimen ID	Buckling length (mm)	Stiffening length (mm)	CFRP thickness (mm)	Number of fiber layer (plies)	Slenderness ratio
Group 1					
NS56BL	560	n/a	n/a	n/a	70
BL56F26-1	560	260	5.30	26	70
BL56F26-2	560	260	5.85	28	70
BL56F34-1	560	340	5.43	27	70
BL56F34-2	560	340	6.02	28	70
Group 2					
NS76BL	760	n/a	n/a	n/a	95
BL76F36	760	360	6.04	30	95
BL76F46	760	460	6.97	30	95

Table 3.2 Properties and specifications of steel bar

Diameter (mm)	Cross section (mm^2)	Moment of inertia (mm^4)	Elastic modulus (MPa)	Yield stress (MPa)	Tensile strength (MPa)	Elongation (%)
32	804.25	51471.85	205000	328	459	33

Table 3.3 Characteristics of carbon fiber

Type	Fiber direction	Sheet thickness (mm)	Fiber weight (gr/m^2)	Density (gr/cm^3)	Elastic modulus (GPa)	Tensile strength (GPa)
BT70-20	0^o	0.056	100	1.8	230	2.9
	90^o	0.056	100	1.8	230	2.9

Table 3.4 Properties of epoxy resin used (curing 7 days at $20\pm1\ ^oC$)

Name	Tensile strength (MPa)	Bending strength (MPa)	Tensile shear strength (MPa)	Compressive strength (GPa)
Epoxy resin E205	>20 *JIS K 7113-1995	>40 *JIS K 7203-1995	>10 *JIS K 6850-1994	>45 *JIS K 7208-1995

*testing reference

Table 3.5 Summary of test results

Specimen ID	Slend. ratio	Max. loads (kN)	P_{max}/P_y	η (%)	Failure mode
Group 1					
NS56BL	70	214	0.81	-	Global buckling (GB)
BL56F26-1	70	249	0.94	+16.4	GB on steel at CFRP end
BL56F26-2	70	228	0.86	+6.3	GB on steel at CFRP end
BL56F34-1	70	250	0.95	+16.8	GB on steel at CFRP end
BL56F34-2	70	234	0.89	+9.0	GB on steel at CFRP end
Group 2					
NS76BL	95	155	0.59	-	Global buckling (GB)
BL76F36	95	183	0.69	+18.3	GB on steel at CFRP end
BL76F46	95	232	0.88	+49.9	GB on steel at CFRP end

Table 3.6 Strength recommendation for the strengthened members

Spec. ID	λ	Max. Stress (MPa)	Euler Buckling Stress (MPa)		λ_{eq} (Low - Up)	Recommended allow. compressive stress (MPa) (Low – Up)		
			Low	Up		AIJ 2005	CAN/CSA S16-09	ANSI/AISC 360-16
BL56F26-1	70	309.6	558.20	608.98	60.20 - 57.64	243.58 - 249.73	243.52 - 250.32	256.49 - 261.80
BL56F26-2		283.5	571.73	629.37	59.49 - 56.70	245.31 - 251.96	245.43 - 252.80	257.98 - 263.72
BL56F34-1		310.8	616.55	674.44	57.29 - 54.77	250.57 - 256.46	251.26 - 257.84	262.53 - 267.59
BL56F34-2		291.0	632.57	697.62	56.56 - 53.85	252.30 - 258.57	253.18 - 260.21	264.01 - 269.41
BL76F36	95	227.5	318.10	352.89	79.75 - 75.72	193.60 - 204.22	192.53 - 202.64	213.03 - 222.29
BL76F46		288.5	355.94	397.55	75.39 - 71.34	205.07 - 215.61	203.46 - 213.94	223.03 - 232.22

Table 3.7 Specimen matrix

Specimens	FE Model	CFRP length (mm)	CFRP thickness (mm)	CFRP layer (plies)	Elastic modulus of CFRP (GPa)	Poisson's ratio of CFRP
NS56BL	NS56BL-FE	-	-	-	-	-
BL56F26-1	BL56F26-1-FE	260	5.30	26	68.72	0.0311
BL56F26-2	BL56F26-2-FE	260	5.85	28	67.49	0.0312
BL56F34-1	BL56F34-1-FE	340	5.43	27	69.94	0.0311
BL56F34-2	BL56F34-2-FE	340	6.02	28	65.06	0.0313

Table 3.8 Comparison between FE analysis and test results

Specimens	FE Model	Ultimate Load (kN)		$P_{exp.}/P_{FE}$
		Exp. ($P_{exp.}$)	FE (P_{FE})	
NS56BL	NS56BL-FE	214	213	1.00
BL56F26-1	BL56F26-1-FE	249	230	1.08
BL56F26-2	BL56F26-2-FE	228	231	0.99
BL56F34-1	BL56F34-1-FE	250	235	1.06
BL56F34-2	BL56F34-2-FE	234	236	0.99

Table 3.9 Parametric study results

FE model	Max. load (kN)	Increase over unstrengthened model (%)	Lateral displacement at max. load (mm)	Decrease over unstrengthened model (%)
Control-120	107.4	-	6.57	-
120-385-10L-E1	119.7	11.4	6.03	8.16
120-385-20L-E1	132.6	23.4	5.69	13.3
120-385-40L-E1	155.5	44.8	3.73	43.2
120-385-50L-E1	164.3	53.0	2.91	55.7
120-385-80L-E1	181.0	68.4	2.05	68.7
120-480-10L-E1	122.6	14.1	5.53	15.8
120-480-20L-E1	140.4	30.7	5.10	22.3
120-480-40L-E1	173.1	61.1	3.35	48.9
120-480-50L-E1	185.4	72.6	2.47	62.3
120-480-80L-E1	204.9	90.7	1.35	79.5
120-625-10L-E1	126.1	17.3	5.48	16.6
120-625-20L-E1	150.0	39.6	4.72	28.1
120-625-40L-E1	200.0	86.2	2.60	60.4
120-625-50L-E1	214.2	99.4	1.70	74.1
120-625-80L-E1	228.5	112.7	0.71	89.1
120-385-10L-E2	119.3	11.0	6.39	2.69
120-385-20L-E2	132.0	22.9	5.19	21.0
120-385-40L-E2	153.9	43.3	4.04	38.5
120-385-50L-E2	162.8	51.6	3.15	52.0
120-385-80L-E2	179.7	67.2	2.16	67.1
Control-100	146.6	-	3.44	-
100-385-10L-E1	164.0	11.9	3.31	3.76
100-385-20L-E1	182.1	24.2	2.68	22.0
100-385-40L-E1	206.2	40.7	1.52	55.8
100-385-50L-E1	212.5	45.0	1.13	67.2
100-385-80L-E1	221.4	51.0	0.82	76.2
Control-70	212.8	-	0.87	-
70-385-10L-E1	226.1	6.25	0.73	16.0
70-385-20L-E1	235.5	10.6	0.60	30.5
70-385-40L-E1	240.4	12.9	0.39	55.0
70-385-50L-E1	241.1	13.3	0.35	59.9
70-385-80L-E1	242.0	13.7	0.25	71.3

Table 3.10 Strength recommendation for the strengthened members

FE Model	Max. stress (MPa)	Euler buckling stress (MPa)		$\lambda_{eq.}$ (Low–Up)	Rec. design strength (MPa) (Low–Up)	σ(rec.)/σ(FEM)	
		Low	Up			Low	Up
120-385-10L-E1	148.8	155.7	160.1	114.0–112.4	135.81–139.12	0.91	0.94
120-385-20L-E1	164.8	173.1	184.1	108.1–104.8	148.39–155.59	0.90	0.94
120-385-40L-E1	193.4	208.2	238.5	98.58–92.10	169.63–184.46	0.88	0.95
120-385-50L-E1	204.3	223.3	264.7	95.19–87.43	177.36–195.26	0.87	0.96
120-385-80L-E1	225.0	254.4	324.2	89.18–79.00	191.22–214.76	0.85	0.95
120-480-10L-E1	152.4	159.2	163.8	112.7–111.1	138.45–141.88	0.91	0.93
120-480-20L-E1	174.6	181.7	194.1	105.5–102.1	154.05–161.72	0.88	0.93
120-480-40L-E1	215.2	230.9	271.2	93.62–86.37	180.97–197.71	0.84	0.92
120-480-50L-E1	230.5	253.5	312.9	89.33–80.41	190.86–211.52	0.83	0.92
120-480-80L-E1	254.8	302.9	420.5	81.73–69.36	208.47–236.64	0.82	0.93
120-625-10L-E1	156.7	164.0	168.0	111.1–109.8	142.01–144.84	0.91	0.92
120-625-20L-E1	186.5	194.3	205.9	102.1–99.13	161.80–168.39	0.87	0.90
120-625-40L-E1	248.7	270.0	318.0	86.56–79.77	197.28–212.99	0.79	0.86
120-625-50L-E1	266.4	309.9	391.3	80.80–71.91	210.62–230.94	0.79	0.87
120-625-80L-E1	284.1	406.9	643.4	70.52–56.08	234.07–264.98	0.82	0.93
120-385-10L-E2	148.3	155.4	159.7	114.1–112.6	135.58–138.84	0.91	0.94
120-385-20L-E2	164.1	172.1	182.7	108.4–105.2	147.71–154.69	0.90	0.94
120-385-40L-E2	191.4	205.6	234.2	99.20–92.95	168.22–182.51	0.88	0.95
120-385-50L-E2	202.5	220.2	259.2	95.85–88.35	175–193.12	0.87	0.95
120-385-80L-E2	223.4	251.3	317.9	89.73–79.78	189.95–212.97	0.85	0.95
100-385-10L-E1	203.9	228.3	234.9	94.14–92.80	179.76–182.86	0.88	0.90
100-385-20L-E1	226.5	259.3	277.0	88.34–85.47	193.15–199.80	0.85	0.88
100-385-40L-E1	256.4	326.0	381.5	78.79–72.83	215.26–228.87	0.84	0.89
100-385-50L-E1	264.3	356.3	436.8	75.36–68.06	223.12–239.53	0.84	0.91
100-385-80L-E1	275.3	421.6	575.4	69.28–59.30	236.83–258.38	0.86	0.94
70-385-10L-E1	281.2	485.0	495.7	64.59–63.89	247.14–248.65	0.88	0.88
70-385-20L-E1	292.8	579.2	611.0	59.10–57.54	258.79–262.00	0.88	0.89
70-385-40L-E1	298.9	823.0	960.8	49.58–45.89	277.61–284.33	0.93	0.95
70-385-50L-E1	299.8	956.2	1198.2	46.00–41.09	284.13–292.49	0.95	0.98
70-385-80L-E1	301.0	1291.4	2083.4	39.58–31.16	294.92–307.08	0.98	1.02

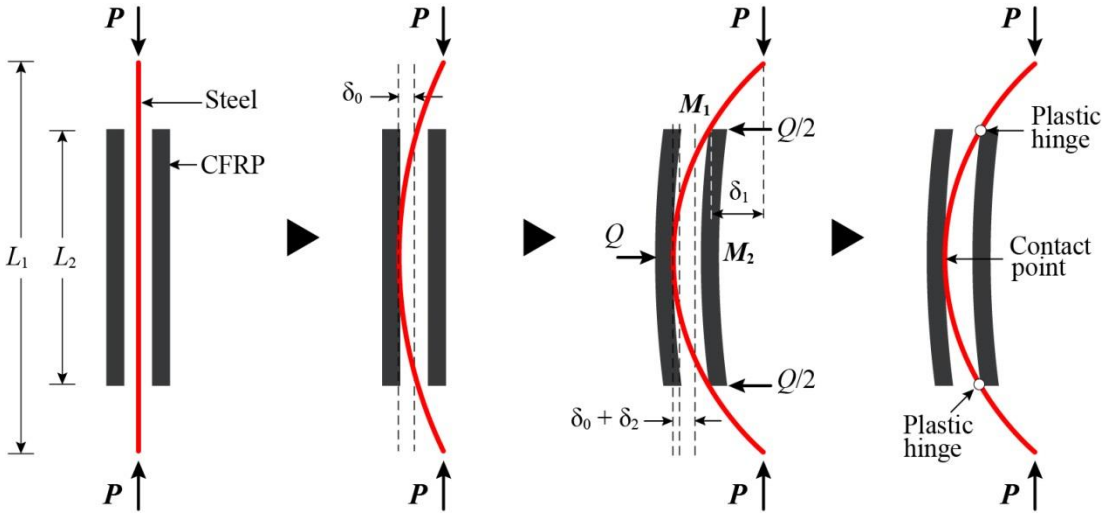

(a) initial position (b) loading condition (c) overall buckling (d) plastic hinge and contact point

Figure 3.1 Developed model for restrainer (CFRP) design

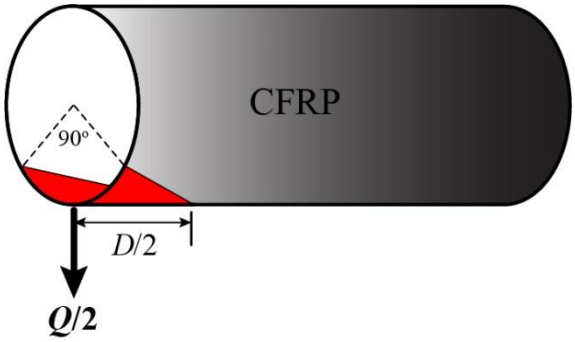

Figure 3.2 Portion of CFRP for bearing load

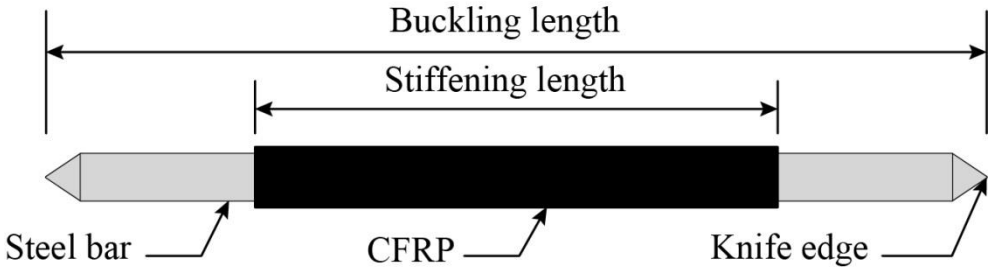

Figure 3.3 Specimen configuration

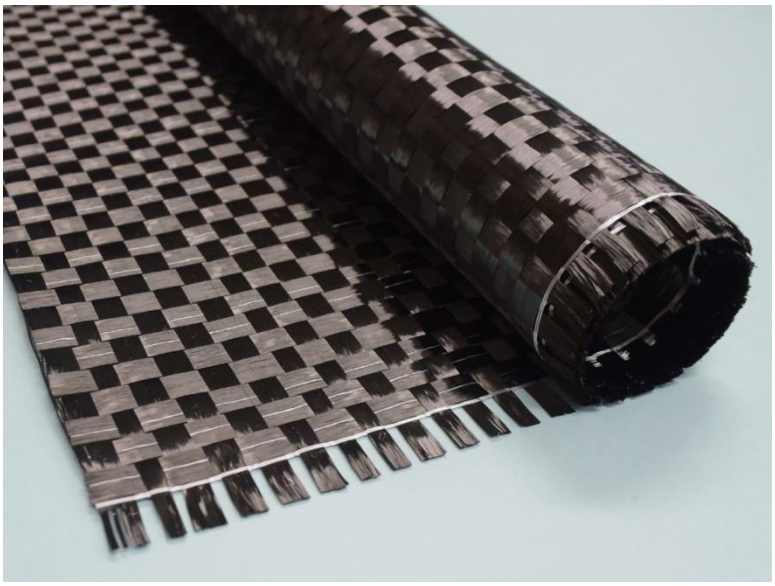

Figure 3.4 Carbon fiber BT70-20

(a) steel before strengthening

(b) molding process

(c) specimen after molding

Figure 3.5 Specimen preparation

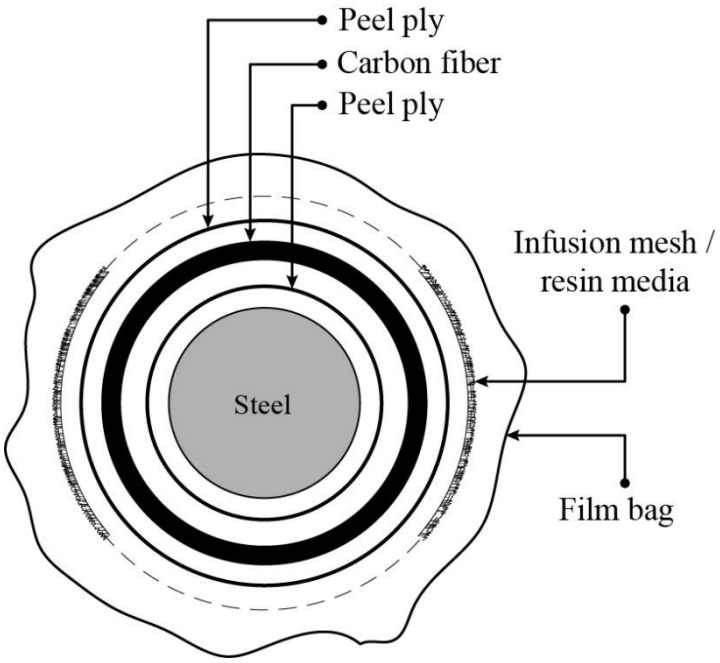

Figure 3.6 Molding cross-section

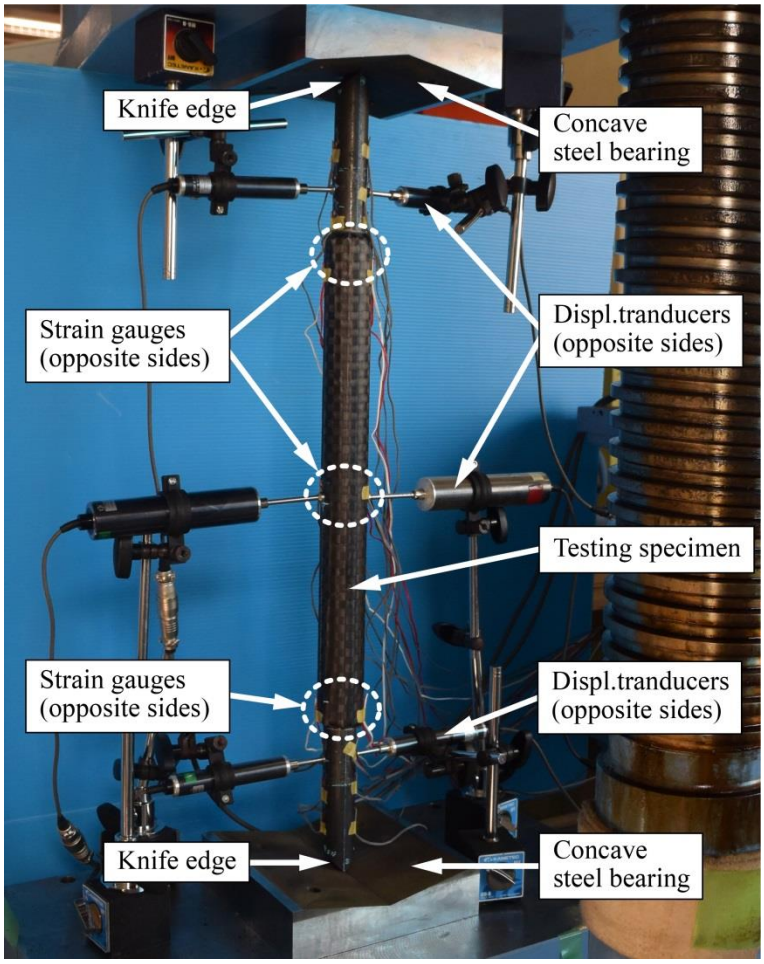

Figure 3.7 Test setup

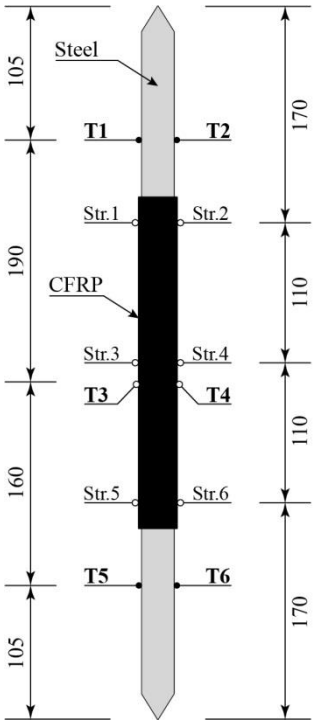

(a) for specimen BL56F26-1 and BL56F26-2

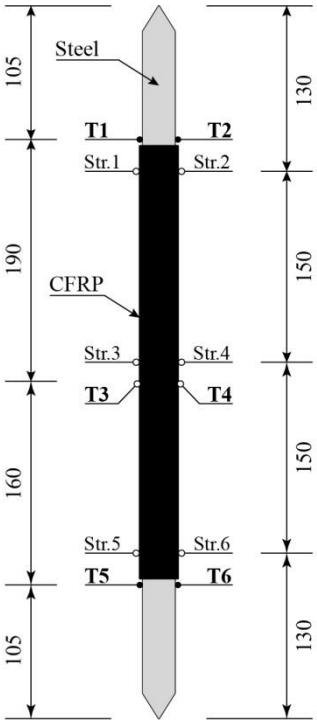

(b) for specimen BL56F34-1 and BL56F34-2

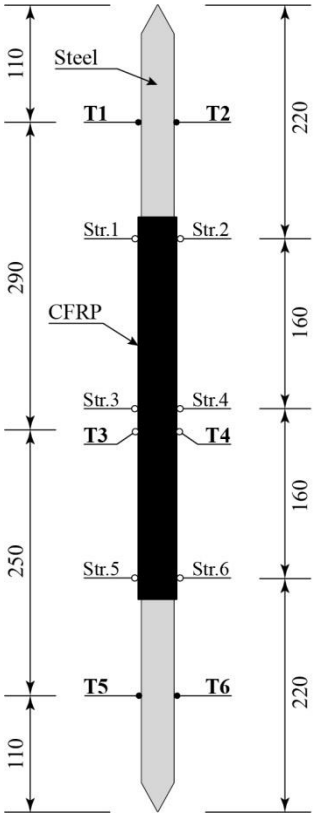

(c) for specimen BL76F36

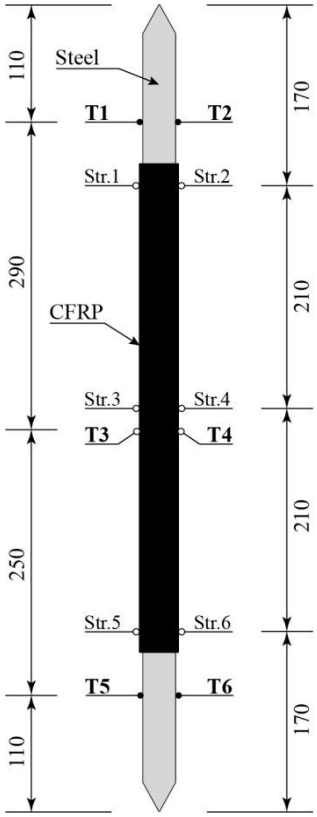

(d) for specimen BL76F46

Figure 3.8 Position of transducers (T1-T6) and strain gauges (Str.1-Str.6)

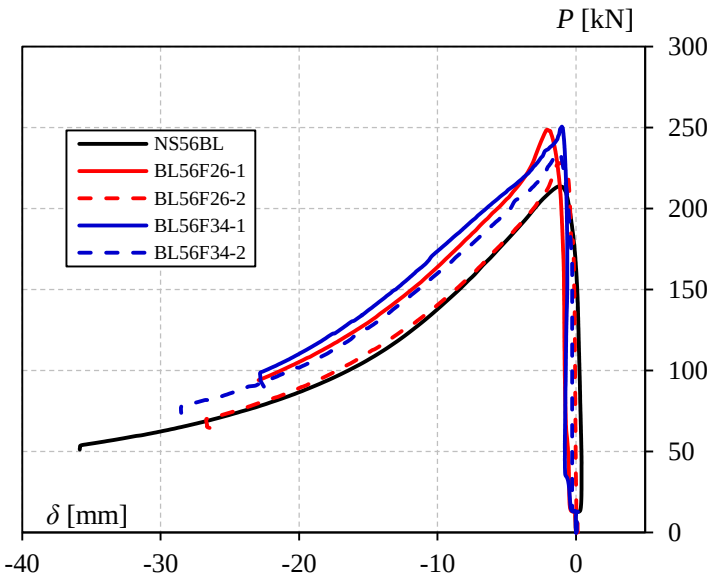

(a) specimens in Group 1

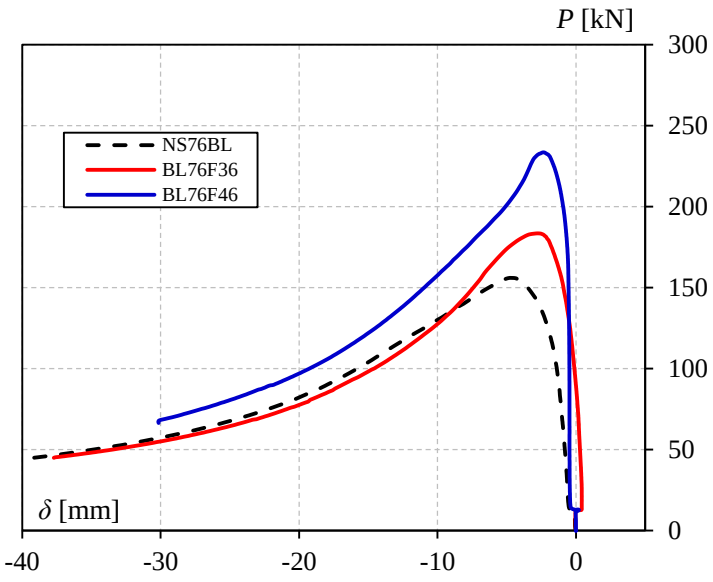

(b) specimens in Group 2

Figure 3.9 Load - lateral midheight displacement response

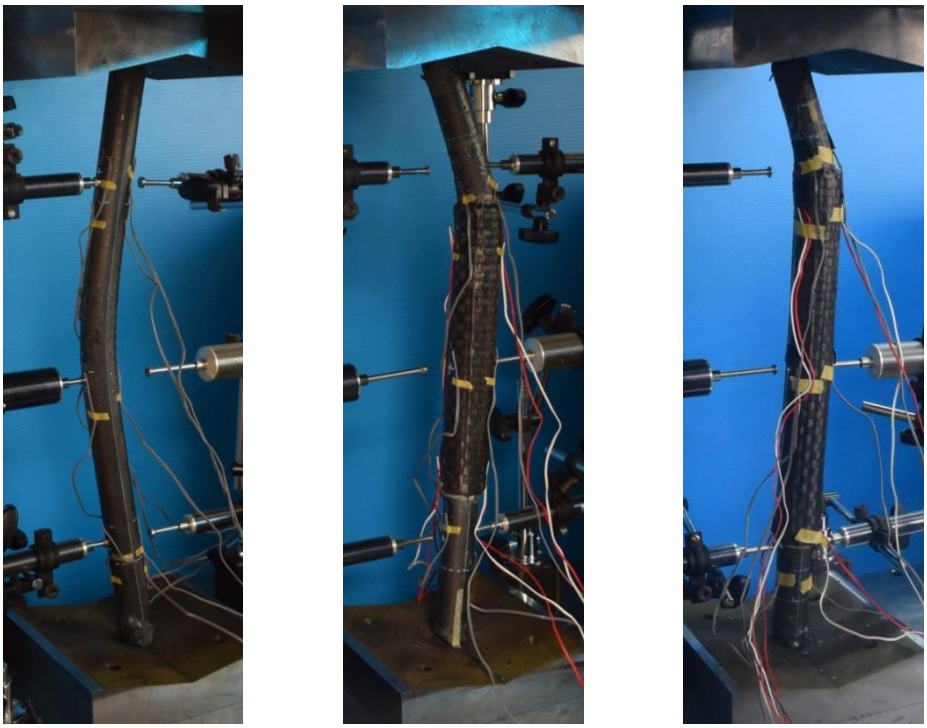

(a) specimen NS56BL (b) typical for specimen BL56F26-1 and BL56F26-2 (c) typical for specimen BL56F34-1 and BL56F34-2

Figure 3.10 Failure modes of specimen in Group 1

(a) specimen NS76BL (b) specimen BL76F36 (c) specimen BL76F46

Figure 3.11 Failure modes of specimen in Group 2

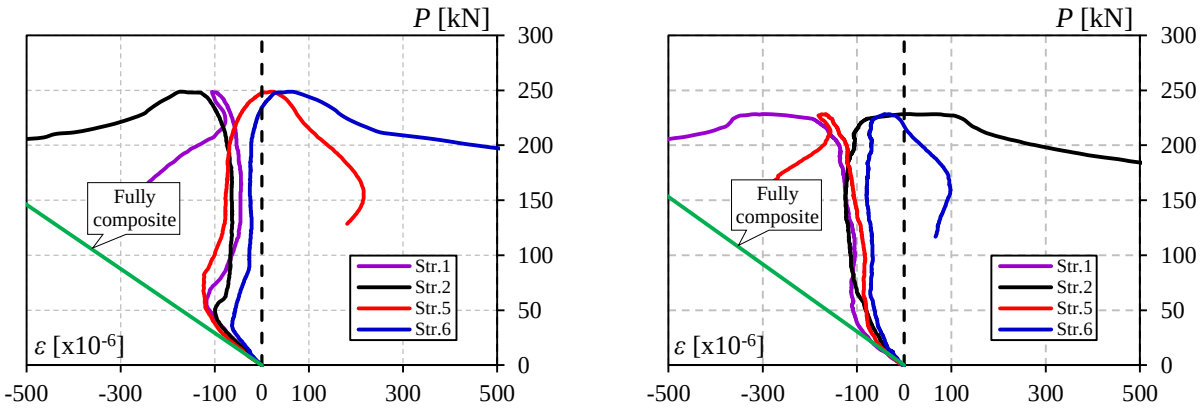

(a) specimen BL56F26-1

(b) specimen BL56F26-2

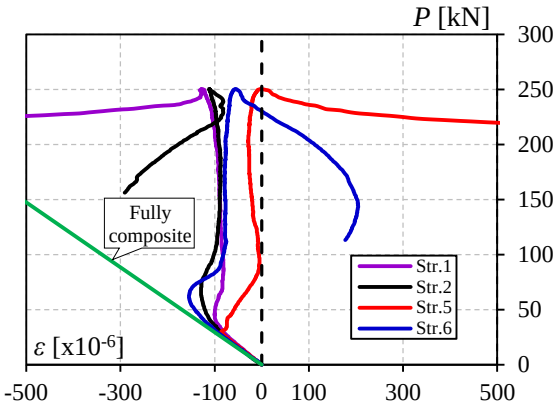

(c) specimen BL56F34-1

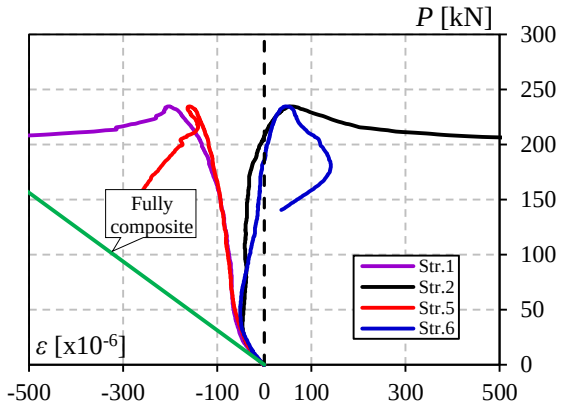

(d) specimen BL56F34-2

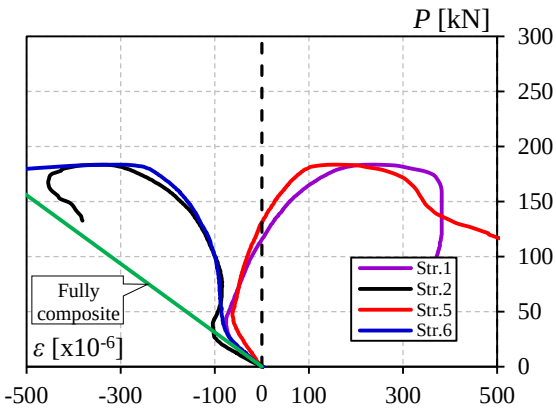

(e) specimen BL76F36

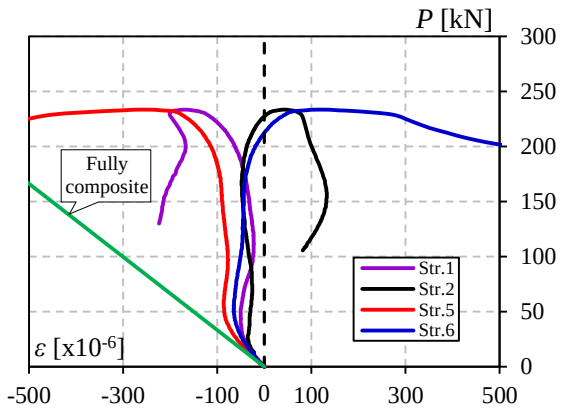

(f) specimen BL76F46

Figure 3.12 Load – longitudinal strain responses at the edge of CFRP

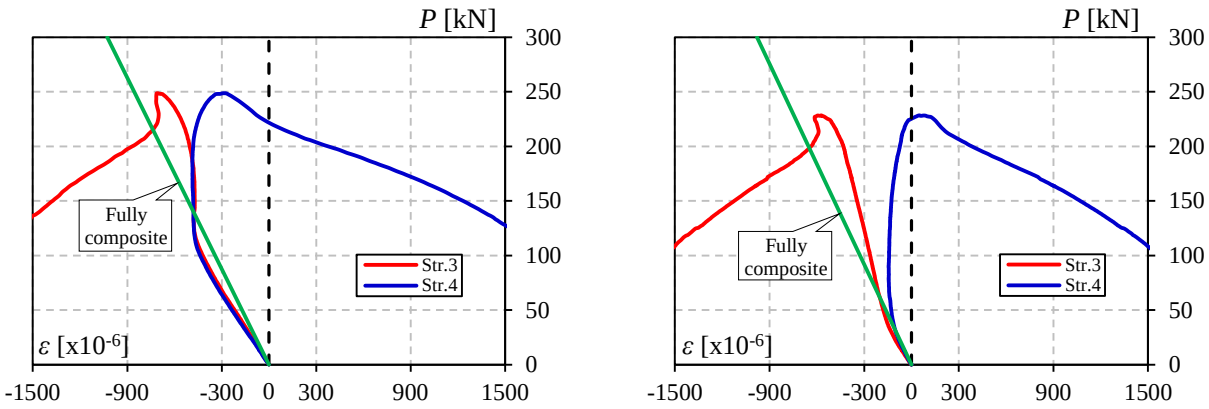

(a) specimen BL56F26-1

(b) specimen BL56F26-2

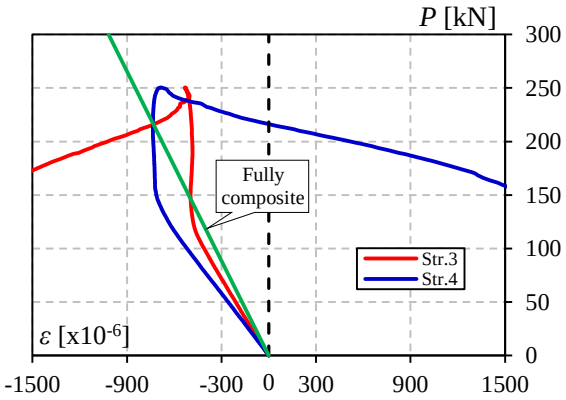

(c) specimen BL56F34-1

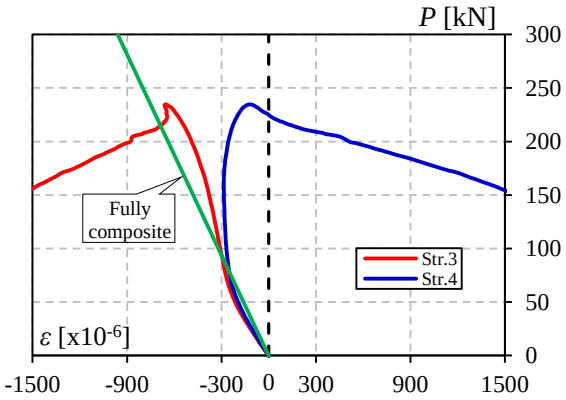

(d) specimen BL56F34-2

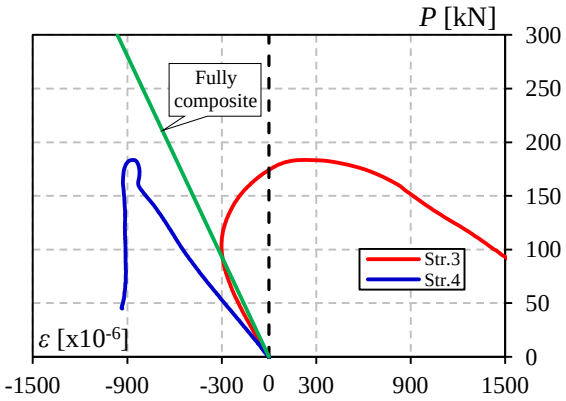

(e) specimen BL76F36

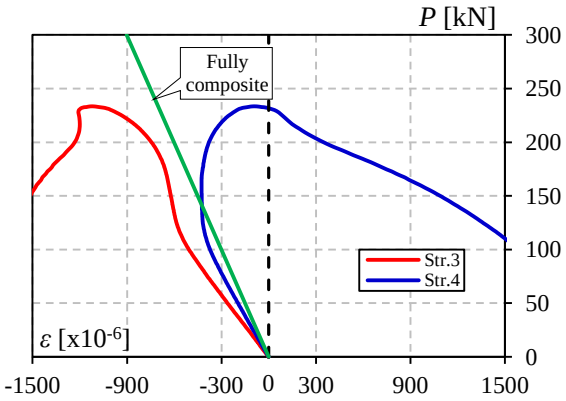

(f) specimen BL76F46

Figure 3.13 Load – longitudinal strain responses at midheight of specimens

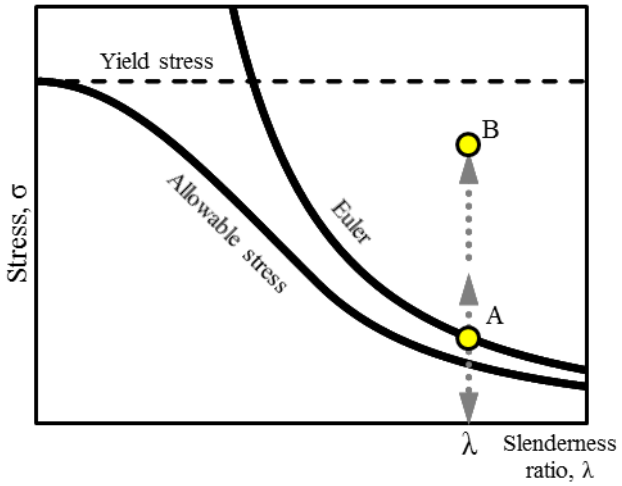

(a) change in Euler stress

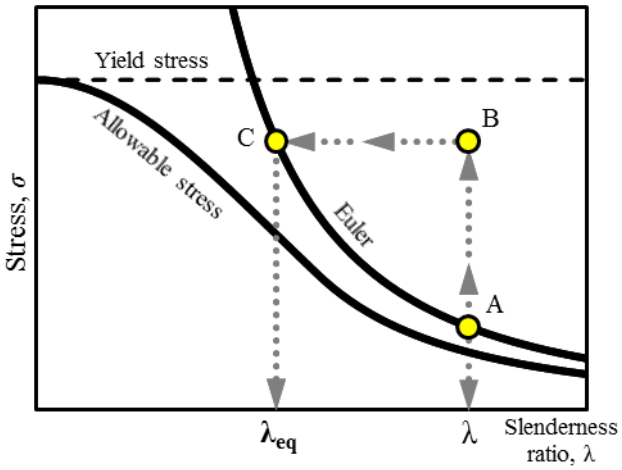

(b) determination Equivalent slenderness ratio

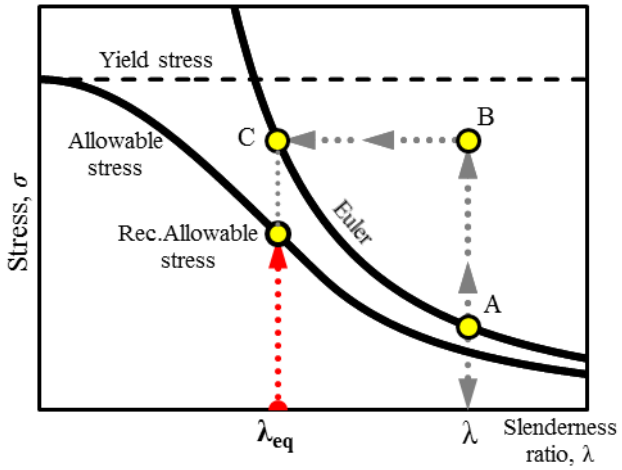

(c) recommended allowable compressive stress

Figure 3.14 Equivalent slenderness ratio for compressive stress design

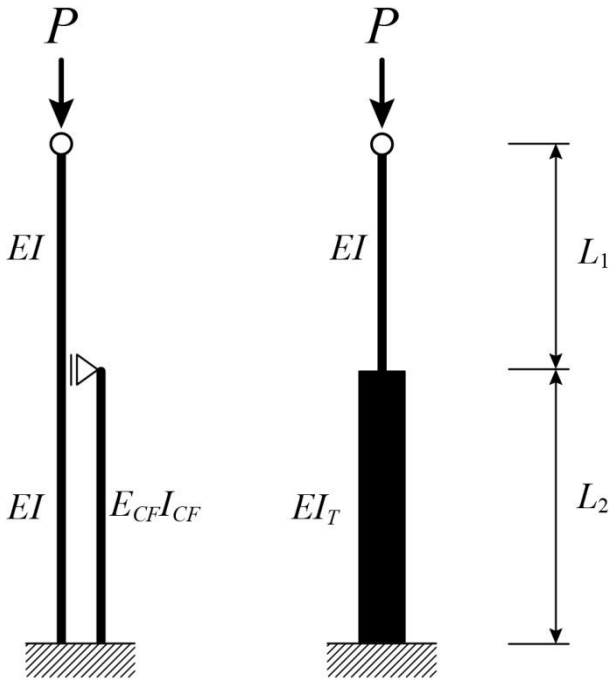

(a) Model 1 (b) Model 2

Figure 3.15 Structural models for strengthened member

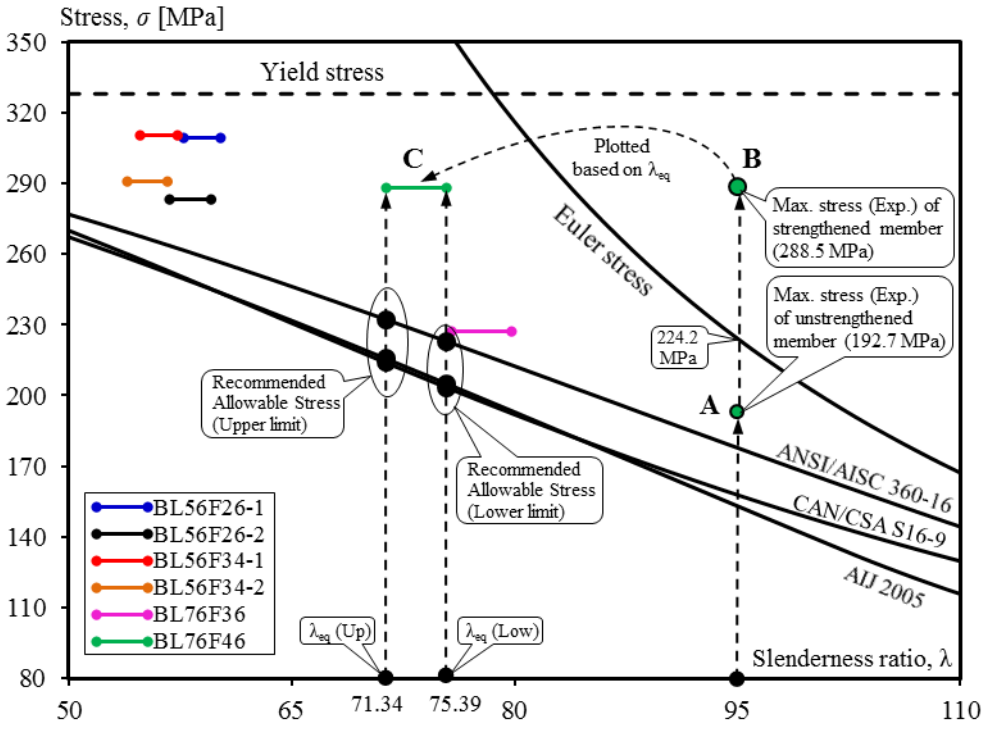

Figure 3.16 Recommended compressive stress for strengthened specimens

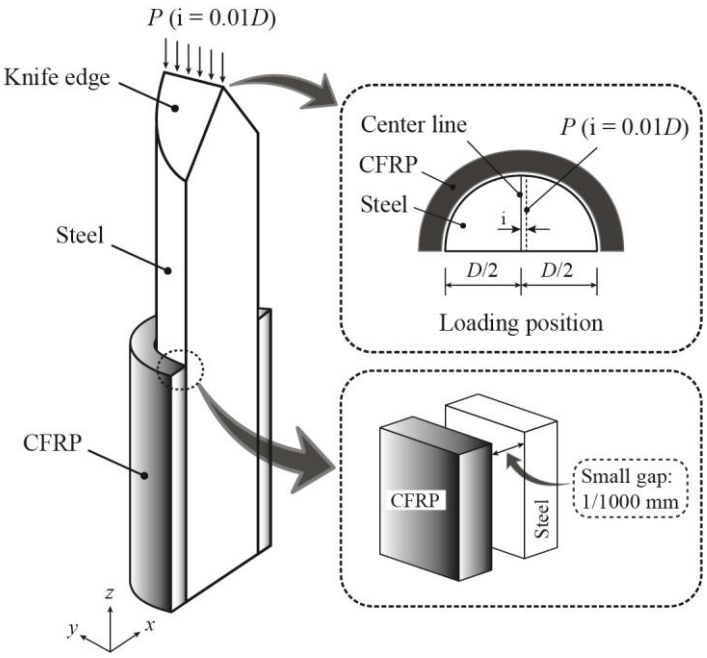

(a) summary of condition

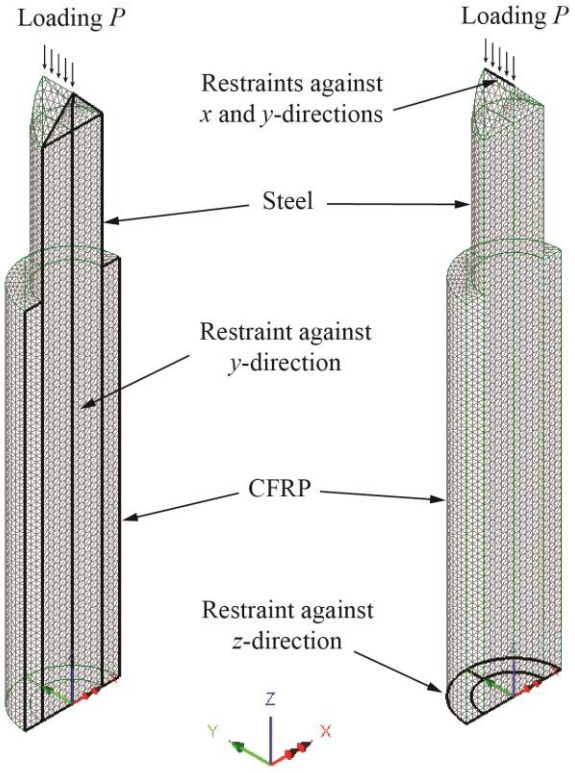

(b) meshing and boundary conditions

Figure 3.17 Features of the FE model along with loading and boundary conditions

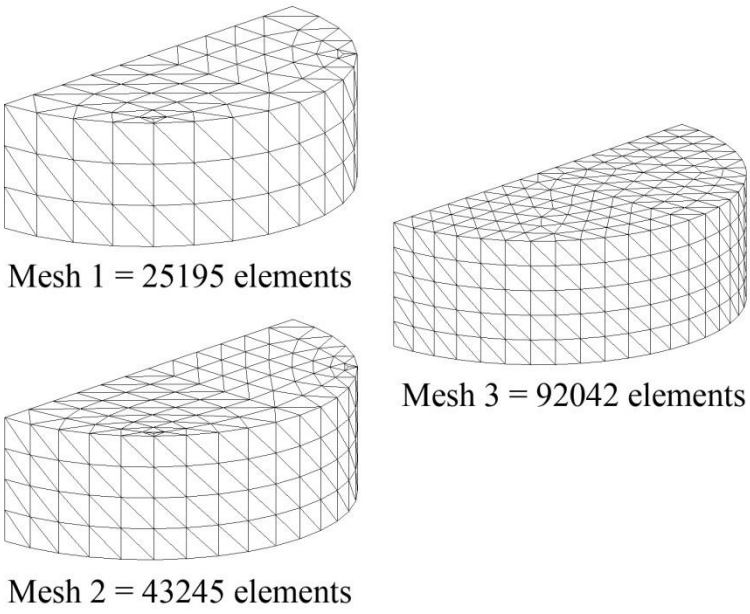

(a) mesh density

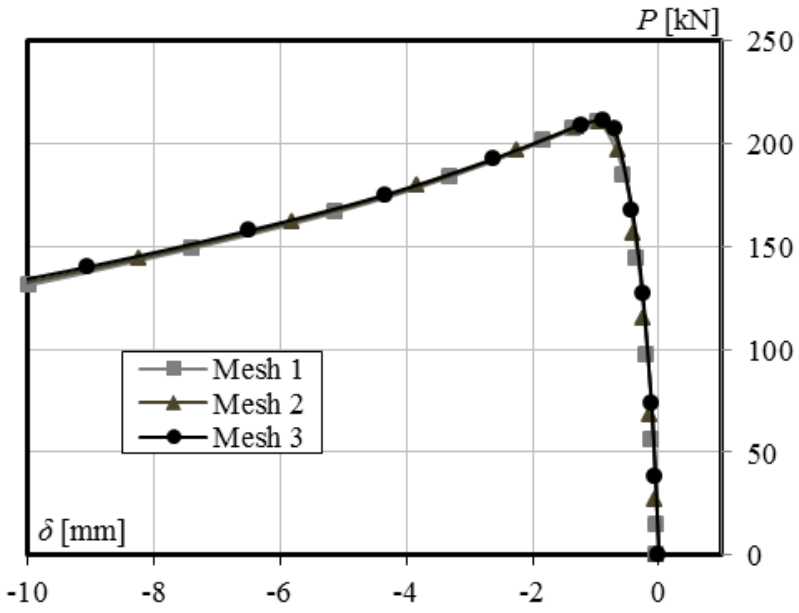

(b) mesh validation

Figure 3.18 Meshing system

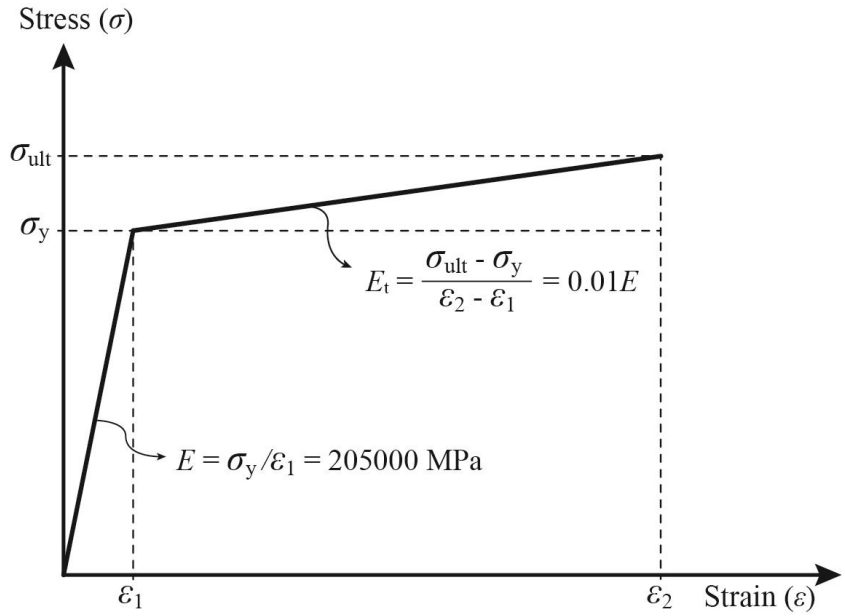

Figure 3.19 Bilinear steel material model

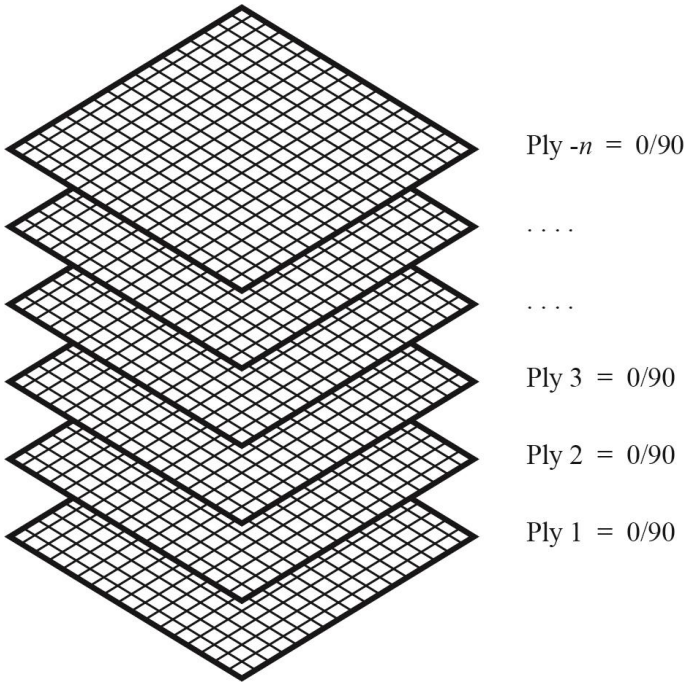

Figure 3.20 Stacking sequence of carbon fiber

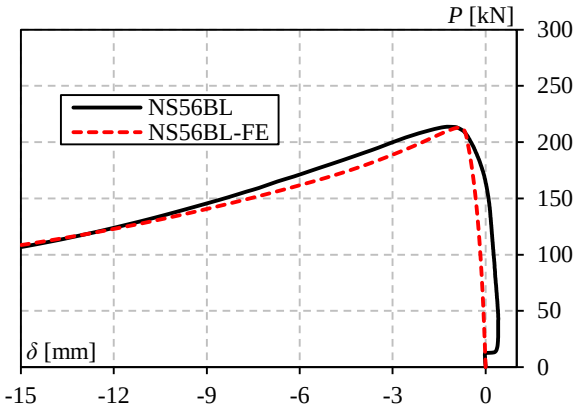

Figure 3.21 Load - lateral midheight displacement for control specimen 560 mm

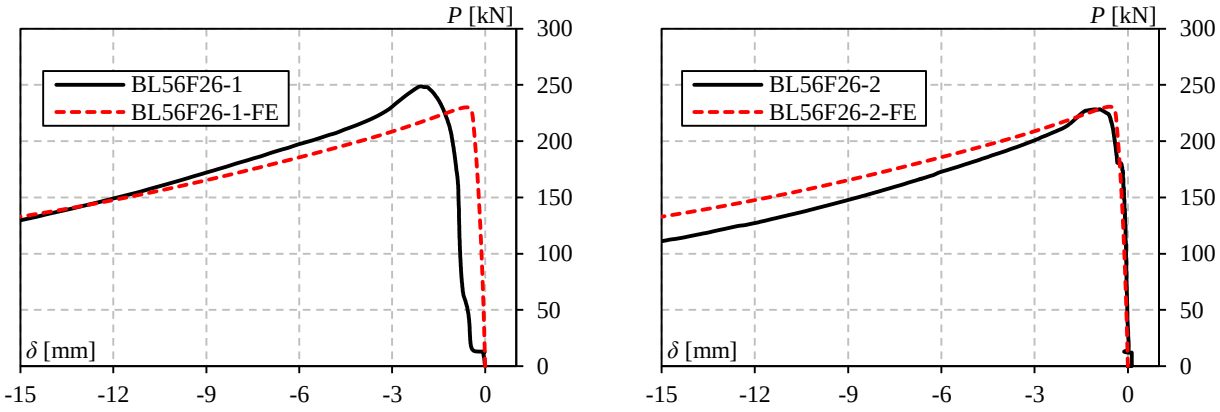

(a) specimen BL56F26-1 (b) specimen BL56F26-2

Figure 3.22 Load - lateral midheight displacement for specimen with 260 mm CFRP

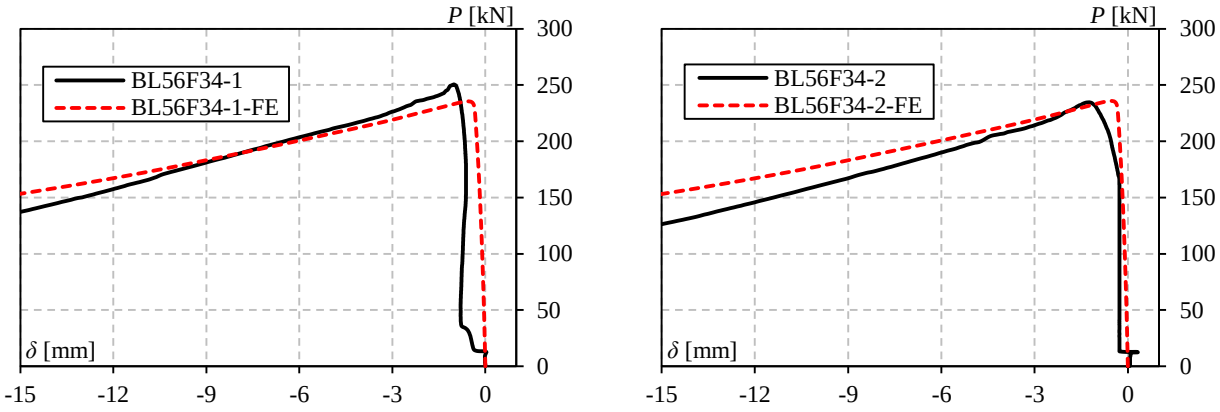

(a) specimen BL56F34-1 (b) specimen BL56F34-2

Figure 3.23 Load - lateral midheight displacement for specimen with 340 mm CFRP

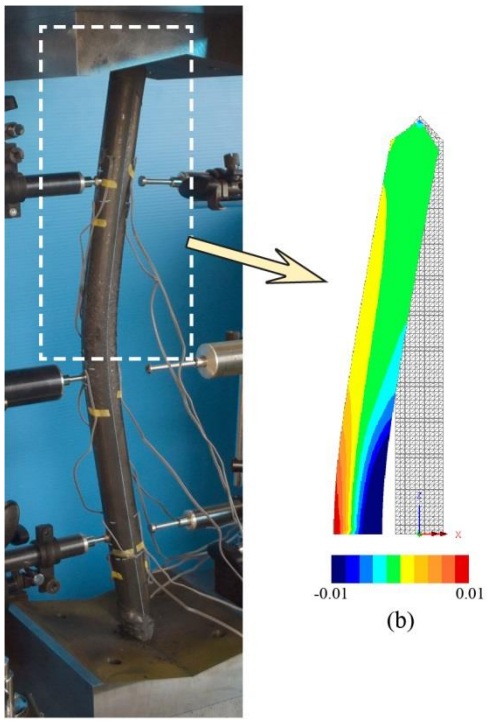

Figure 3.24 Failure mode of control unstrengthened specimen: (a) NS56BL and (b) NS56BL-FE along with longitudinal (*z*) strain contour

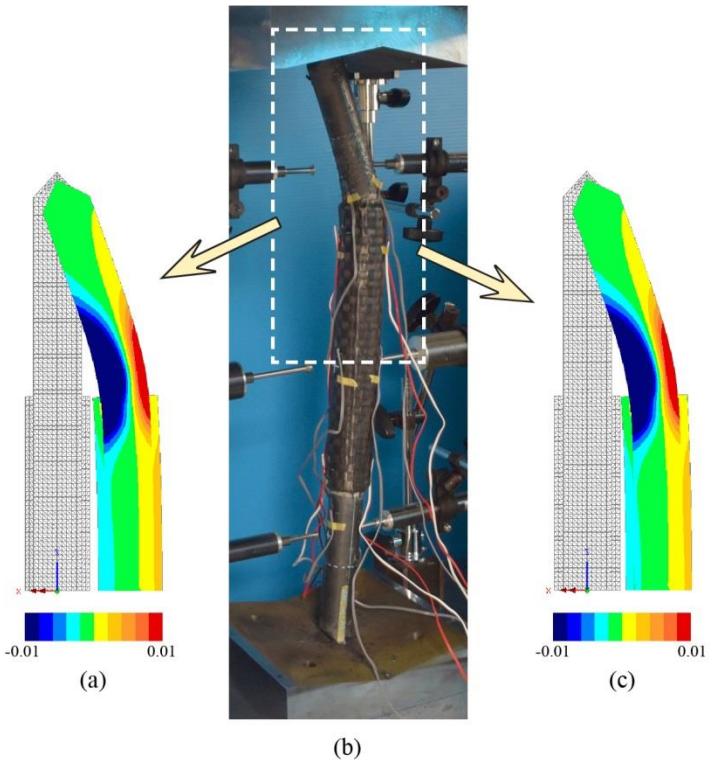

Figure 3.25 Failure mode of specimen with 260 mm CFRP: (a) BL56F26-1-FE along with longitudinal (*z*) strain contour, (b) typical experimental failure for BL56F26-1 and BL56F26-2, and (c) BL56F26-2-FE along with longitudinal (*z*) strain contour

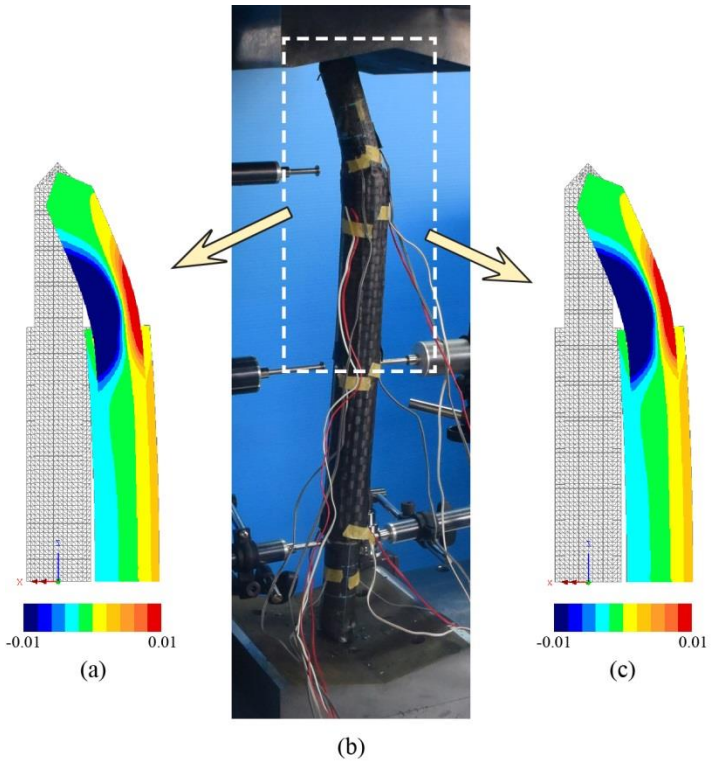

Figure 3.26 Failure mode of specimen with 340 mm CFRP: (a) BL56F34-1-FE along with longitudinal (*z*) strain contour, (b) typical experimental failure for BL56F34-1 and BL56F34-2, and (c) BL56F34-2-FE along with longitudinal (*z*) strain contour.

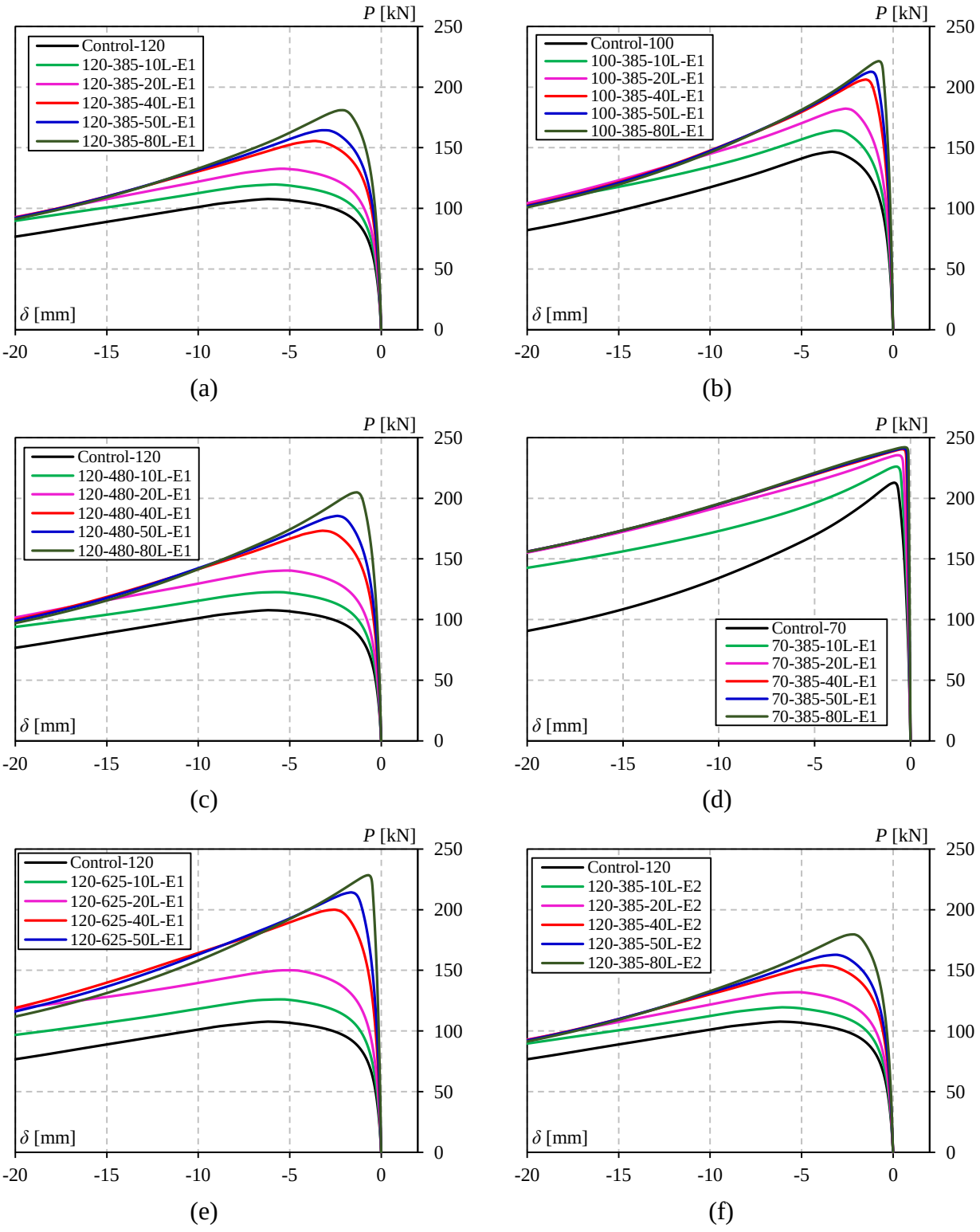

Figure 3.27 Load-lateral displacement behavior of all specimens: (a), (c), and (e) The member having slenderness ratio 120 with CFRP length of 385mm, 480mm, and 625mm, respectively; (b) and (d) The member having CFRP length of 385mm with slenderness ratio 100 and 70, respectively; (f) The member having slenderness ratio 120, CFRP length of 385mm, and CFRP modulus 68.72 GPa.

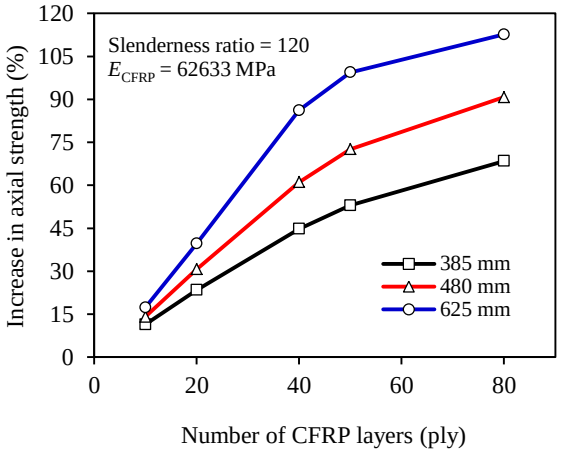

(a) effect of CFRP length on strength increase

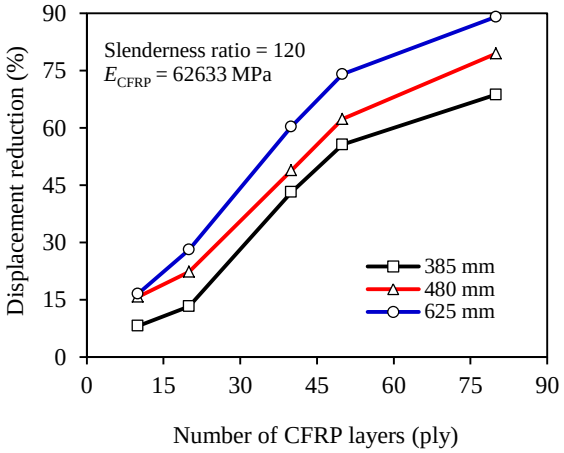

(b) effect of CFRP length on displacement reduction

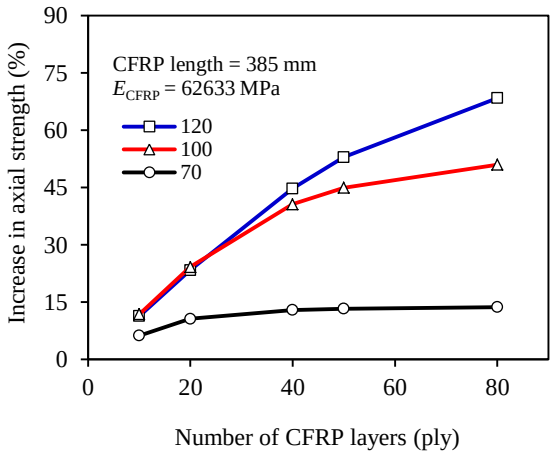

(c) effect of steel's slenderness ratio on strength increase

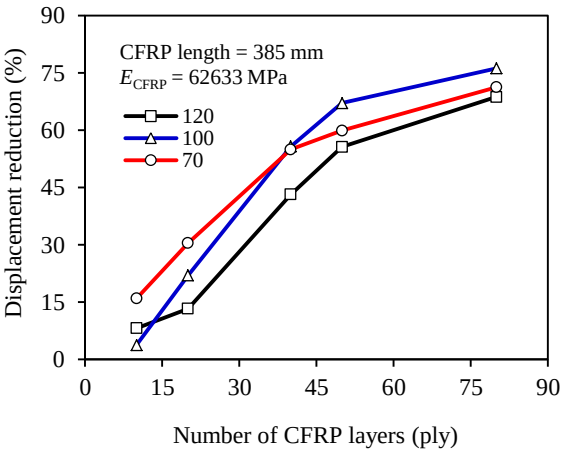

(d) effect of steel's slenderness ratio on displacement reduction

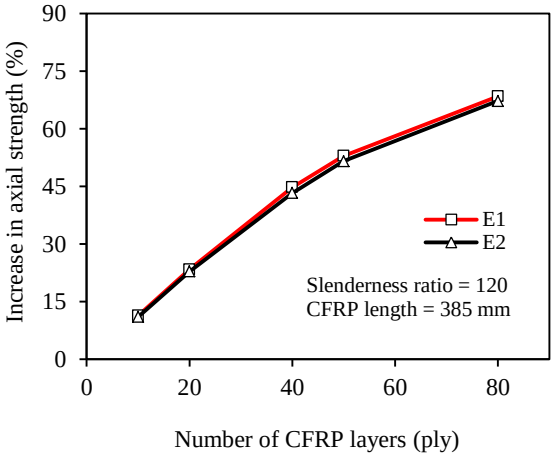

(e) effect of CFRP's elastic modulus on strength increase

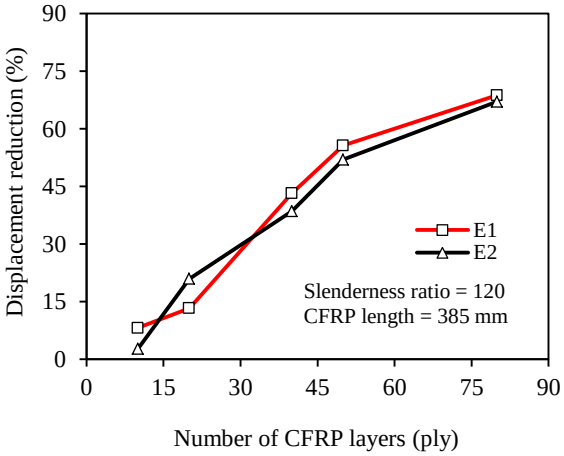

(f) effect of CFRP's elastic modulus on displacement reduction

Figure 3.28 Parametric study results

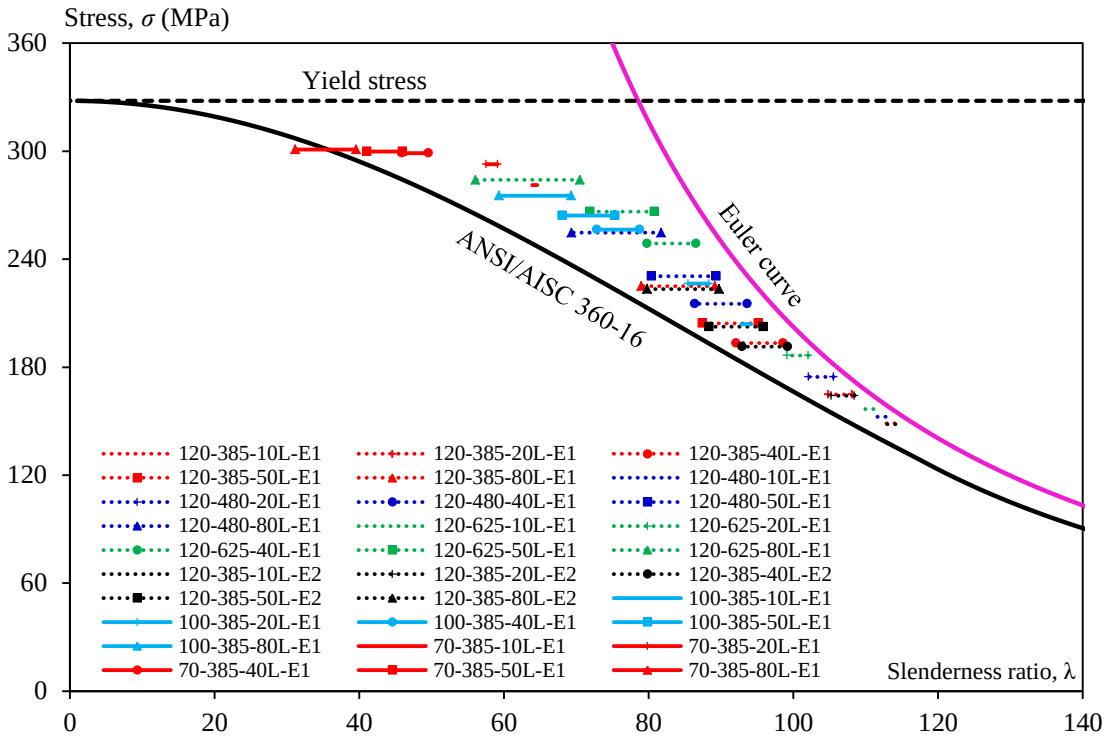

Figure 3.29 Compressive stress of strengthened steel members plotted based on equivalent slenderness ratio

CHAPTER 4
ANGLE STEEL FULLY-JACKETED CROSS SECTION

4.1 Introduction

In this chapter, the proposed unbonded CFRP strengthening is scaled up to be used for strengthening a real or large-scale steel member. Angle steel is chosen because it is very popular used as lateral resisting element in steel buildings. Due to this crucial role, it is very prone to buckling failure. Experimental test is conducted to investigate the buckling performance of specimens in their weak axis only. The test specimens are prepared and designed following criteria developed in the previous chapter. Specimens strengthened with unbonded CFRP are compared with control unstrengthened specimen for evaluation. Strengthening effect of the CFRP is scrutinized for a different number of CFRP layers, CFRP lengths, and the angle steel's slenderness ratio. At the end of this chapter, the effectiveness of the proposed method of equivalent slenderness ratios for strength design of the unbonded CFRP strengthened angle steel is then validated.

4.2 Experimental program

4.2.1 Description of the Test Specimens

A total of twelve specimens, including two control bare steel, are tested in this experiment to investigate the effectiveness of unbonded CFRP laminates in enhancing buckling performance of angle steels. The specimens are divided into two different groups based on the specimen length (L), i.e., 1618 mm and 1218 mm. In the first group, besides of bare steel, three specimens are strengthened with 1000 mm length CFRP and the other three are strengthened with only 500 mm length. However, in Group 2, with also one control unstrengthened angle steel, all other four specimens are strengthened with a same CFRP length, namely 500 mm. The CFRP is positioned at middle part of the angle steel (Figure 4.1). Total number of carbon fiber layers (n_{CF}) in the CFRP laminates is also varied to allow investigation of the strengthening effect in more detail. Table 4.1 summarizes all the test specimens and its parameters that are used in this study. To simplify identification, the specimens are designated as follow: the first letter-number ("C1" and "C2") indicates group of specimen (Group 1 and 2, respectively) and the second letter-number is specimen's name.

4.2.2 Material Properties

The experimental program uses an angle steel L-65x6 which is manufactured as grade SS400 conforming to JIS G3101 (Japanese Industrial Standard). This type of steel is selected as it is widely used for steel buildings in Japan. No tensile coupon test carried out to determine its material properties. Modulus of elasticity (E_s) of the steel is assumed to be 205 GPa which is common for commercial purpose steel. And then, its yield stress (F_y) and tensile strength (F_u) are obtained from manufacturer's inspection certificate as shown in Table 4.2. The angle steel cross-section is shown in Figure 4.2 while descriptions of the symbol including its wall thickness t are given in Table 4.2. Although a nominal wall thickness data is available, the actual wall thickness t_a of 5.56 mm is obtained from measurement.

The bi-directional carbon fiber cloth (BT70-20, see Figure 3.4) is also used in this experiment as the main material for CFRP laminates. Its properties are given in Table 3.3. Epoxy resin used has excellent durability, high strength, and ultra-low viscosity. Its measured tensile material properties (JIS K 7161-1:2014) are given in Table 4.3 and a representative stress-strain curve from one of the test specimens is shown in Figure 4.3.

4.2.3 Specimen Preparation

The angle steel is firstly cut into specific length (i.e., 1200 mm and 1600 mm). At the same time of cutting at different place, two square steel plates having the same thickness of 9 mm are also prepared. The steel plates are then carefully welded to both ends of the angle steel (Figure 4.4a). Specimen length (L) is a sum of the steel length and thickness of these two steel plates (see Figure 4.1). The steel plates have bolt hole around each corner to accommodate installation of knife edges later on. The knife edges are prepared to ensure free-ends rotation can be achieved in all specimens during the compression test.

The unbonded CFRP laminates in all strengthened specimens are processed by a Vacuum-assisted Resin Transfer Molding (VaRTM) technique. The bare angle steel is firstly wrapped with one layer peel ply. The peel ply installed is ensured to cover a whole surface of angle steel along the designated area for CFRP strengthening (strengthened zone in Figure 4.1), so that the CFRP does not stick directly to steel when the molding process is complete. The peel ply serves as separator between steel and CFRP. It should be noted that there are no surface treatments carried out on steel prior to wrapping of peel ply.

Following the peel ply, carbon fiber sheet which has been prepared beforehand is then wrapped around the specimen until it reaches the number of layers as designed in Table 4.1. The carbon fiber is installed so that its 0^o and 90^o of fiber orientation angles lay into longitudinal and transversal direction of the angle steel respectively. Afterwards, an additional layer of peel ply is installed again to cover the carbon fibers before continuing with the installation of resin media (infusion mesh), nylon hose (resin feed line), and a film bag with firmly gum tape connection. After installing all of those needs, the specimen is now ready for resin impregnation (Figure 4.4b). The resin is prepared with its components mixing ratio (by weight) of 3 resin : 1 hardener, as suggested by manufacturer. The resin impregnation process was carried out by utilizing a vacuum pump with a recorded pressure of 0.67 Pa. During the process of impregnation, the specimens are tilted. One edge of specimen which is a suction side is positioned higher than the other edge (injection side). This position is maintained to facilitate air bubbles escape easily so that the possibility for it being trapped inside the mold can be decreased and thus resin can spread evenly. After completing the impregnation process, the final step is that specimens are cured for about one week (or longer) prior to testing (Figure 4.4c). This is to ensure the laminates harden properly. Figure 4.5 shows the cross-section of the strengthened specimens during molding process whereas Figure 4.6 shows detail of the cross-section after demolding.

4.2.4 Test Setup and Instrumentation

The compression test is carried out on all specimens using a testing machine with 2000 kN loading capacity, as presented in Figure 4.7. The specimens are tested under pin-ended conditions which are achieved through knife edges provided on both end of the specimens. The knife edges are designed to coincide with the weak axis (*v*-*v*) of angle steel (Figure 4.2) to allow them buckle in this direction only. The applied load is measured by a load cell built-in within the machine. A total of 20 strain gauges are affixed to measure longitudinal strains on the strengthened specimen. But for control unstrengthened angle steel, there are only twelve strain gauges utilized. In addition to strain gauges, displacement transducers are also mounted to measure out-of-plane displacement during the test. The lateral displacements are measured at mid-height of the specimen and near the top and/or the bottom edge of CFRP. Detail position of the strain gauges and transducers for control and strengthened specimens is shown in Figure 4.8.

4.3 Experimental Results

A summary of the results is presented in Table 4.4. The slenderness ratios given in this table, which is also presented in Table 4.1, are calculated based on the buckling length (L_{cr}). The buckling length is a total of both specimen length (L) and additional bolted steel plates (high strength steel) at top and bottom, (see Figure 4.7). Also given in Table 4.4 are thickness of CFRP, fiber volume content, maximum loads, and strength increases, which are given for the individual specimens.

4.3.1 Fiber Volume Content

Wall thickness of the strengthened angle steel ($t_{s\text{-}CFRP}$, see Figure 4.6) as given in Table 4.4 is an average value of thickness measurements conducted at six different locations along the strengthened zone (see Figure 4.1). By knowing this thickness, the thickness of CFRP (t_{CFRP}) can then be easily determined by halving the value after discarding actual wall thickness t_a of steel (see Figure 4.6). This must be carried out since CFRP exists on both inner and outer side of the steel cross-section and is considered to have same thickness. The fiber volume content (V_f) will depend on the thickness of CFRP and is determined by Eq. (21). In this case, n_{CF} denotes number of carbon fiber layers used and t_{CF} is nominal thickness of a carbon fiber sheet (BT70-20), namely 0.112 mm.

$$V_f = \frac{2n_{CF}t_{CF}}{\left(t_{S\text{-}CFRP} - t_a\right)} \times 100\% \quad \ldots (21)$$

It can be seen from Table 4.4 that the fiber content of all strengthened specimens exceeds 50% and varies between 58.2%-62.7%. This result is higher than findings of a similar investigation by Mieda et al. (2019) whom perform a VaRTM process on creating CFRP for strengthening steel with bonding technique. The fiber content obtained ranges from 49.7% to 51.3%. However, the highest fiber content in the current study (62.7%) is almost equal to investigation results given by Kim et al. (2006), namely 64.0% (resin content 36.0%). The possibility of producing higher fiber content (> 50%) of CFRP laminates through a VaRTM process will lead to producing higher stiffness CFRP which is highly expected for unbonded strengthening as being investigated in this study. This result proves and reconfirms the advantage of VaRTM process over hand-layup.

The percentage gain in axial strength given in Table 4.4 is calculated as the ratio of axial strength of the strengthened specimens (after deduction with strength of the appropriate control specimen) and its appropriate unstrengthened control specimen (C1S0 or C2S0). It is clear that positive and varied strengthening effects can be confirmed due to the application of unbonded CFRP. The highest strength increase is attained in specimen C1S3, i.e., 54.3% whereas the lowest increase is found in specimen C1S4, which is only 8.5%. The variation in strength increase can be viewed as an effect of several factors, namely, number of CFRP layers, CFRP length, and steel's slenderness ratio.

Figures 4.9a and 4.9b present the relationship between applied compressive load and axial displacement for specimens of Group 1 and 2, respectively. In each figure, the responses of both strengthened and control specimens are plotted. The increase in axial strength for all strengthened specimens due to the presence of CFRP laminates can be confirmed from these figures. However, axial stiffness of the specimens remains unchanged. This is reasonable because, in addition to not being applied throughout the steel length, the CFRP is not bonded onto steel surface and the angle steel buckling is only prevented through flexural rigidity of the CFRP used. It means that no effects will occur on the elastic behavior of structure. The difference found from the two groups of specimen is that axial displacement of specimens in Group 1 increased rapidly soon after reaching the maximum load while this behavior start to happen at about 50% of maximum load for specimens in Group 2.

The load versus lateral displacement responses at mid-height of specimens are shown in Figures 4.10a and 4.10b. The unbonded CFRP successfully delays the lateral displacement. This behavior tends to happen before and after reaching maximum load for specimens of Group 2 and occurs as increasing number of CFRP layers. This similar behavior is also experienced by the strengthened specimens of Group 1 but it can only be confirmed before maximum load.

4.3.2 Effect of Different Parameters

The effect of number of CFRP layers on increasing the compression strength can be seen in Table 4.4. It is also demonstrated in Figure 4.9 and Figure 4.10. The strength increases in Group 1 ranged from 8.5% to 54.3%, whereas in Group 2, the increases are varied between 10.6% and 35.0%. The findings prove that compressive strength increases as increasing number of CFRP layers. This trend occurs among specimens in

both Group A and Group B except for specimen C2S4. Number of CFRP layers in this specimen is the highest (30 layers) among others in Group 2 but its strength increase (28.9%) is lower than that of specimen C2S3 (35.0%) which has only 25 layers. This is thought to be closely related to higher imperfection in specimen C2S4. Although not measured in this study, it is implied from load-lateral displacement behavior as shown in Figure 4.10b. The curve of specimen C2S4 (before reaching maximum load) is less steep compared to that of specimen C2S3.

The effect of CFRP length can be seen from specimens in Group 1. The specimens are same in buckling length (1636 mm) but different in CFRP length. The first three strengthened specimens in Group 1, namely C1S1, C1S2, and C1S3, have CFRP length of 1000 mm, whereas the other three strengthened specimens (C1S4, C1S5, and C1S6) are with 500 mm CFRP length. It is indicated from the first (C1S2 and C1S4) and the second (C1S3 and C1S5) comparable specimens (same number of CFRP layers) that axial strength increases as increasing length of CFRP. Even with small number of CFRP layers with longer CFRP, the strength increase can still be higher than that of specimens having many layers of CFRP but short in CFRP length. It is evident from a comparison between specimen C1S1 having strength gain of 24.96% and specimen C1S6 with only 16.77%.

Besides CFRP length and number of CFRP layers, the difference in angle steel's slenderness ratio also affects compressive strength increase of the strengthened specimens. It is found in this study (angle steels are same in cross-section) that strength gain increases as the slenderness ratio (λ) is decreased. Table 4.4 and Figure 4.11 record this finding for strengthened specimens with CFRP length of 500 mm. Specimen C1S4 (λ = 128.4), for example, has strength increase of 8.5% while specimen C2S2 (λ = 97.02) has 14.7%. There is difference in strength increase, i.e., 14.7% - 8.5% = 6.2%. A higher difference (22.4%) is found between specimens C1S5 and C2S3 (both has 25 CFRP layers), where strength increase of specimen C1S5 (λ = 128.4) is 12.6% and specimens C2S3 (λ = 97.02) is of 35.0%. Another higher strength increase can also be seen from comparison between specimen C2S4 (λ = 97.02; 30 CFRP layers) and specimen C1S6 (λ = 128.4; 30 CFRP layers), although the difference in their strength increase does not exceed that of between specimen C1S5 and C2S3, namely 12.1%. This is most probably due to higher imperfection of specimen C2S4 as previously mentioned. Therefore, restating the finding that, smaller angle steel's slenderness ratio provides greater strength increase of the strengthened specimens. Even with small

number of CFRP layers (specimen C2S1) the strength increase can still be higher than that of specimens with many CFRP layers but higher slenderness ratio (specimen C1S4).

4.3.3 Failure Mode and Strain Response

Figure 4.12 shows the modes of failure of all specimens tested in this experiment. As predicted, two control specimens which are not strengthened with CFRP undergo failure of classical global buckling of pin-ended column (Figure 4.12a and Figure 4.12j). Plastic hinge occurs at mid-height of the specimens. Meanwhile, all the strengthened specimens except C1S1 have different deformed shape compared to control specimens. There is a change in curvature where the plastic hinge moves around the edge of CFRP. Moreover, no material crush on CFRP can also be observed. This represents the favorable behavior of the unbonded CFRP for strengthening axial loaded steel members. The CFRP can optimally perform its function as a stiffener.

Although failure modes in almost all of strengthened specimens has demonstrated effectiveness of CFRP as stiffener in this study, the failure mode of specimen C1S1 is still similar with that of control specimen (C1S0) where plastic hinge located at mid-height (Figure 4.12b). The CFRP is also confirmed to have damage at this location (Figure 4.12e and Figure 4.12f). This becomes an indication that strength capacity of the CFRP may have been exceeded prior to failure as what is experienced by the other strengthened specimens. This failure mode is not recommended. Even so, the unbonded CFRP laminates can still provide contribution in buckling strength of the angle steel at around 25%.

The load versus longitudinal strain responses for control specimens are shown in Figure 4.13 and Figure 4.15, while the responses for the strengthened specimens are presented in Figure 4.14 and Figure 4.16. The measurements conducted at three different heights on the control specimen show that compressive strains develop, with almost no difference in the rate of increase, until reaching maximum load. After maximum load, only compressive strain at the mid-height of specimen develops and reaches the angle steel material yield strain at approximately 0.16%. This confirms the failure mode of two control specimens (i.e., C1S0 and C2S0), as mentioned previously.

The different load–longitudinal strain responses of unbonded CFRP strengthened specimens can be seen in Figure 4.14 and Figure 4.16. In general, by observing comparable specimens (the same in both CFRP length and angle steel length),

compressive strains in the CFRP increases, but the rate of increase become smaller as the number of CFRP layers used increases. Other than that, the rate of increase in compressive strains at the CFRP ends is also smaller than that of the mid-height of the specimen. The existence of strain growth on the CFRP is believed to have been caused by minor bonding between the steel and peel ply and/or between the peel ply and CFRP, which cannot be avoided. It is worth noting that the CFRP is created through VaRTM process so that the peel ply between steel and CFRP will also be impregnated with resin during the specimen molding process.

Although the compressive strains exist, the strain growth at CFRP ends only occurs up to a certain load (before maximum load). After reaching this load, the strains no longer grow and tend to return to zero. This behavior indicates that the unbonded condition has occurred/started, since the load is reached (named "debonding load"). The unbonded condition also occurs earlier with the increasing flexural rigidity of the CFRP. This is evident from the smaller debonding load for the strengthened specimen with a higher number of CFRP layers. A comparison of all curves of the strengthened specimens in Figure 4.16 can more easily demonstrate this behavior. The unbonded condition of CFRP can even be achieved from the first application of load (strains almost do not develop at all), as observed for specimen C2S4 (Figure 4.16d). In addition, the smaller strain growth at the CFRP ends as compared with at the mid-height of the specimen, as previously mentioned, confirms the experimental finding that the unbonded condition of the CFRP in reality is initiated at the CFRP ends and then propagated to the mid-height of specimens.

4.3.4 Strength Evaluation

Strength evaluation is carried out through determining equivalent slenderness ratios for the CFRP-strengthened specimens. The procedure for determining equivalent slenderness ratio and design strength have been described in Chapter 3. In this section, the only structural model considered is that no bond at all between the CFRP and steel, or fully unbonded condition (see Figure 3.15a). Therefore, the design values obtained will be safer (lower bound solution). Here, for effectiveness, the provision of AIJ 2005 is chosen as representative of the other existing provisions.

The maximum stress of each specimen is plotted based on the value of equivalent slenderness ratio (given in Table 4.5), as shown in Figure 4.17. The design strength of the strengthened specimens is also calculated based on the equivalent slenderness ratio and

then listed in Table 4.5 along with safety factor, standard deviations, and coefficient variations for each set. One set consists of specimens with the same buckling length and CFRP length. It can be clearly seen from Figure 4.17 and Table 4.5 that the slenderness ratio after modification is smaller than that of bare steel. The decrease in the slenderness ratio occurs as the number of CFRP layers increases. However, this allows for a reasonable design solution. It means that if the slenderness ratio is much smaller and uncontrolled, the proposed design strength (recommendation strength value) is unsafe because the design value exceeds the actual maximum stress. Furthermore, the safety factor obtained in this study varied from 1.14 to 1.34. The standard deviation for each set is 0.03, 0.01, and 0.06, which provides coefficient variation of 2.2%, 0.6%, and 5.2%, respectively. This finding is sufficient to ensure that the proposed equivalent slenderness ratio for determining design strength of the unbonded CFRP strengthened specimens falls into an acceptable category.

4.4 Post-buckling Prediction

The following steps are used to predict the post-buckling response of the strengthened specimens. This procedure is based on the model developed as in Figure 4.18.

1. set the initial condition for horizontal and vertical deflections equal to zero ($\delta h_i = \delta v_i = 0$)
2. assume that the increament for horizontal deflection (δh_{inc}) equals to 0.1 mm
3. calculate the values of $\alpha_i, \alpha_i', \beta_i, \beta_i'$, and $\delta v_i'$ using Eq. (22) to Eq. (26), where l_1 is the length of the unstrengthened zone at one edge of the specimen (see Fig.2) and l_2 is the length of the specimen excluding l_1

$$\alpha_i = \sin^{-1}\left(\frac{\delta h_i}{l_1}\right) \quad \ldots (22)$$

$$\alpha_i' = \sin^{-1}\left(\frac{\delta h_i + \delta h_{inc}}{l_1}\right) \quad \ldots (23)$$

$$\beta_i = \sin^{-1}\left(\frac{\delta h_i}{l_2}\right) \quad \ldots (24)$$

$$\beta_i' = \sin^{-1}\left(\frac{\delta h_i + \delta h_{inc}}{l_2}\right) \quad \ldots (25)$$

$$\delta v_i' = l_1(\cos\alpha_i - \cos\alpha_i') + l_2(\cos\beta_i - \cos\beta_i') \quad \ldots (26)$$

4. by virtual work, solve the value of compression load *P* using the plastic momen M_P (Eq. (27))

$$P.\ \delta v_i' = \{(\alpha_i' - \alpha_i) + (\beta_i' - \beta_i)\}\,.M_P \quad \ldots (27)$$

5. calculate the horizontal and vertical deflections for the current step of iteration (*i*) using Eq. (28) and Eq. (29)

$$\delta h_{i+1} = \delta h_i + \delta h_{inc} \quad \ldots (28)$$

$$\delta v_{i+1} = \delta v_i + \delta v_i' \quad \ldots (29)$$

6. back to step 3
7. stop the iteration when the vertical deflection reaches a value equals to the maximum axial displacement obtained from experiment.

The comparison of post-buckling curve, which is determined from the procedure described above, against the experimental results is shown in Figure 4.19 and 4.22. The curve is plotted starting from the design value which has been obtained as in Table 4.5. The experimental curves is plotted after fixing the unloaded condition at the beginning stage of loading. It can be seen from Figure 4.19 and 4.22 that the post-buckling curve prediction and the experimental curves provide a good correspond.

4.5 Summary and Conclusions

Experimental test was conducted to investigate the effect of unbonded CFRP in strengthening angle steel against buckling. The CFRP was created by VaRTM process. Totally twelve specimens including control unstrengthened angle steel were prepared and tested to failure with several experimental variables, i.e., number of CFRP layers, CFRP lengths, and the angle steel's slenderness ratio. The test results are used to validate the proposed method of equivalent slenderness ratio for strength recommendations. Based on the investigation results, following conclusions can be drawn:

1. The unbonded CFRP strengthening can improve the buckling performance of angle steel. Load capacity of the angle steel can be increased by 8.5%-54.3%.
2. The VaRTM process was able to produce CFRP with higher fiber contents. Volume fiber content of the CFRP varied from 58.2% to 62.7%.
3. The increase in load capacity occurred with the increasing number of CFRP layers and CFRP length. However, for the strengthening with same number of layers and CFRP length, a greater capacity increase was attained in specimens with smaller steel slenderness ratios.

4. The method of equivalent slenderness ratio can be used for determining strength recommendations for the unbonded CFRP strengthened angel steel specimens. The safety factor obtained fell within the range of 1.14-1.34 with coefficient variations of 2.2%, 0.6%, and 5.2% depending on strengthening variations.
5. The step-by-step procedure developed in this study can be used to predict the axial compression response of the strengthened specimen after buckling (post-buckling response).

Table 4.1 Specimen details

Specimen ID	Specimen length (mm)	CFRP layer (plies)	CFRP length (mm)	Steel's slenderness ratio
Group 1				
C1S0	1618	-	-	128.4
C1S1	1618	10	1000	128.4
C1S2	1618	18	1000	128.4
C1S3	1618	25	1000	128.4
C1S4	1618	18	500	128.4
C1S5	1618	25	500	128.4
C1S6	1618	30	500	128.4
Group 2				
C2S0	1218	-	-	97.02
C2S1	1218	10	500	97.02
C2S2	1218	18	500	97.02
C2S3	1218	25	500	97.02
C2S4	1218	30	500	97.02

Table 4.2 Dimension and properties of angle steel

Cross-section dimensions (mm)				Elastic modulus (GPa)	Yield stress (MPa)	Tensile strength (MPa)
AxB	t	r_1	r_2			
65x65	6.0	8.5	4.0	205	333	448

Table 4.3 Properties of resin

Specimen No.	Elastic modulus (GPa)	Poisson's ratio	Tensile strength (MPa)
1	1.204	0.46	16.694
2	1.403	0.49	16.893
3	1.252	0.45	17.565
4	1.345	0.46	15.416
5	1.248	0.46	15.171
6	1.257	0.46	17.085
Average	1.285	0.46	16.471
CV (%)	5.754	2.949	5.826

Table 4.4 Test results

Spec. ID	Buckling length (mm)	Slend. ratio	$t_{s\text{-}CFRP}$ (mm)	CFRP thickness (mm)	Fiber content (%)	Max. load (kN)	Axial strength (MPa)	Strength increase (%)
Group 1								
C1S0	1636	128.4	-	-	-	77.2	110.2	-
C1S1	1636	128.4	9.33	1.89	59.4	96.5	137.7	24.9
C1S2	1636	128.4	12.49	3.47	58.2	106.4	151.9	37.8
C1S3	1636	128.4	14.58	4.51	62.1	119.1	170.0	54.3
C1S4	1636	128.4	12.14	3.29	61.3	83.8	119.6	8.5
C1S5	1636	128.4	14.52	4.48	62.5	86.9	124.1	12.6
C1S6	1636	128.4	16.54	5.49	61.2	90.2	128.7	16.8
Group 2								
C2S0	1236	97.02	-	-	-	122.7	175.1	-
C2S1	1236	97.02	9.39	1.92	58.5	135.7	193.8	10.6
C2S2	1236	97.02	12.19	3.32	60.8	140.7	200.8	14.7
C2S3	1236	97.02	14.49	4.47	62.7	165.7	236.5	35.0
C2S4	1236	97.02	16.71	5.58	60.3	158.2	225.8	28.9

Table 4.5 Strength design for specimens

Specimen. ID	Max. stress (MPa)	Design method				
		Modified slend. ratio	Strength design (MPa)	Safety Factor	Standard deviation	Coefficient variation (%)
Group 1						
C1S0	110.2	128.4	84.99	-	-	-
C1S1	137.8	116.6	103.0	1.34	0.03	2.2
C1S2	151.9	108.8	118.4	1.28		
C1S3	170.1	103.2	131.5	1.29		
C1S4	119.6	117.9	100.8	1.19	0.01	0.6
C1S5	124.1	115.0	105.9	1.17		
C1S6	128.7	113.2	109.3	1.18		
Group 2						
C2S0	175.1	97.0	148.1	-	-	-
C2S1	193.8	90.7	165.1	1.17	0.06	5.2
C2S2	200.8	86.7	176.0	1.14		
C2S3	236.5	83.9	183.8	1.29		
C2S4	225.8	82.0	188.9	1.20		

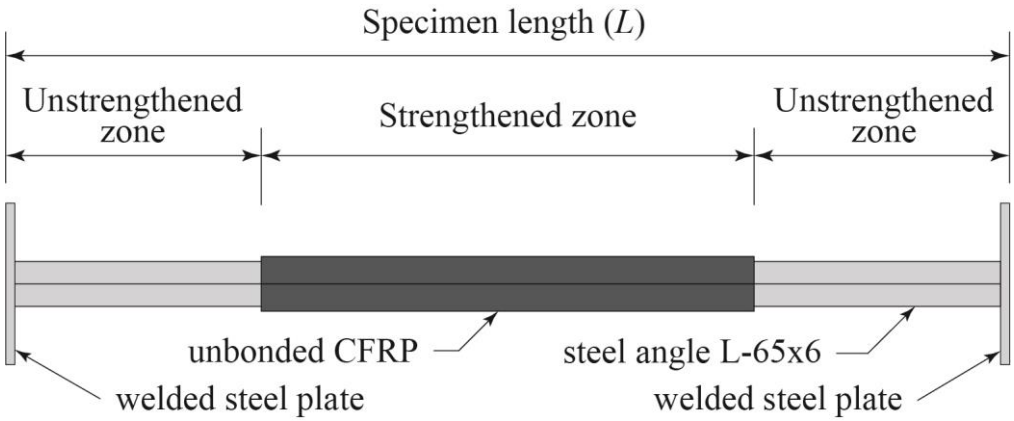

Figure 4.1 Specimen configuration

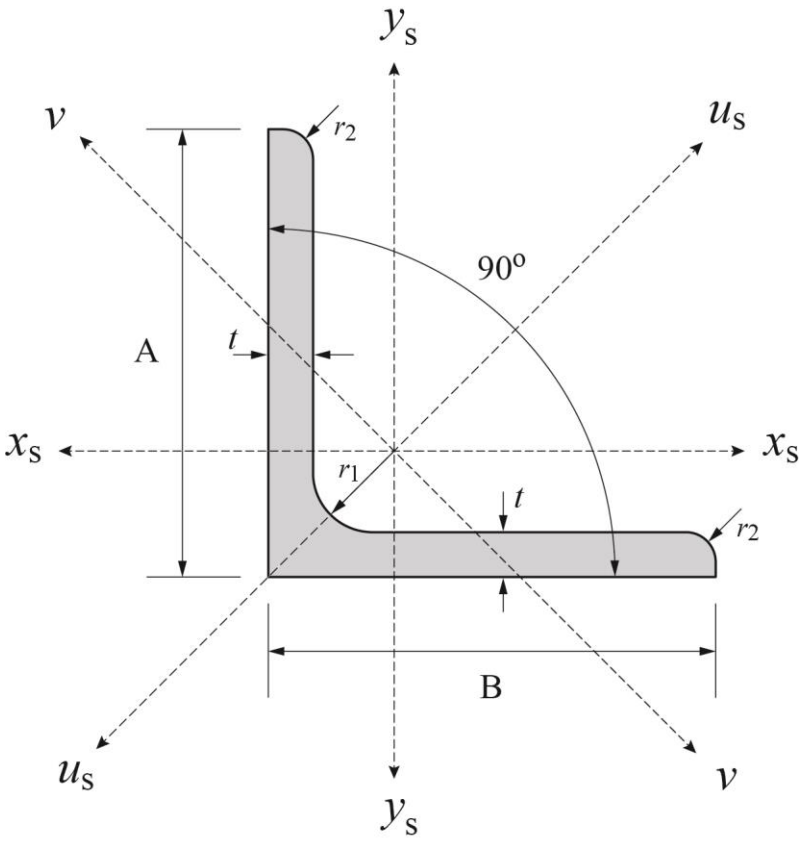

Figure 4.2 Cross-section of angle steel

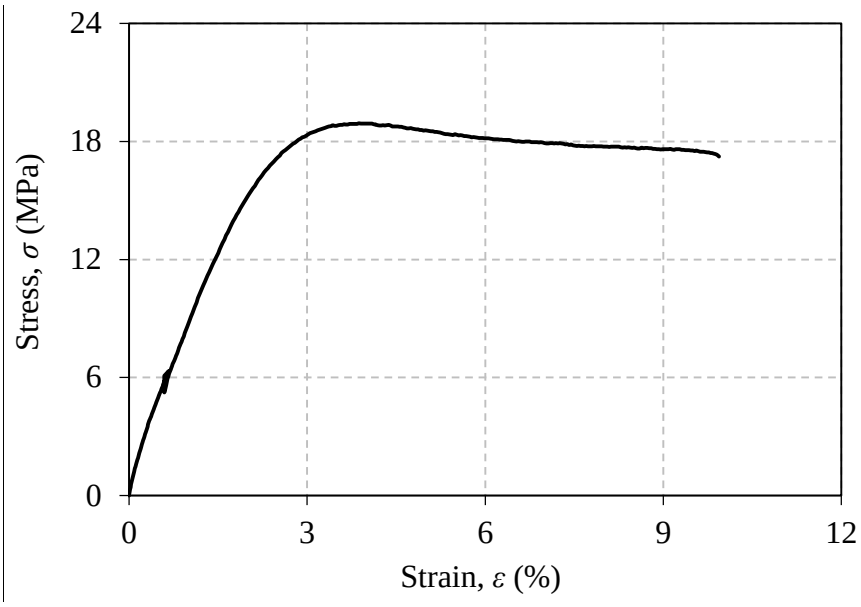

Figure 4.3 Stress-strain curve of resin

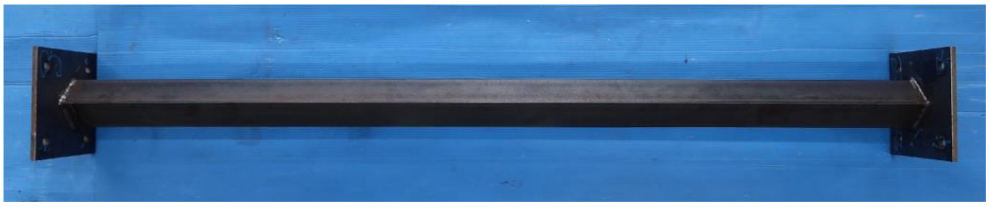

(a) angle steel before strengthening

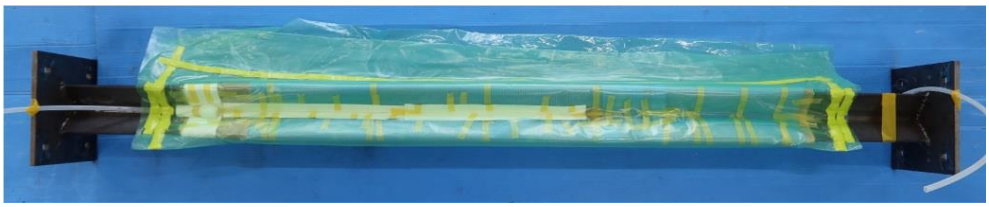

(b) molding process

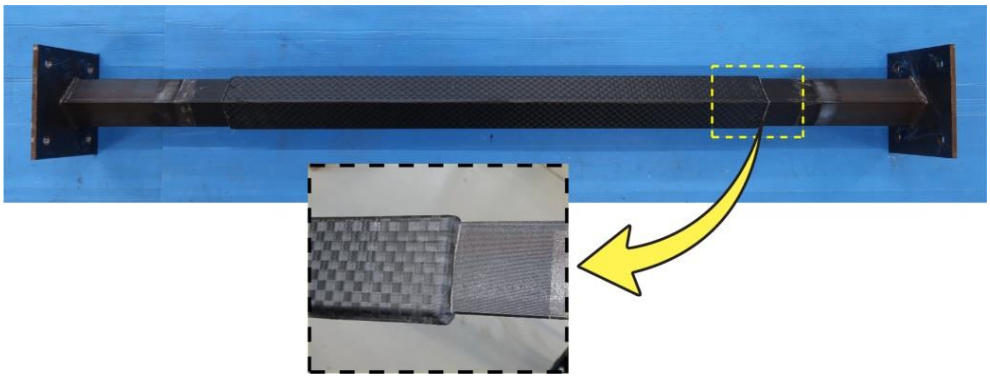

(c) specimen after molding

Figure 4.4 Specimen preparation

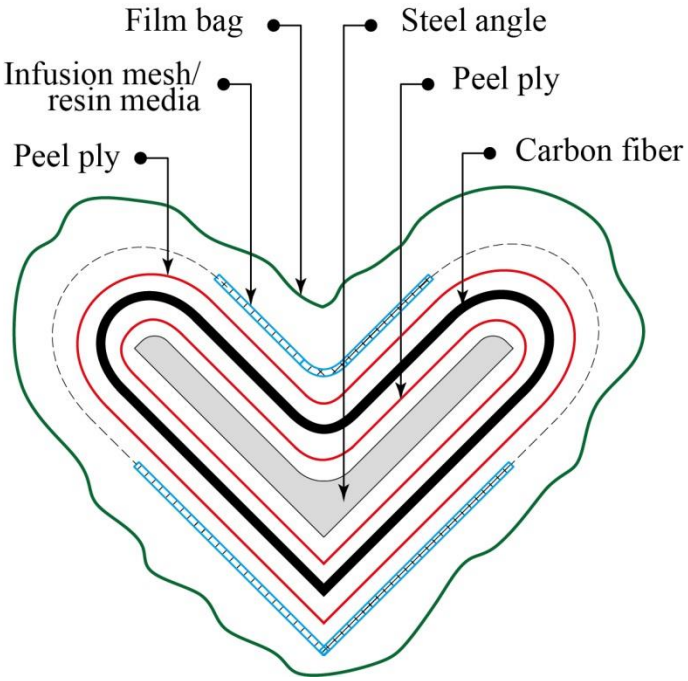

Figure 4.5 Specimen molding cross-section.

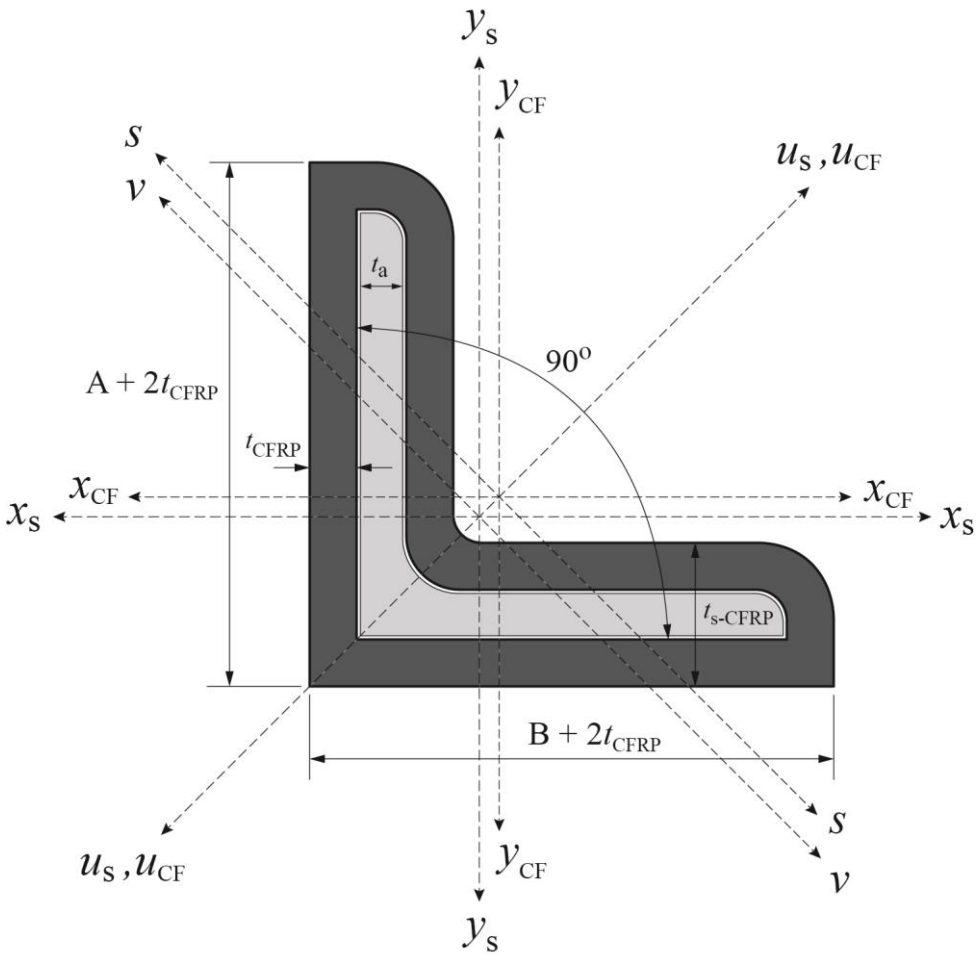

Figure 4.6 Cross-section of specimen at strengthened zone

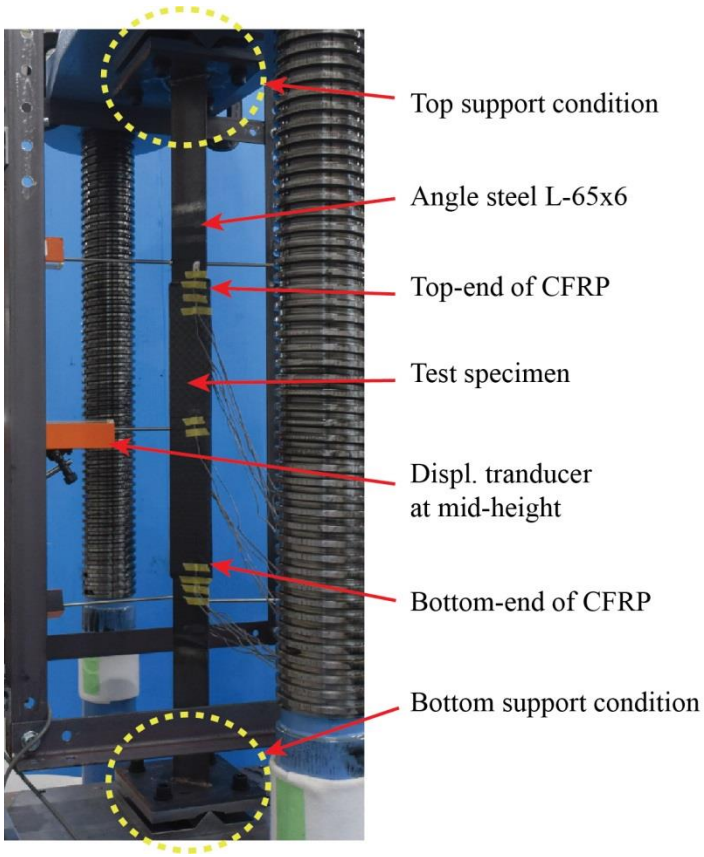

(a) test setup

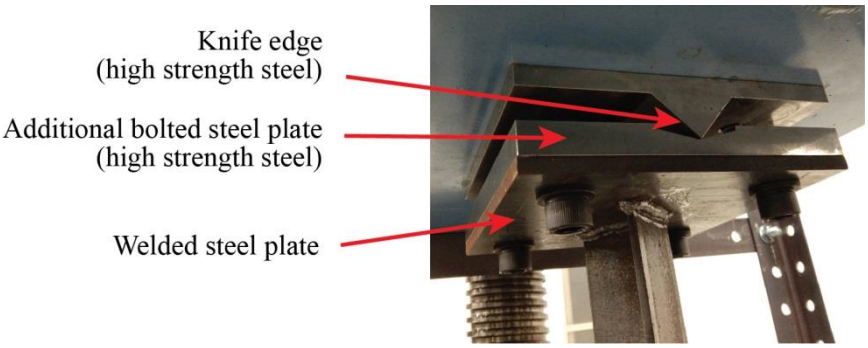

(b) top support condition

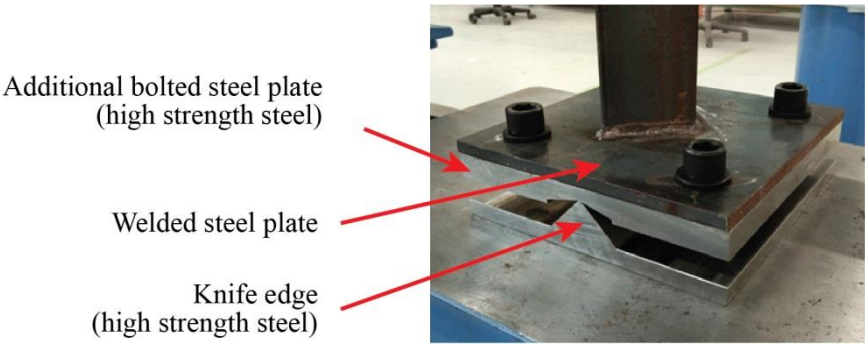

(c) bottom support condition

Figure 4.7 Specimen buckling test setup

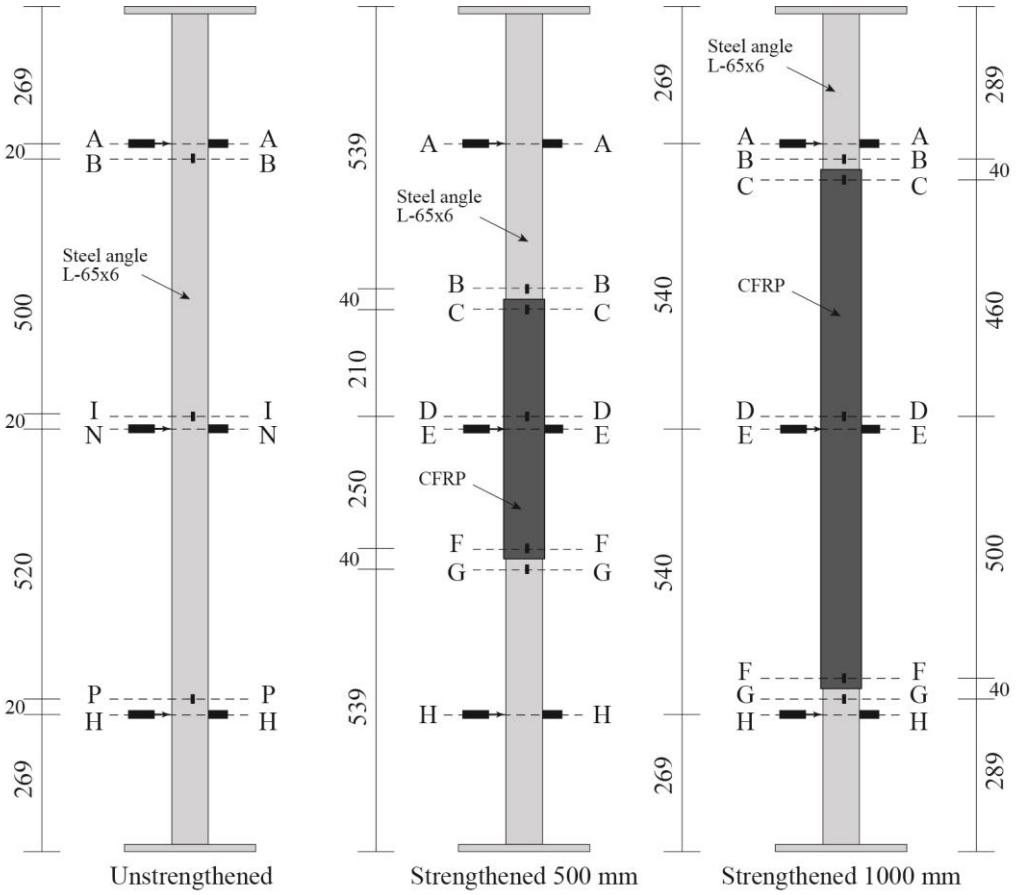

(a) Specimens of Group 1

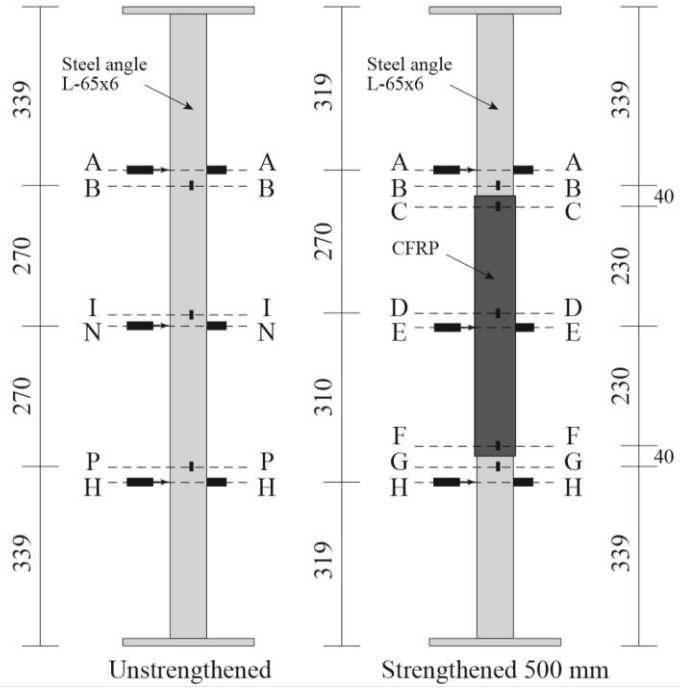

(b) Specimens of Group 2

Figure 4.8 Position of displacement transducers and strain gauges

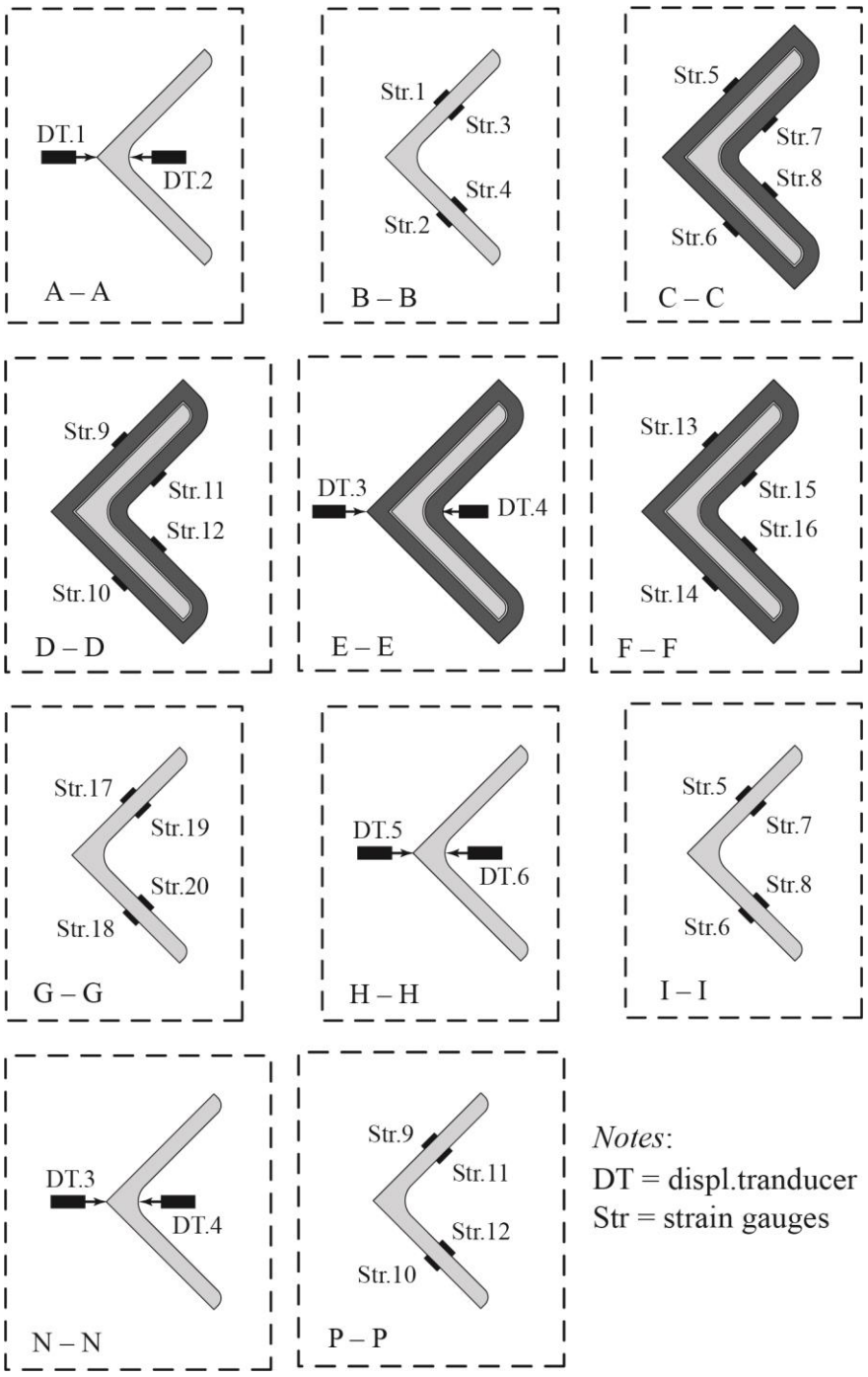

(c) Detail in cross-section

Figure 4.8 Position of displacement transducers and strain gauges (Continued.)

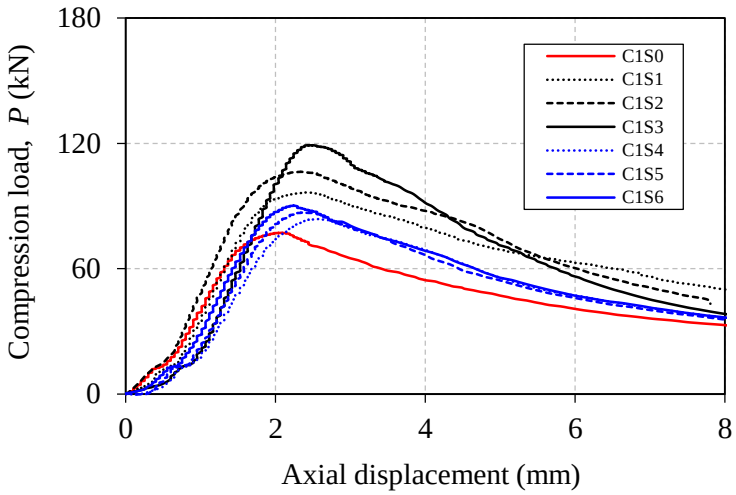

(a) Specimens of Group 1

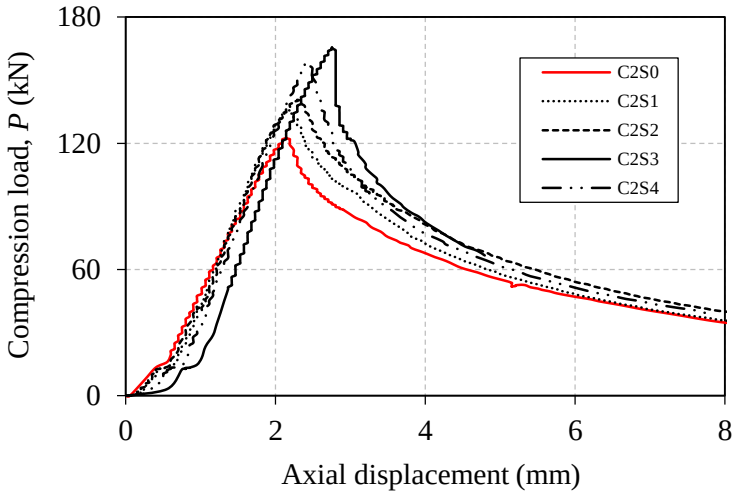

(b) Specimens of Group 2

Figure 4.9 Load – axial displacement relationships

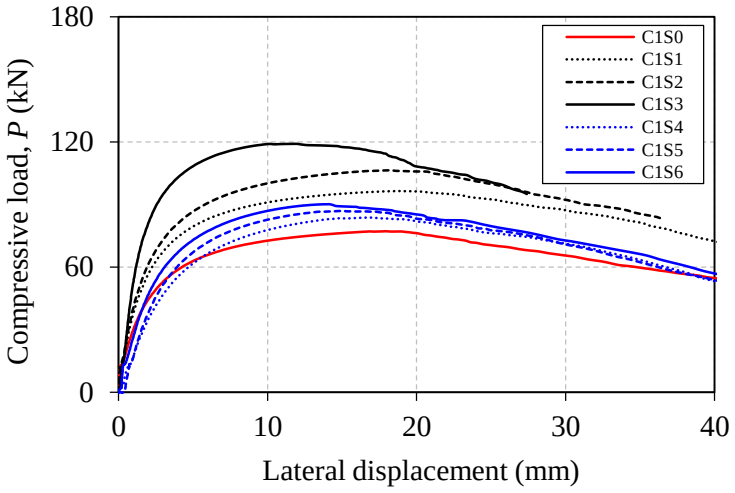

(a) Specimen of Group 1

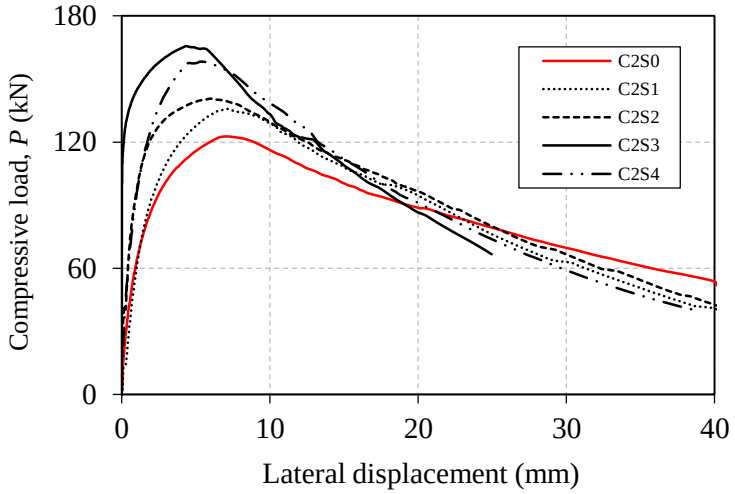

(b) Specimen of Group 2

Figure 4.10 Load – lateral mid-height displacement relationships

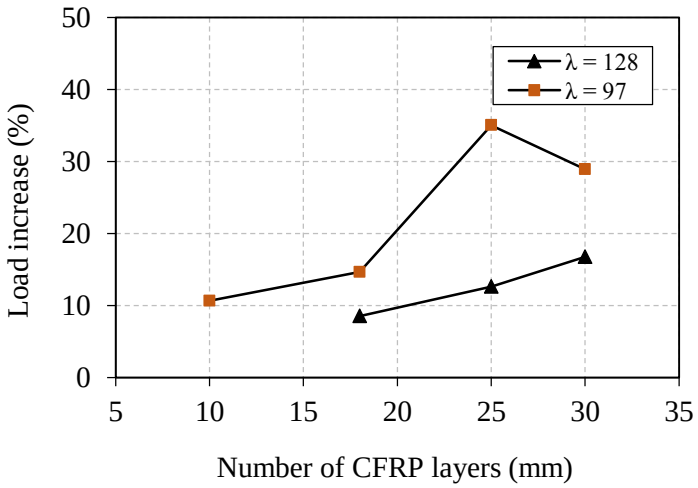

Figure 4.11 Effect of steel's slenderness ratio

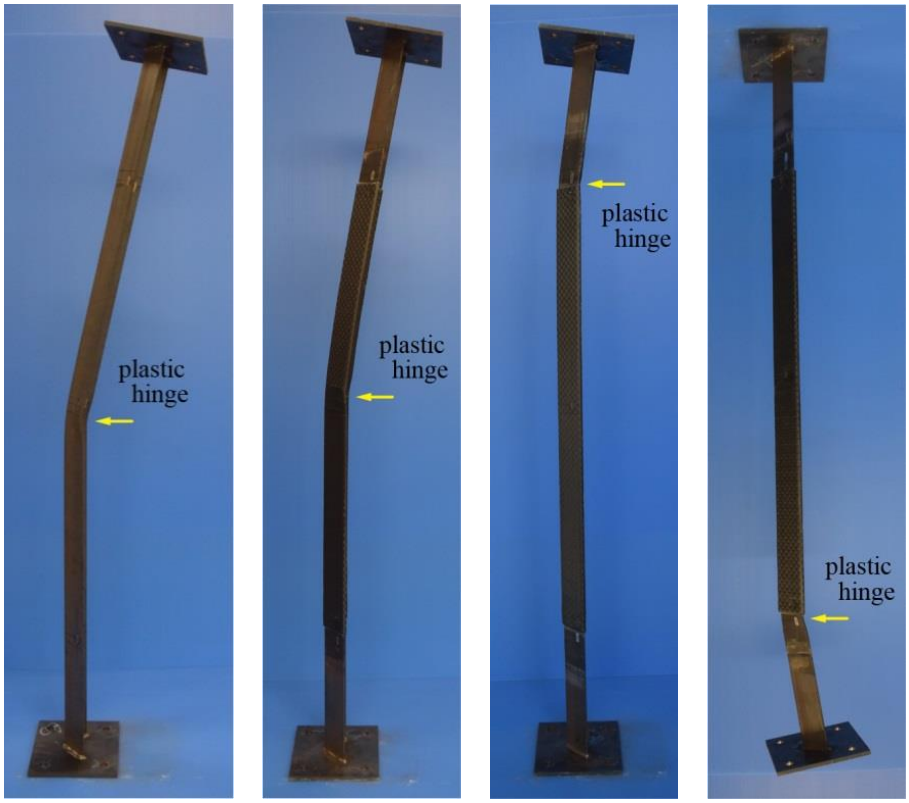

(a) C1S0 (b) C1S1 (c) C1S2 (d) C1S3

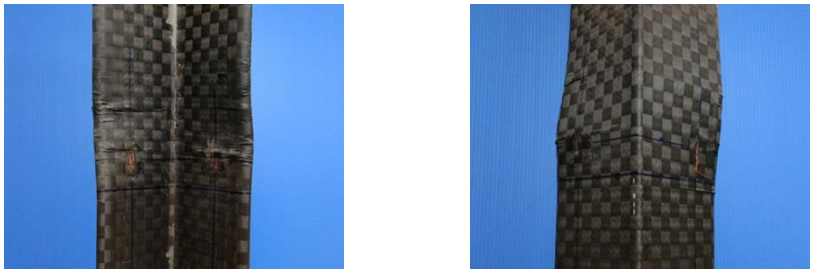

(e) CFRP break C1S1 (front) (f) CFRP break C1S1 (back)

Figure 4.12 Failure modes

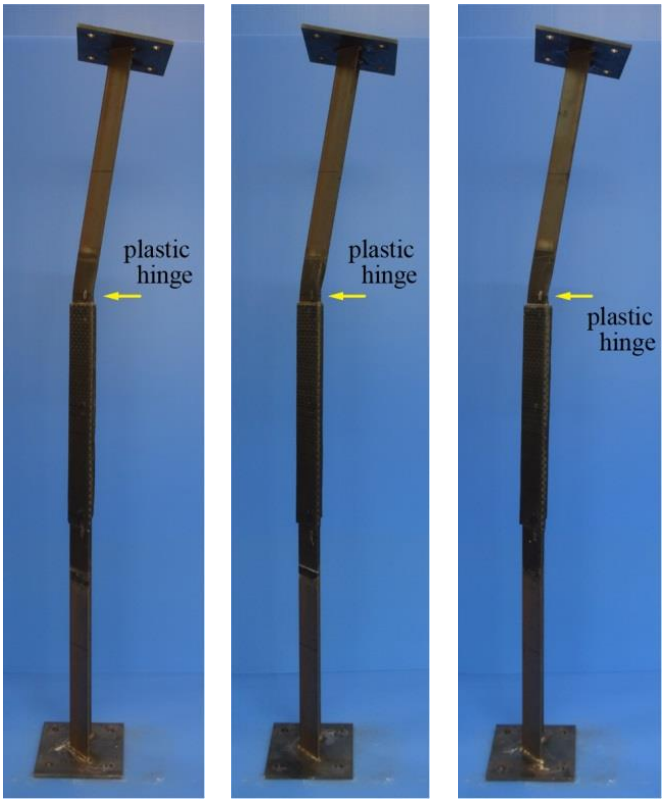

(g) C1S4 (h) C1S5 (i) C1S6

(j) C2S0 (k) C2S1 (l) C2S2 (m) C2S3 (n) C2S4

Figure 4.12 Failure modes (Continued.)

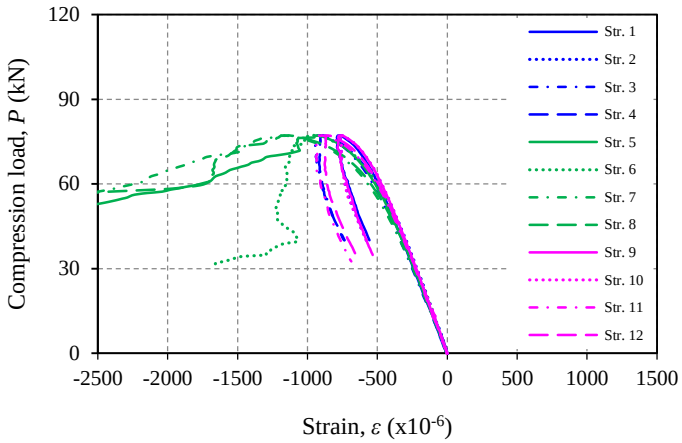

Figure 4.13 Strain responses for specimens C1S0

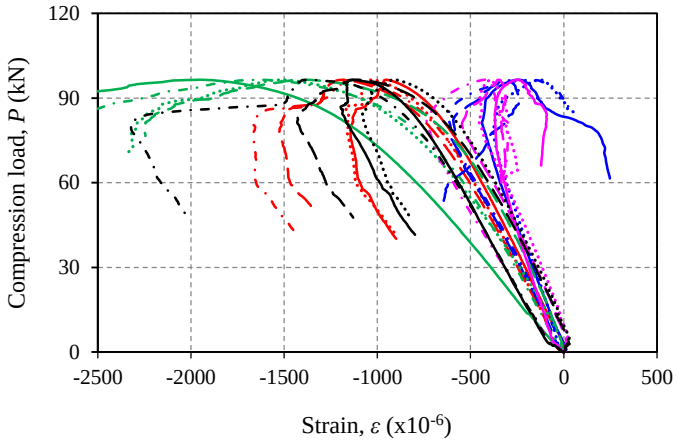

(a) Specimen C1S1

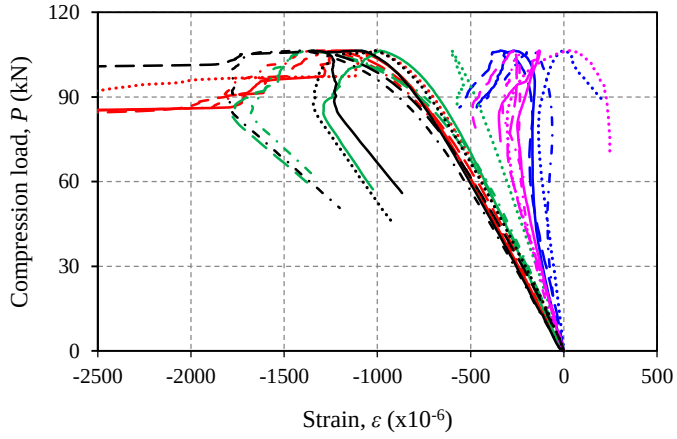

(b) Specimen C1S2

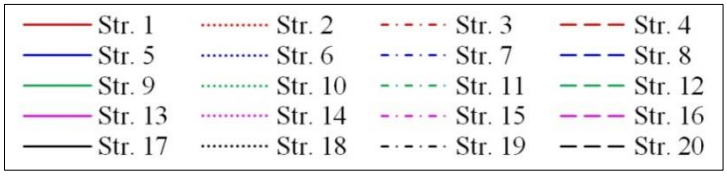

Figure 4.14 Strain responses for specimens of Group 1

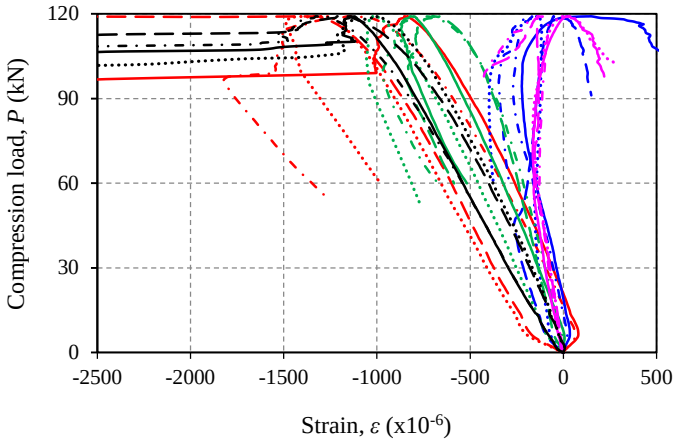

(c) Specimen C1S3

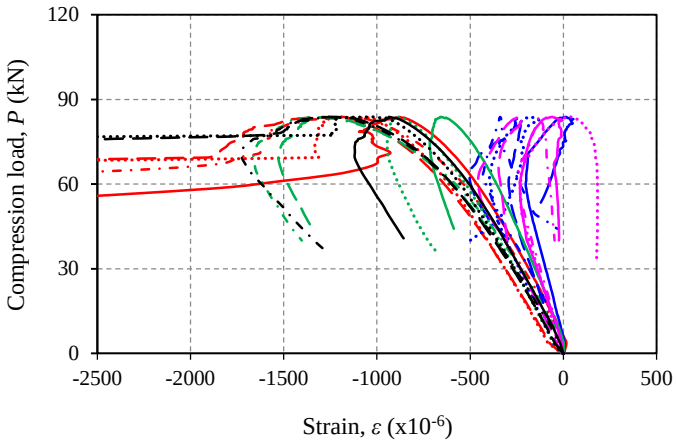

(d) Specimen C1S4

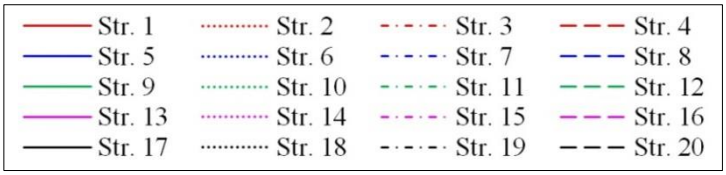

Figure 4.14 Strain responses for specimens of Group 1 (Continued.)

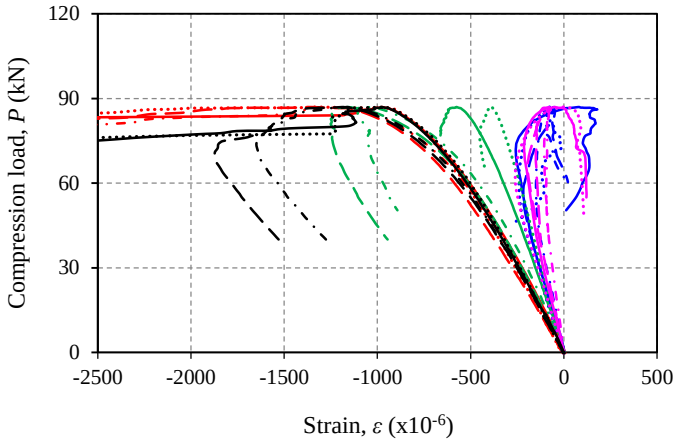

(e) Specimen C1S5

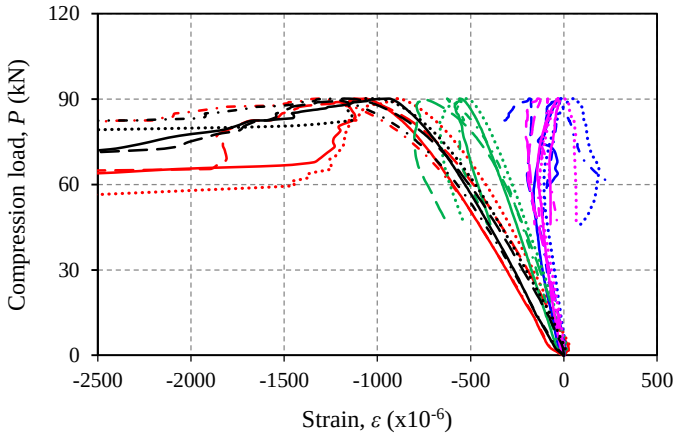

(f) Specimen C1S6

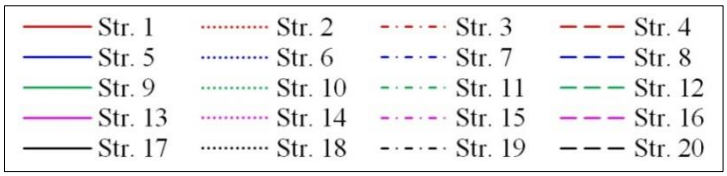

Figure 4.14 Strain responses for specimens of Group 1 (Continued.)

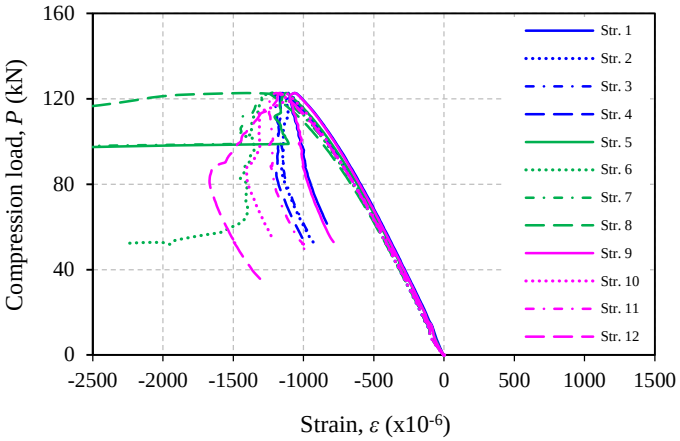

Figure 4.15 Strain responses for specimens C2S0

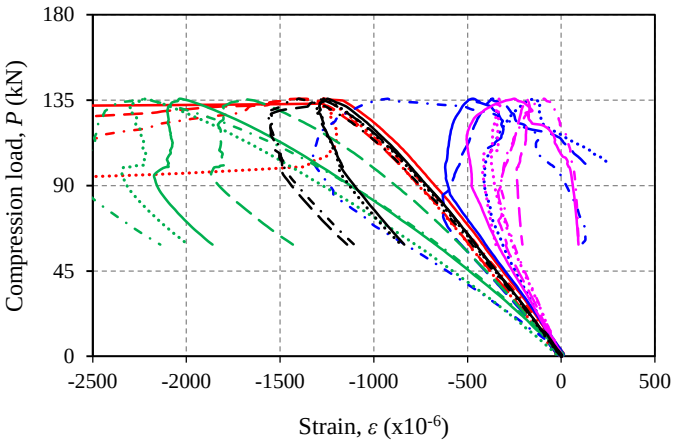

(a) Specimen C2S1

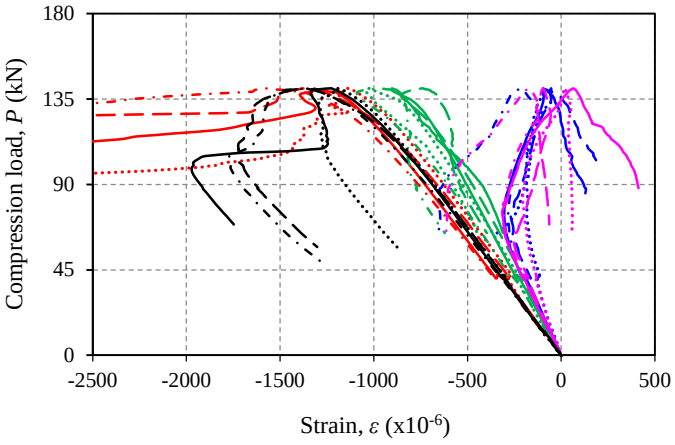

(b) Specimen C2S2

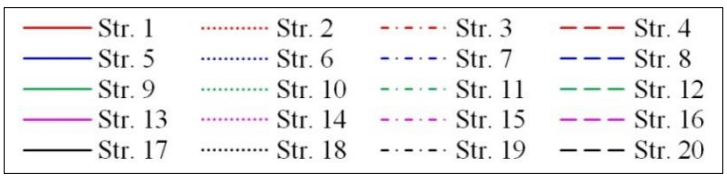

Figure 4.16 Strain responses for specimens of Group 2

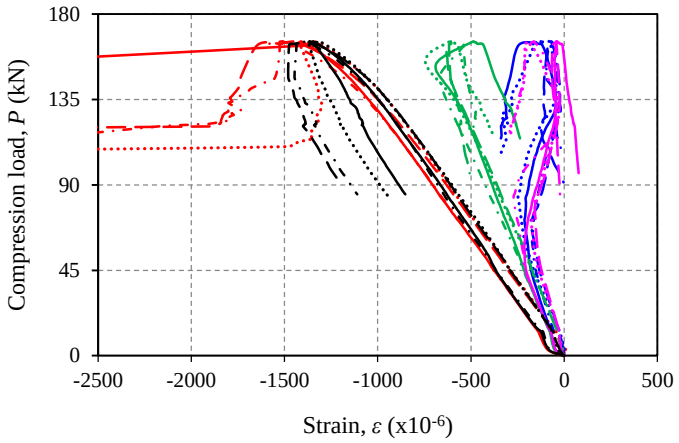

(c) Specimen C2S3

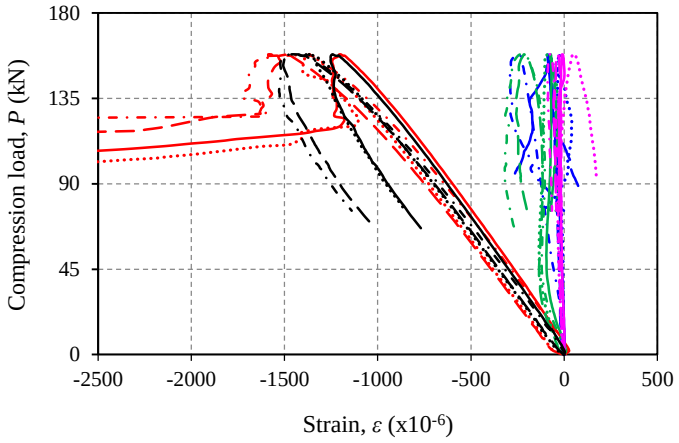

(d) Specimen C2S4

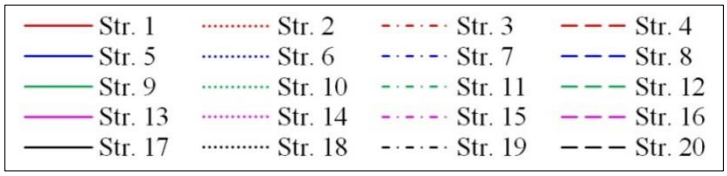

Figure 4.16 Strain responses for specimens of Group 2 (Continued.)

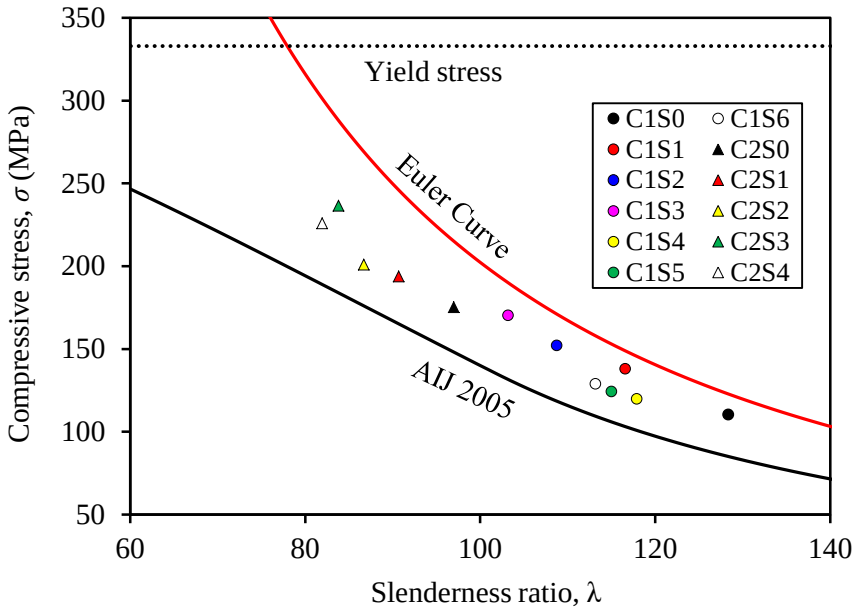

Figure 4.17 Strength design for strengthened specimen

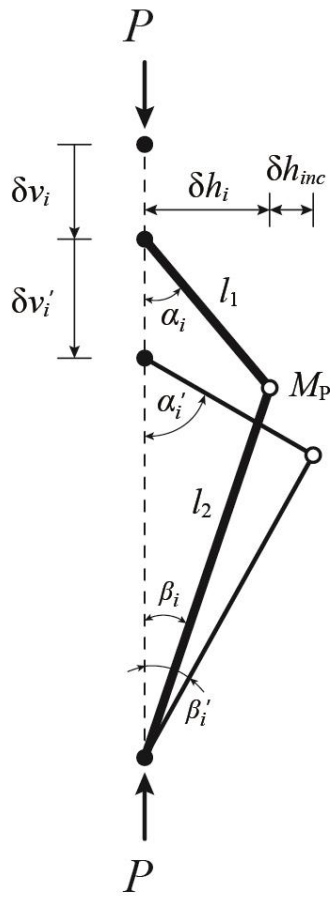

Figure 4.18 The strengthened specimen model for post-buckling prediction

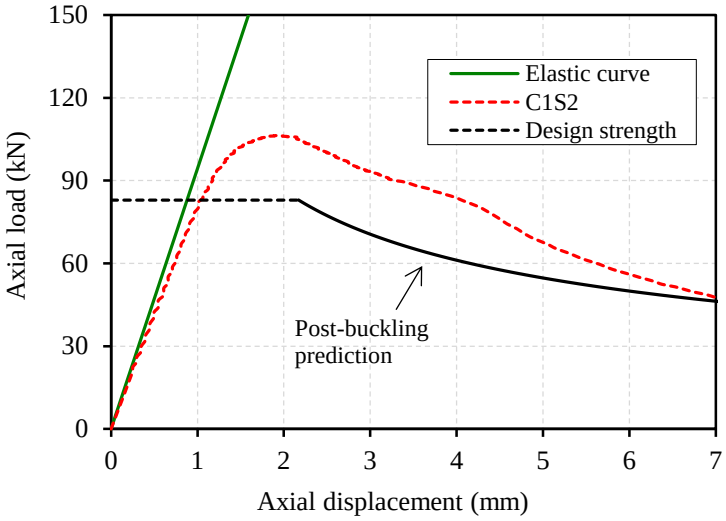

(a) Specimen C1S2

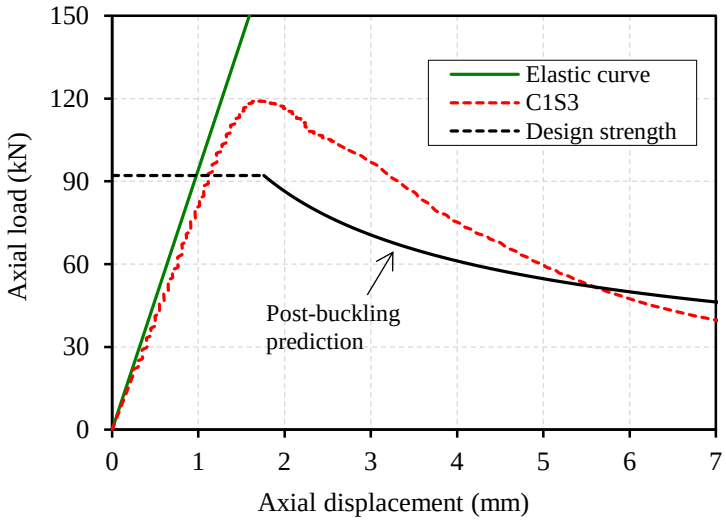

(b) Specimen C1S3

Figure 4.19 Post-buckling prediction for specimens C1S2 and C1S3

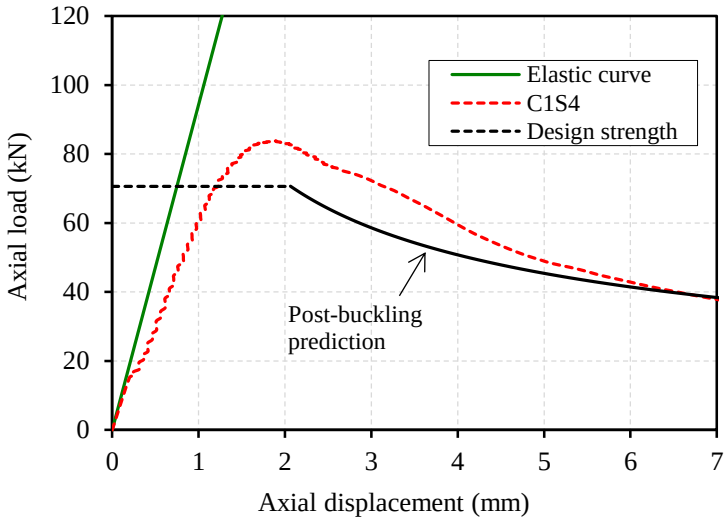

(a) Specimen C1S4

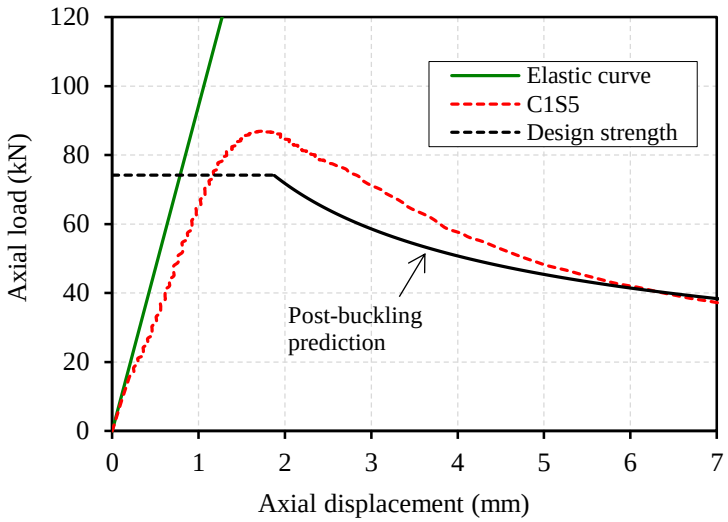

(b) Specimen C1S5

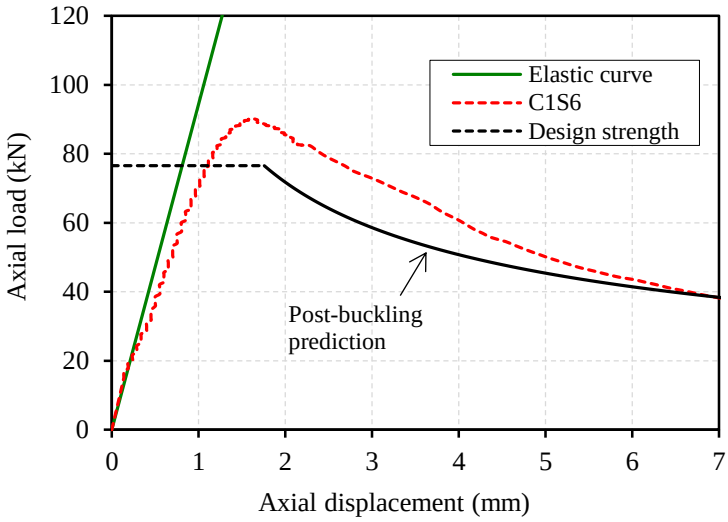

(c) Specimen C1S6

Figure 4.20 Post-buckling prediction for specimens C1S4, C1S5, and C1S6

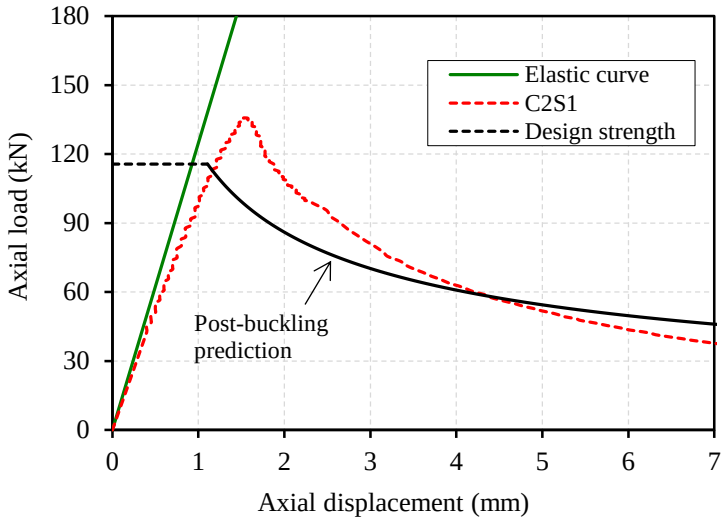

(a) Specimen C2S1

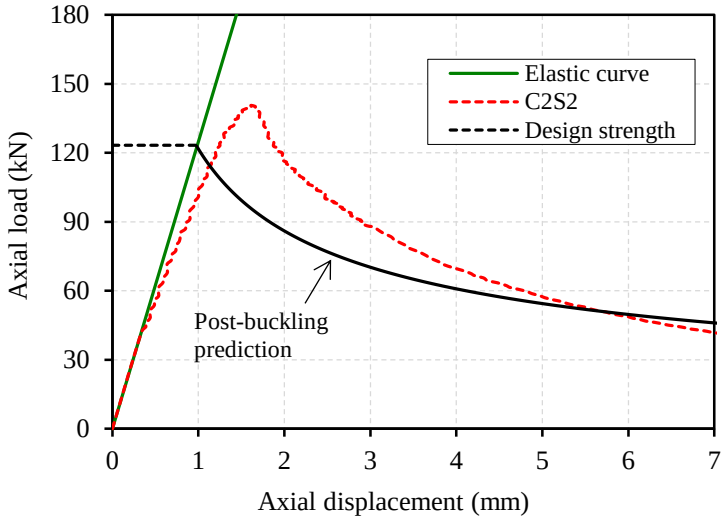

(b) Specimen C2S2

Figure 4.21 Post-buckling prediction for specimens C2S1 and C2S2

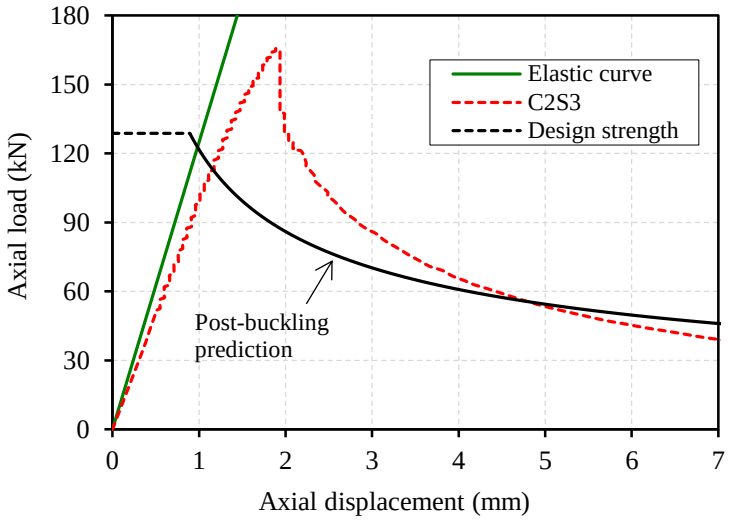

(a) Specimen C2S3

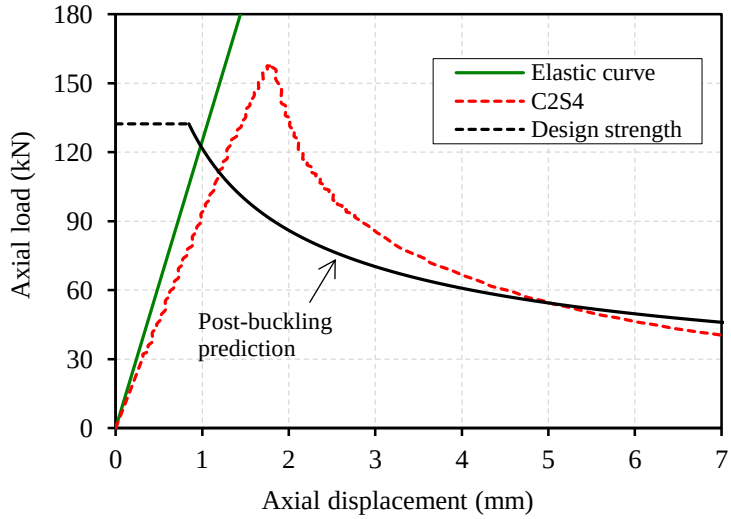

(b) Specimen C2S4

Figure 4.22 Post-buckling prediction for specimens C2S3 and C2S4

CHAPTER 5
ANGLE STEEL PARTIALLY-JACKETED CROSS SECTION

5.1 Introduction

This chapter also investigates the using of unbonded CFRP for strengthening angle steel. Unlike investigation in chapter 4, the angle steel is strengthened in scheme of partially-jacketed cross section. Unbonded CFRP is only applied in both legs of the angle steel. This experimental program is carried out to explore another alternative strengthening scheme that allows reduction in amount of CFRP usage. Experimental variables involved within this investigation, namely: number of CFRP layers, length of CFRP, and angle steel's slenderness ratio. Specimens strengthened with the proposed unbonded CFRP are then compared to control unstrengthened specimen to evaluate the improvement in buckling performance.

5.2 Experimental Program

5.2.1 Description of the Test Specimens

The specimens tested consist of two groups of angle steel with different slenderness ratio (λ). Each group has one control specimen that is not strengthened with CFRP. Specimens of Group A (λ = 128.4) are divided into two different CFRP lengths, i.e., 1000 mm and 500 mm, while specimens of Group B (λ = 97.02) has only 500 mm of CFRP length. Number of CFRP layers in strengthened specimens is varied to further investigate the effect of strengthening. The CFRP is positioned at middle part of angle steel as shown in Figure 5.1. Total specimens tested are thirteen where their detailed parameters as given in Table 5.1. As shown in the table, specimens are labeled for easy identification. The first combination of 'letter-number' describes angle steel and its buckling length, the second combination is CFRP length, and the last combination indicates number of CFRP layers. For instance, A16S10L25 identifies a specimen with 1636 mm buckling length, 1000 mm CFRP length, and 25 CFRP layers. Here, buckling length is a total of specimen length *L* (Figure 5.1) and thickness of additional steel plate (up to knife edge) at both ends of specimen (see Figure 5.5).

5.2.2 Material Properties

Angle steel L-65x6 is also used as the main material in this experiment. It has a grade SS400 according to JIS G3101. Figure 4.2 shows cross-section of the steel with values of each symbol given in Table 4.2 (see in Chapter 4). It should be noted that the measured wall thickness t_a is slightly smaller compared with the nominal wall thickness t given in the table, namely 5.56 mm. Material properties of the angle steel (i.e., elastic modulus, yield stress, and tensile strength) which are also presented in the table, are obtained from inspection certificate issued by manufacturer. No tensile coupon test is conducted for this study.

The CFRP laminates are made of bi-directional carbon fiber cloth (BT70-20). It is sheet-like shape. In one sheet, this carbon fiber has two directions of fiber which are perpendicular each other (see Figure 3.4). By this configuration, CFRP laminate having same properties in 0^o and 90^o directions of the weave can be easily produced. That is the reason behind of choosing this material in this study. Properties and characteristics of the carbon fiber BT70-20 are shown in Table 3.3. All the data given are based on manufacturer's data sheet. Besides carbon fiber, adhesive used is epoxy resin. This material has elastic modulus 1.285 GPa, Poisson's ratio 0.46, and tensile strength 16.47 MPa. These data are average values obtained from tensile test of six specimens which is conducted according to JIS K 7161-1:2014. Figure 5.2 shows representative of stress-strain curve of the epoxy resin.

5.2.3 Specimen Preparation

Both ends of angle steel are welded onto steel plate which will be used for installation of knife edges later on. Welding is carried out so that weak axis of the angle steel coincides with center line of the steel plate. All CFRP in strengthened specimens are created by method of Vacuum-assisted Resin Transfer Molding (VaRTM). The process begins by wrapping the angle steel at strengthening location (middle part) using a layer of peel ply. It is conducted without being preceded by any treatments on steel surface. Carbon fiber with a predetermined number of layers is then installed following the peel ply. The fiber direction of 0^o is positioned in same direction with longitudinal axis of the angle steel. The carbon fiber is installed so that CFRP will be created covering both legs of angle steel only, not in full cross-section (Figure 5.3). Afterwards, another peel ply is used again to cover the carbon fiber. Infusion meshes (resin media) are also attached after the peel ply to facilitate resin transfer during impregnation

process. A vacuum bag with strong gum tape connection is applied at the same time of installation PVC hose in both injection and suction sides. The next process is to impregnate resin by suction. After CFRP is molded, specimens are cured for at least one week before being tested. Figure 5.4 summarizes the steps of specimen preparation.

5.2.4 Test Setup and Instrumentation

All the strengthened and control specimens are tested under compression load using a 2000 kN capacity of Maekawa testing machine (Figure 5.5). The specimens are in pinned-end conditions and designed to buckle only in their weak axis (*v*-*v*, see Figure 4.2). To reach these goals, knife edge is installed at both ends of specimen where it must coincide with weak axis (*v*-*v*) of the angel steel (Figure 5.5). During the test, the applied load is measured by a load cell within the machine. A total of 20 strain gauges are installed scattered along the strengthened specimen to measure its longitudinal strain response. Meanwhile, for control specimen, only 12 strain gauges are utilized. Out-of-plane lateral displacement is measured by displacement transducers. The lateral displacement is measured at three different locations: around the bottom edge of CFRP, mid-height of specimen, and around the top edge of CFRP. Detail position of strain gauges and displacement transducers for both control and strengthened specimens are shown in Figure 5.6.

5.3 Experimental Results

Table 5.2 summarizes the test results, namely maximum load capacity, CFRP thickness, and fiber volume content of the laminates. Also presented in Table 5.2 is strengthening effect due to the application of unbonded CFRP. The strengthening effect is given as ratio of difference in maximum load capacity of each specimen (compared with control unstrengthened specimens) and maximum load capacity of the appropriate control unstrengthened specimen (A16S00L00 or A12S00L00). Based on Table 5.2, it is clear that unbonded CFRP provides positive strengthening effect. The highest effect can be found in specimen A16S10L35 namely 69.13%, whereas the lowest is attained by specimen A16S05L18 (7.123%). Generally, the positive strengthening effect and its variation in values are attributed to delaying overall buckling due to higher as well as different values of flexural stiffness of the unbonded CFRP existed in each specimen. The difference in flexural stiffness of CFRP becomes a certainty as several parameters have been applied, e.g., number of CFRP layers and CFRP length. Besides that, another factor that also exists is the difference in fiber content of CFRP in each specimen, as

presented in Table 5.2. The fiber content also contributes to flexural stiffness of CFRP, although not as much as of number of CFRP layers or CFRP length, through creating elastic modulus of the laminates. Theoretically, the higher fiber volume content, the higher elastic modulus of CFRP will be created, and thus the higher flexural stiffness will be produced.

5.3.1 Fiber Volume Content

The fiber content, as presented in Table 5.2, is a ratio between total thickness of carbon fiber used (number of layers x 0.112 mm) and thickness of CFRP. The thickness of CFRP (t_{CF}) is calculated by involving wall thickness of specimen at strengthened part (t_{tot}) and wall thickness of angle steel (t_a = 5.56 mm), namely $t_{CF} = 0.5\ (t_{tot} - t_a)$. It is evident from Table 5.2 that all CFRP has fiber content higher than 50%. Therefore, besides of being as expected, this also confirms an advantage of the VaRTM process in producing CFRP laminates over other techniques (e.g., hand-layup).

5.3.2 Load-displacement Response

Figure 5.7 shows the load versus axial-displacement response of all specimens in Group A and B. It can be seen from the figure that the curves provide a steep initial response before reaching maximum load. After maximum load, the axial displacement increases rapidly as the compressive load gradually decreases. Figure 5.7 graphically proves that the presence of unbonded CFRP increases maximum load but it does not affect initial axial stiffness of the strengthened specimens. Slope of the curves remains unchanged compared to control unstrengthened specimen. This is reasonable as the CFRP is not directly stuck onto steel (unbonded), which mean that elastic behavior of the structure will not be affected.

The load-lateral displacement responses at mid-height of specimens are provided in Figure 5.8. The curves show a steep response before overall buckling occurs. Afterward, lateral displacement increases rapidly. Displacement curve of specimen A16S10L35 appears in negative value indicating that this specimen buckles in opposite direction of the others. It is clear from Figure 5.8 that unbonded CFRP reduces the lateral deflection.

5.3.3 Effect of Different Parameters

The increasing number of CFRP layer gives positive effect in enhancing buckling strength of the angle steel. It is confirmed from Figure 5.9 and Table 5.2. Moreover, it can also be seen from Figures 5.7 and 5.8. The strength increases for strengthened

specimens in Group A ranged from 7.123% to 69.13%, but in Group B the increases are only varied between 7.742% and 25.67%. The trend of increasing strength as increasing number of CFRP layers is experienced by all strengthened specimens with appropriate CFRP length in both Group A and B. However, an exception is only for specimen A12S05L30 which has 30 CFRP layers. The strength increase of this specimen, i.e., 22.45%, is not larger than that of specimen A12S05L25 (25.71%) which has only 25 CFRP layers. A reason behind this is most likely due to higher imperfection owned by A12S05L30. The imperfection is indeed not measured in this study but it can be reflected by load-lateral displacement curve of this specimen (see Figure 5.8a). The curve is known to be less vertical (before reaching ultimate load) as compared to that of specimen A12S05L25.

The effect of CFRP length can be well captured through comparison of specimens in Group 1 (see Table 5.2), where two kinds of CFRP lengths are investigated, namely 500 mm and 1000 mm. For easy visualization, the comparison is presented in Figure 5.9a. It is clear from Figure 5.9a and Table 5.2 that strength increase is higher for specimens with longer CFRP. The difference in strength increase between specimens A16S10L18 (34.03%) and specimen A16S05L18 (7.12%), both have 18 layers of CFRP, is 34.04% - 7.12% = 26.92%. This value is almost unchanged compared with the difference in strength increase of other specimens (A16S10L25 and A16S05L25), where the number of CFRP layers is increased to 25, i.e., 46.28% - 17.97% = 28.31%. However, for larger than 25 CFRP layers, specimens with 1000 mm of CFRP length (e.g., A16S10L30) tend to have more higher strength increase compared to specimen with 500 mm CFRP length (A16S05L30).

Figure 5.9b shows the effect of different angle steel's slenderness ratio (λ) on strength increase of the strengthened specimens. Detail percentage of the increases is presented in Table 5.2. It is found from Figure 5.9b and Table 5.2 that a higher strength increase belongs to specimens with smaller steel’s slenderness ratio. This condition is clearly demonstrated by all comparable specimens (similar number of CFRP layers) between Group A and B having CFRP length of 500 mm. Even in one case, compared to specimen with larger λ (A16S05L18, 18 CFRP layers), a higher strength increase is still owned by specimen with smaller λ (A12S05L10) even though fewer layers of CFRP are used (only 10 layers).

5.3.4 Failure Mode and Strain Response

All control specimens undergo failure due to overall buckling of pinned-end columns, as shown in Figure 5.10a and 5.10i. Plastic hinge is confirmed at mid-height of the specimens. For the unbonded CFRP strengthened angle steel, three different failure modes can be observed. The first mode of failure is that the plastic hinge is located around the edge of the CFRP (outside CFRP strengthening zone), not at mid-height of the specimens, as shown in Figure 5.10(c-d, f-h, and k-m). The buckling curvatures are similar to each other, toward the inner side of the angle steel. In this case, the CFRP laminates can perform their duty as a stiffener without suffering damage. In the second mode, the specimen fails when the plastic hinge lies within the strengthening zone, as shown in Figure 5.10 (b and j). The direction of the curvature remains the same as the former failure mode, i.e., to the inner side of the angle steel. This mode of failure occurs when the number of CFRP layers is lower (A16S10L18 and A12S05L10), meaning that the CFRP does not have the appropriate stiffness to overcome overall buckling of the angle steel. Thus, the CFRP at the outer side of the angle steel peels off and the CFRP at the inner side of the angle steel is under compression, which can be damaged when excessive load is applied (see Figures 5.10b and 5.10j).

The last failure mode occurs when the plastic hinge is within the CFRP strengthening zone but the buckling curvature occurs towards the outer side of the angle steel, as experienced by specimen A16S10L35 (Figure 5.10e). This type of failure mode tends to occur as the number of CFRP layers increases. This trend can be easily seen in specimens belonging to Group A which have a CFRP length of 1000 mm (Figure 5.8a). It is clear from Figure 5.8a that the lateral deflection curve (before reaching maximum load) becomes steeper as the number of CFRP layers increases from 18 (A16S10L18) to 25 (A16S10L25). It is only within the extreme condition of the use of 30 CFRP layers that the specimen curve (A16S10L30) becomes perfectly vertical. Beyond this, a larger number of layers makes the curve response change to a negative value (specimen A16S10L35). This means that the buckling curvature occurs in the opposite direction (Figure 5.10e). The reason behind this failure mode is that, in addition to the increase in the CFRP stiffness due to the increase in the number of CFRP layers, loading eccentricity (in terms of the centroid of the CFRP's cross section) also increases. The larger number of CFRP layers leads to a larger change in the centroid of the CFRP cross section, but the position of the applied load remains unchanged on the weak axis of the angle steel cross section.

Figures 5.11 to 5.14 show the load versus longitudinal strain response of all specimens tested in this study. It is confirmed by Figures 5.11 and 5.13 (control specimens) that only compressive strain at mid-height of the specimens continues to develop and reaches the angle steel yield strain at about 0.16%. This finding corresponds to the failure modes previously discussed. For strengthened specimens, the strain on CFRP also increases, but the rate of increase at the end of CFRP is smaller than that of at the middle, and it only occurs up to a certain load (the load where strain stops developing or returns to zero), e.g., in specimen A12S05L18 (see Figure 5.14b for easy visualization, the load is around 60 kN). In other specimens, the strains in CFRP may not develop at all or develop only up to a very small load, for example, specimens A12S05L25 or A12S05L30 (Figures 5.14(c or d)). These two specimens have higher CFRP stiffness as a result of many layers of CFRP and shorter CFRP length. In some other specimens (mainly in Group A), the load at which the strain stops developing may not be easily identified. The increase in compressive strains on CFRP in all of the strengthened specimens indicates the existence of a minor bond of CFRP to steel. This is highly possible because during the VaRTM process, the resin will also impregnate into the peel ply.

5.4 Summary and Conclusions

Experimental test was conducted to angle steels which were strengthened using unbonded CFRP in scheme of partially-jacketed cross section. The CFRP was applied in both legs of the angle steel through a process of VaRTM. Based on the experimental investigation, the following findings can be drawn:

1. The unbonded CFRP with partially-jacketed cross section strengthening scheme could increase buckling capacity of the angle steel by up to 69.13%.
2. Buckling capacity of the angle steel increased with increasing number of CFRP layers and CFRP length. In addition, for the same CFRP length, the increase in buckling capacity was greater for specimens with shorter angle steel.
3. Based on position of plastic hinge, failure modes of the strengthened specimens could be divided into two: plastic hinge around the end of CFRP (outside CFRP strengthening zone) and plastic hinge within the CFRP strengthening zone. Both failure modes were affected by flexural stiffness of the CFRP laminates.
4. The VaRTM process could produce CFRP laminates with a higher fiber volume content (around 60%).

Table 5.1 Detail parameter of test specimens

Specimen name	CFRP layer (plies)	CFRP length (mm)	Buckling length (mm)	Angle steel's slenderness ratio
Group A				
A16S00L00	-	-	1636	128.4
A16S10L18	18	1000	1636	128.4
A16S10L25	25	1000	1636	128.4
A16S10L30	30	1000	1636	128.4
A16S10L35	35	1000	1636	128.4
A16S05L18	18	500	1636	128.4
A16S05L25	25	500	1636	128.4
A16S05L30	30	500	1636	128.4
Group B				
A12S00L00	-	-	1236	97.02
A12S05L10	10	500	1236	97.02
A12S05L18	18	500	1236	97.02
A12S05L25	25	500	1236	97.02
A12S05L30	30	500	1236	97.02

Table 5.2 Test results

Specimen name	CFRP thickness (mm)	Fiber content (%)	Max. Load (kN)	Strengthening effect (%)
Group A				
A16S00L00	-	-	77.22	-
A16S10L18	3.34	60.35	103.5	34.03
A16S10L25	4.58	61.15	113.0	46.34
A16S10L30	5.50	61.11	125.9	63.04
A16S10L35	6.38	61.47	130.6	69.13
A16S05L18	3.39	59.44	82.72	7.123
A16S05L25	4.65	60.22	91.10	17.97
A16S05L30	5.62	59.84	92.05	19.20
Group B				
A12S00L00	-	-	122.7	-
A12S05L10	1.97	56.76	132.2	7.742
A12S05L18	3.30	61.17	140.8	14.75
A12S05L25	4.78	58.59	154.2	25.67
A12S05L30	5.60	59.96	150.2	22.41

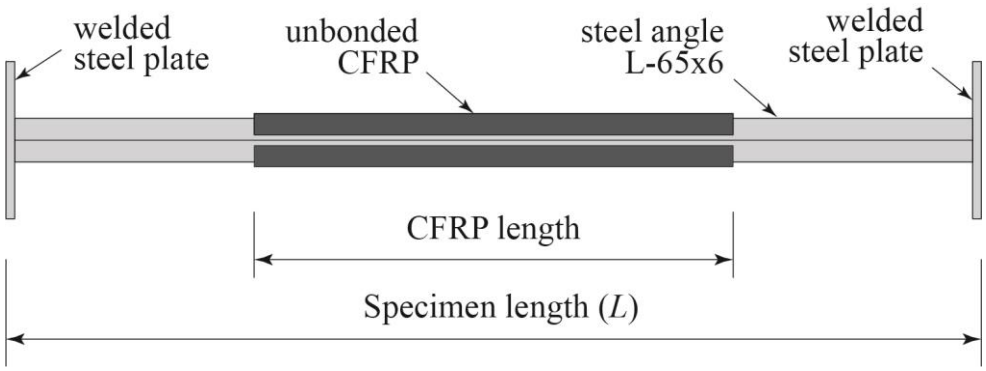

Figure 5.1 Configuration of test specimen

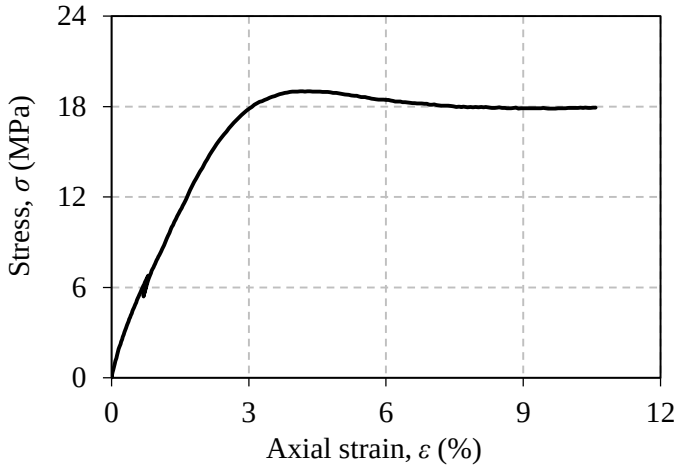

Figure 5.2 A representative stress-strain curve of resin

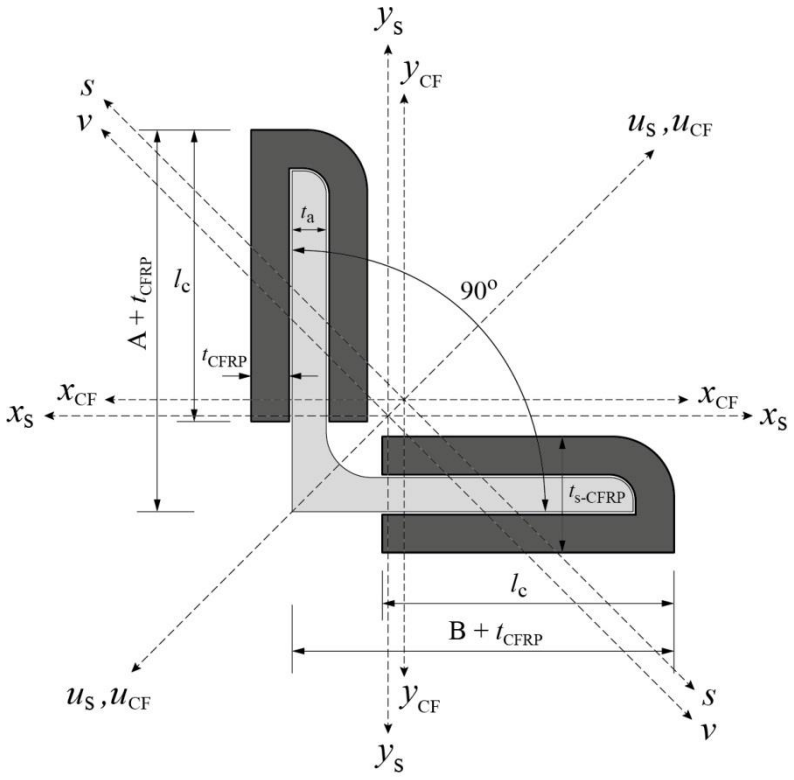

Figure 5.3 Strengthening scheme of angle steel

Figure 5.4 Specimen preparation

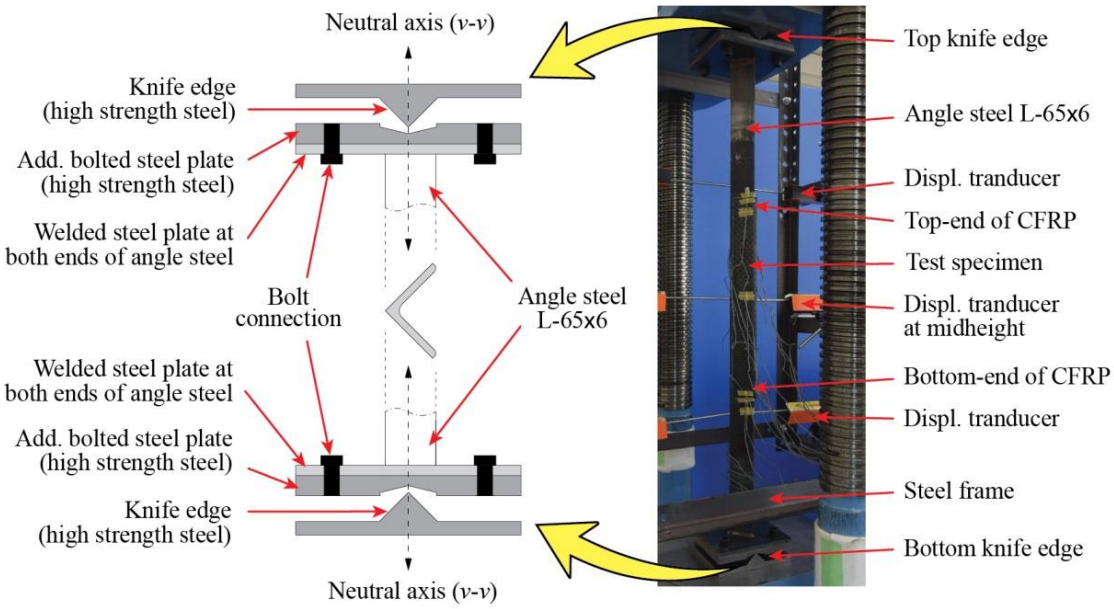

Figure 5.5 Test setup

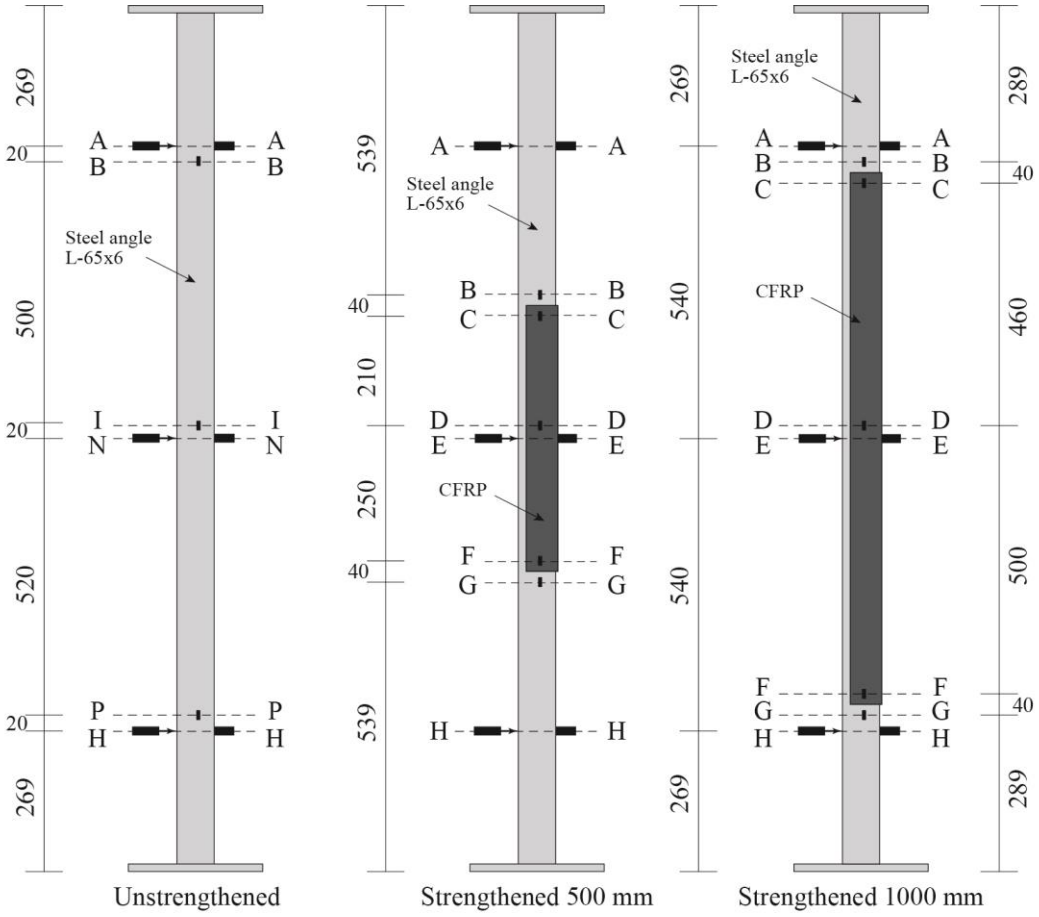

(a) Specimens of Group A

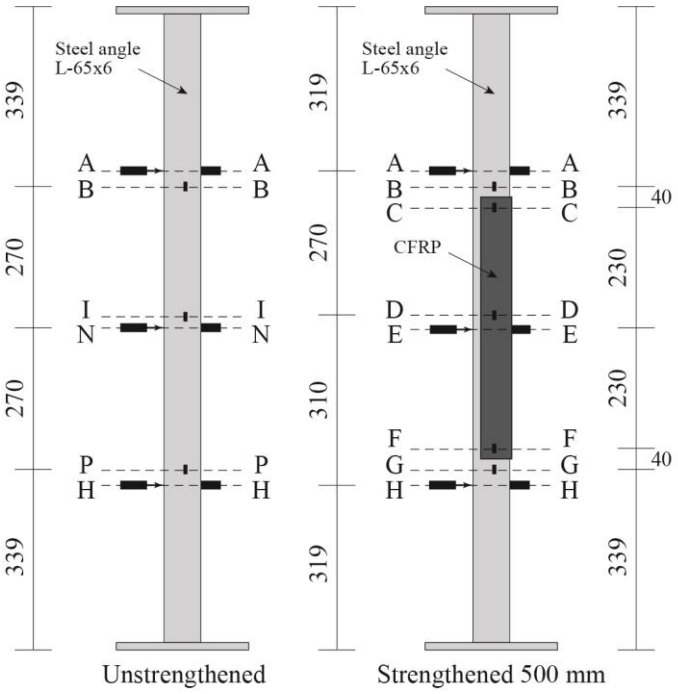

(b) Specimens of Group B

Figure 5.6 Position of displacement transducers and strain gauges

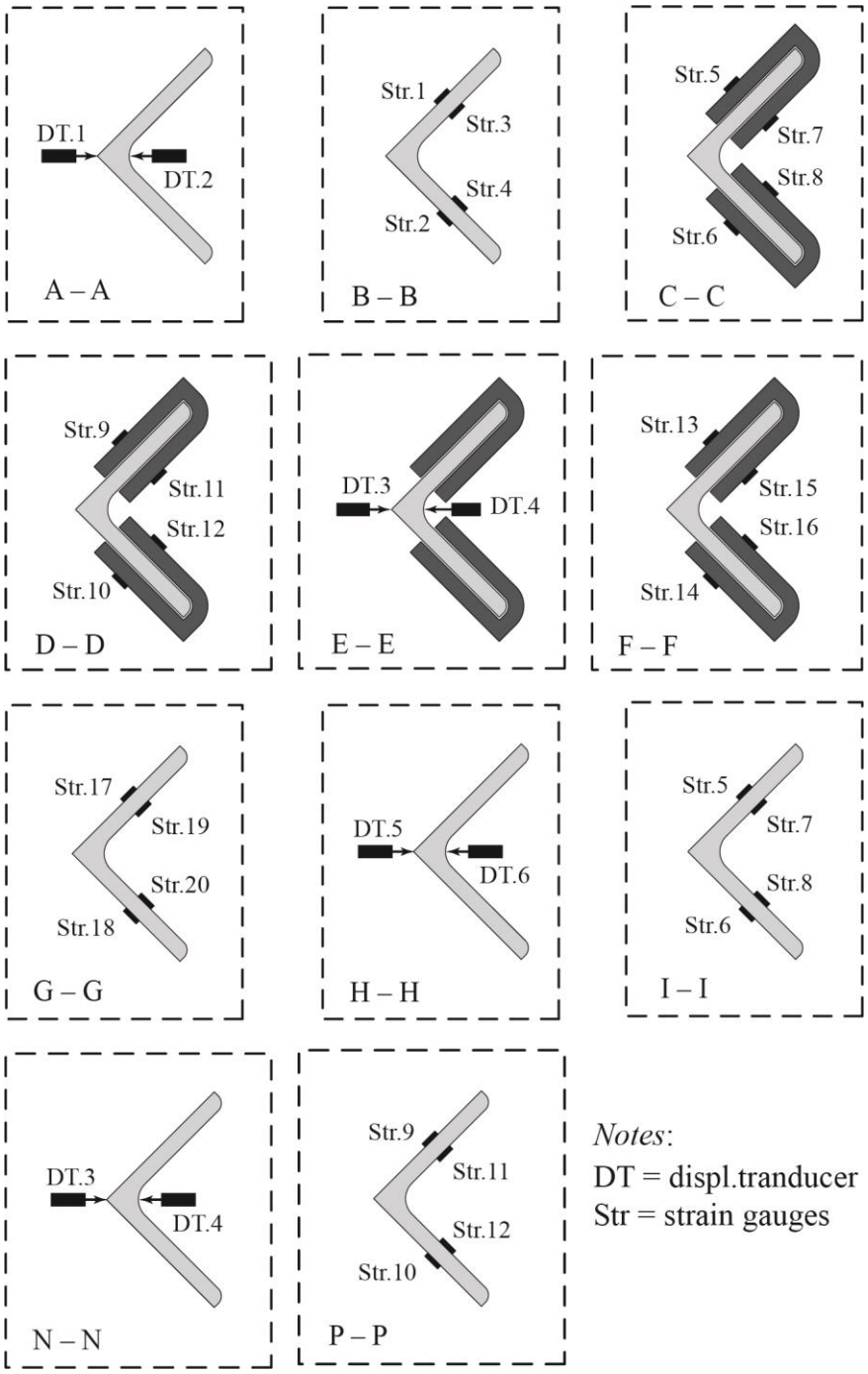

(c) Detail in cross-section

Figure 5.6 Position of displacement transducers and strain gauges (Continued.)

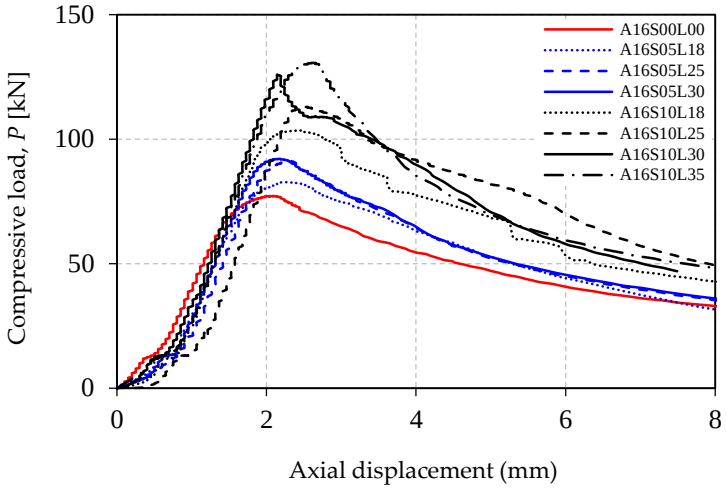

(a) Specimens of Group A

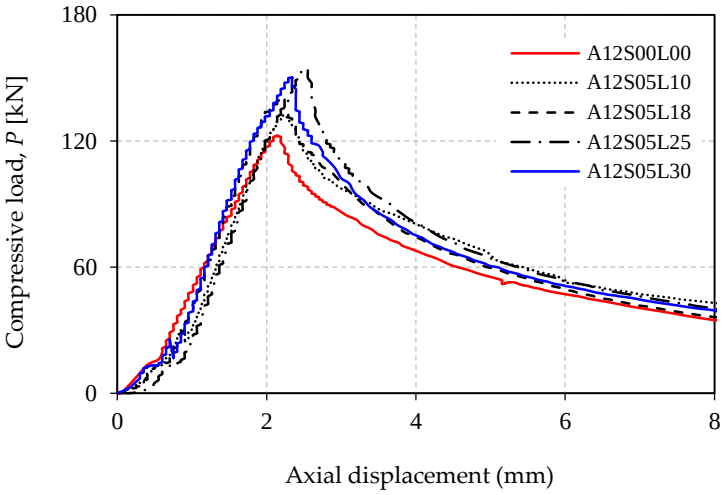

(b) Specimens of Group B

Figure 5.7 Load - axial displacement relationships

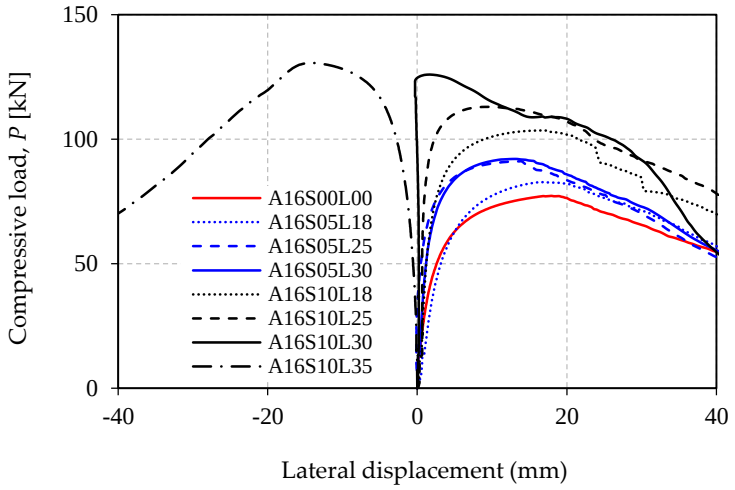

(a) Specimen of Group A

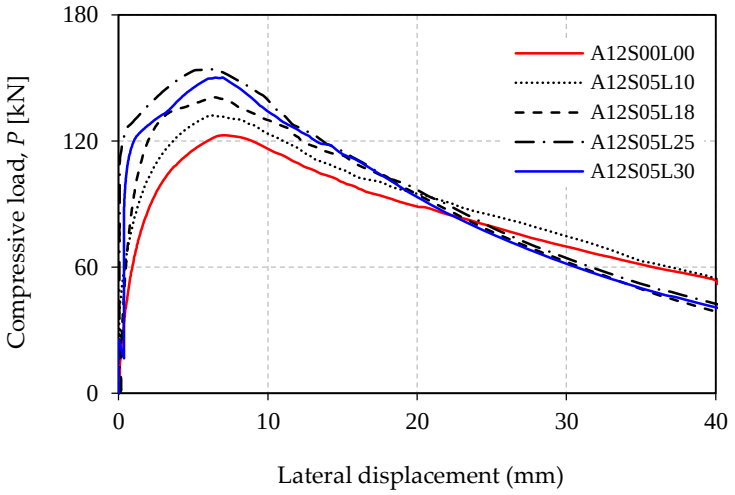

(b) Specimen of Group B

Figure 5.8 Load - lateral midheight displacement relationships

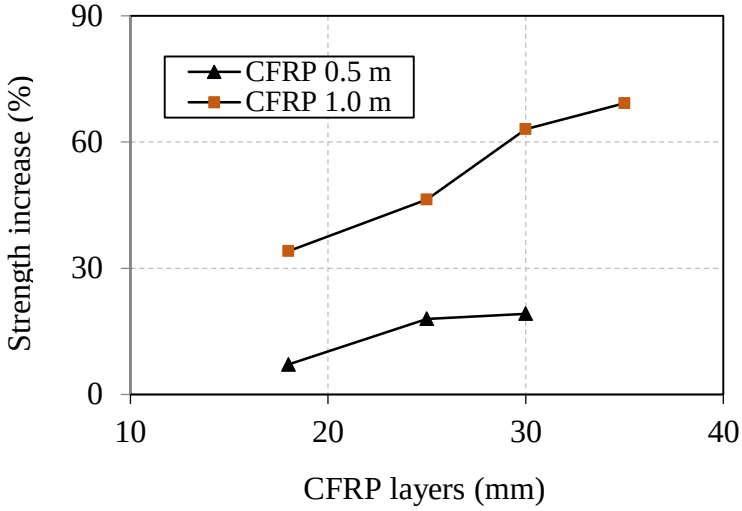

(a) effect of CFRP length (λ = 128.4)

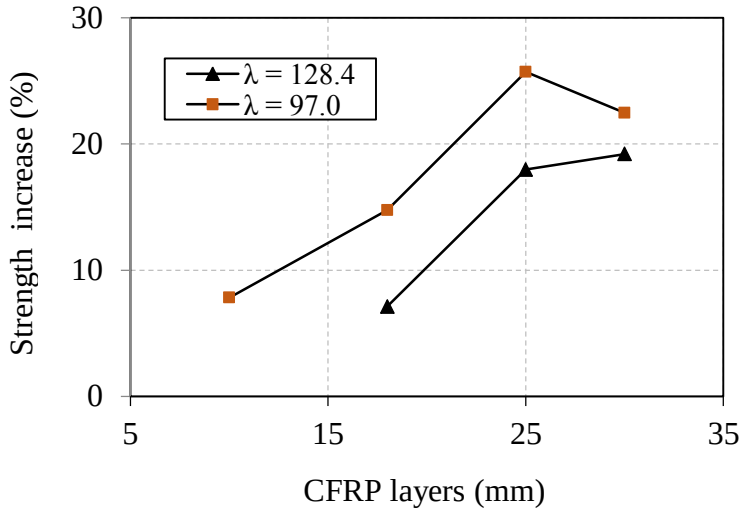

(b) effect of angle steel's slenderness ratio (CFRP length = 500mm)

Figure 5.9 Effect of different parameters

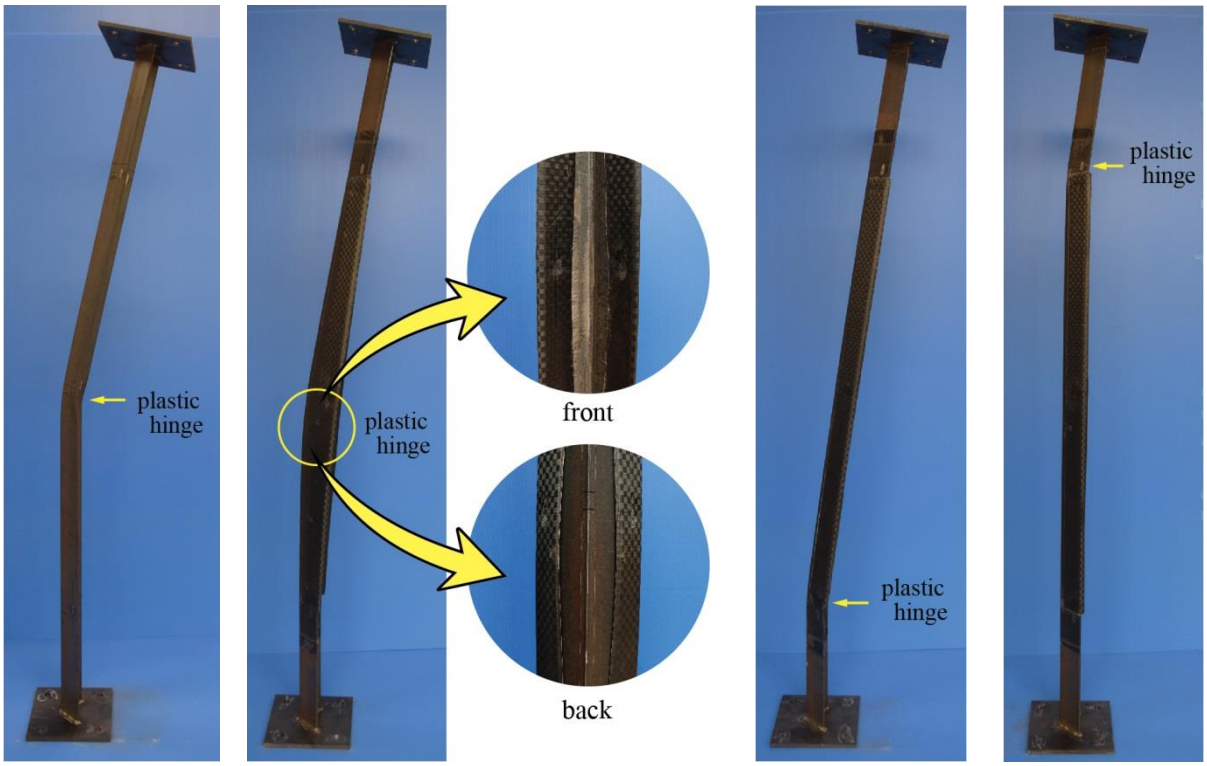

(a) A16S00L00 (b) A16S10L18 (c) A16S10L25 (d) A16S10L30

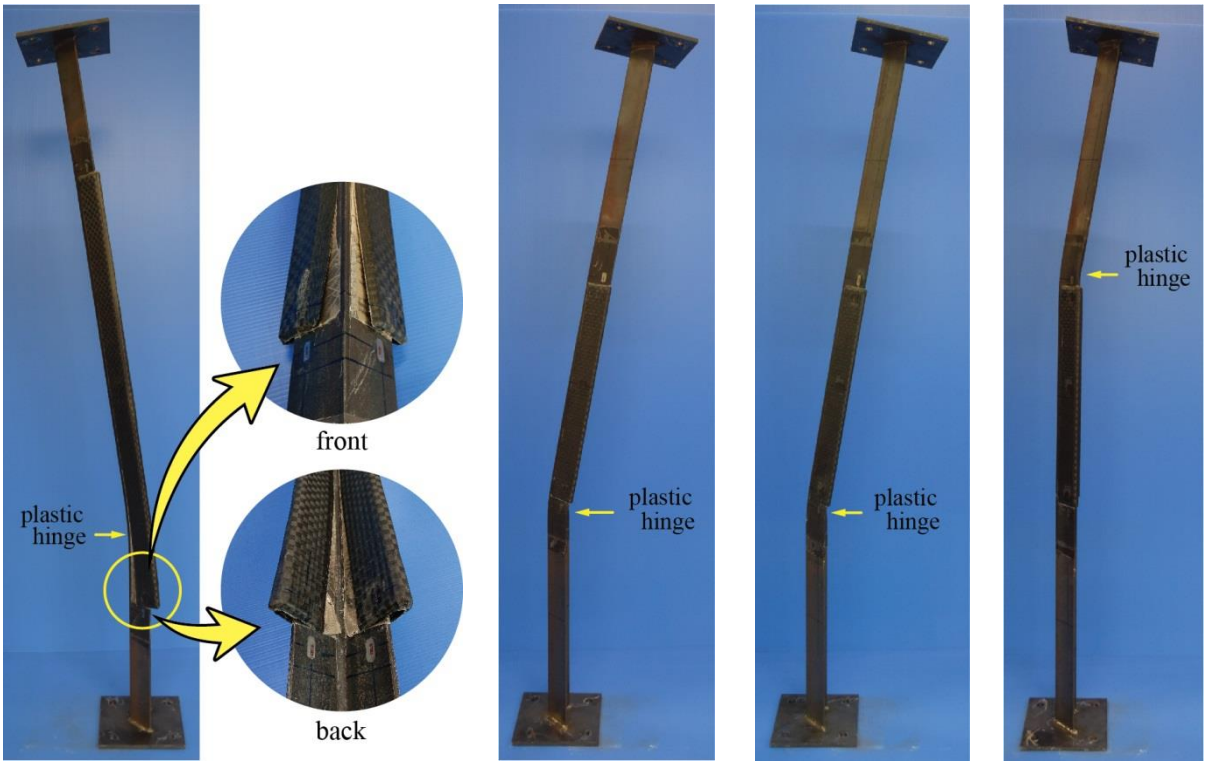

(e) A16S10L35 (f) A16S05L18 (g) A16S05L25 (h) A16S05L30

Figure 5.10 Failure modes

(i) A12S00L00

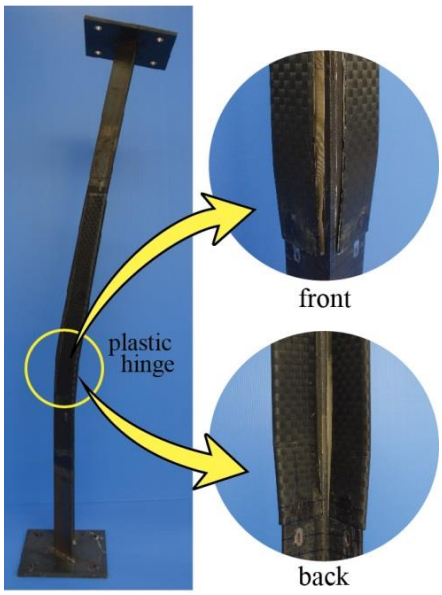

(j) A12S05L10

(k) A12S05L18

(l) A12S05L25

(m) A12S05L30

Figure 5.10 Failure modes (Continued.)

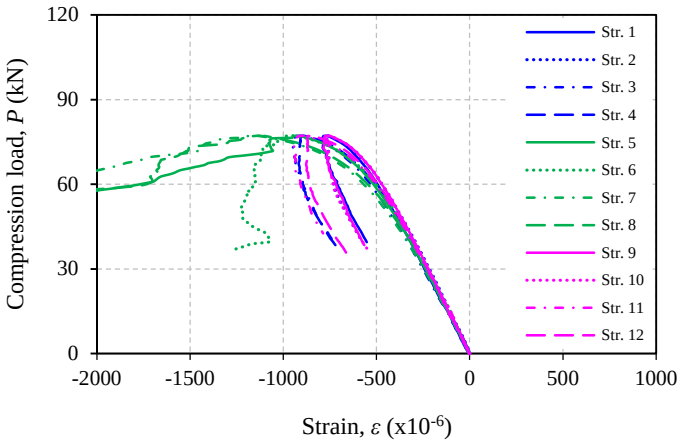

Figure 5.11 Strain responses for specimens A16S00L00

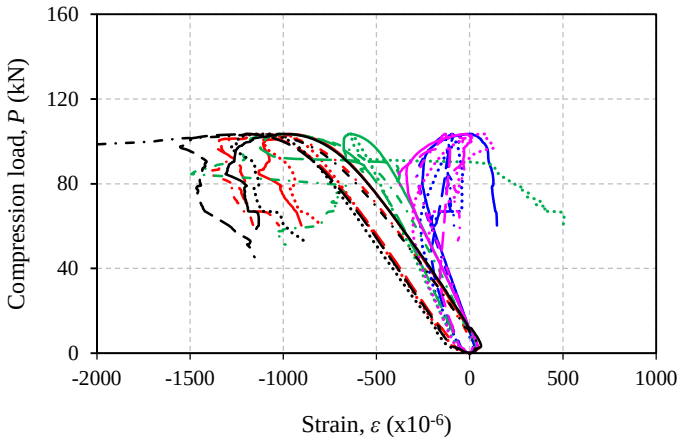

(a) Specimen A16S10L18

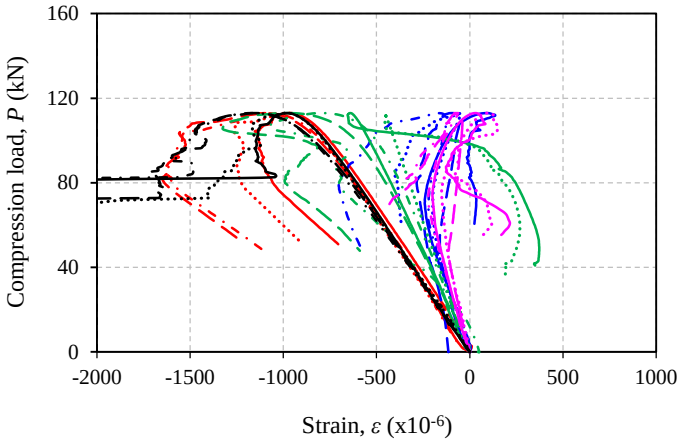

(b) Specimen A16S10L25

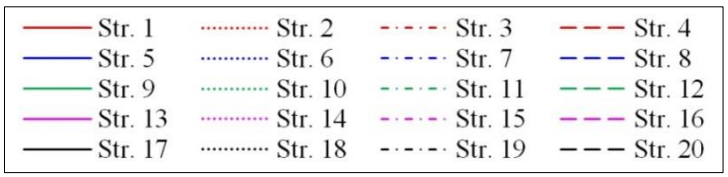

Figure 5.12 Strain responses for specimens of Group A

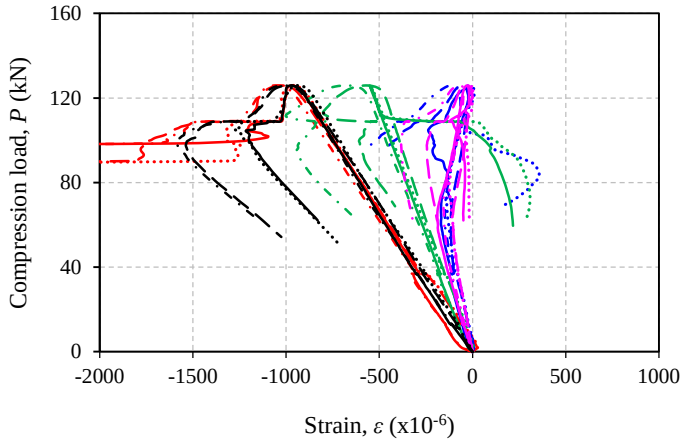

(c) Specimen A16S10L30

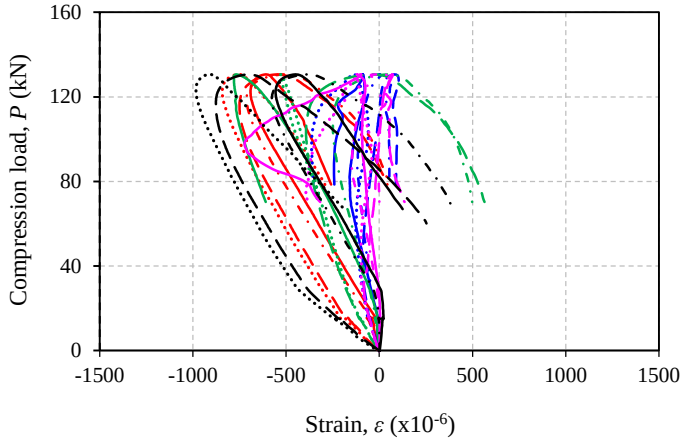

(d) Specimen A16S10L35

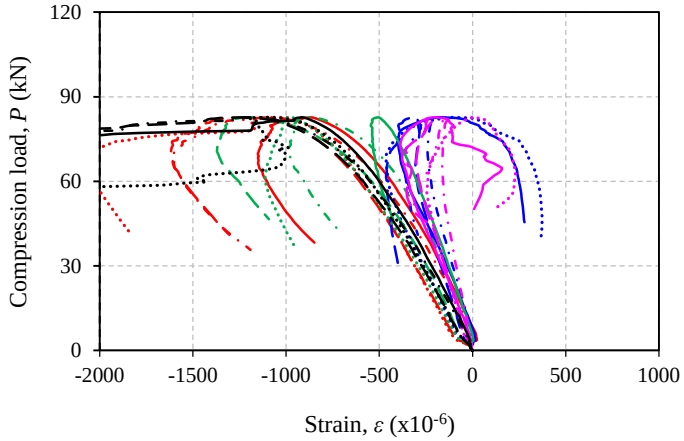

(e) Specimen A16S05L18

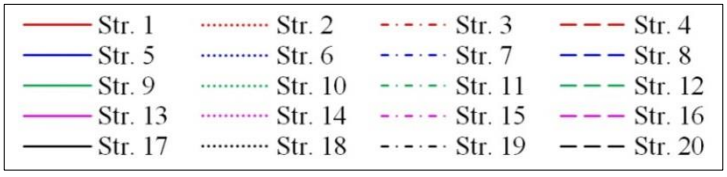

Figure 5.12 Strain responses for specimens of Group A (Continued.)

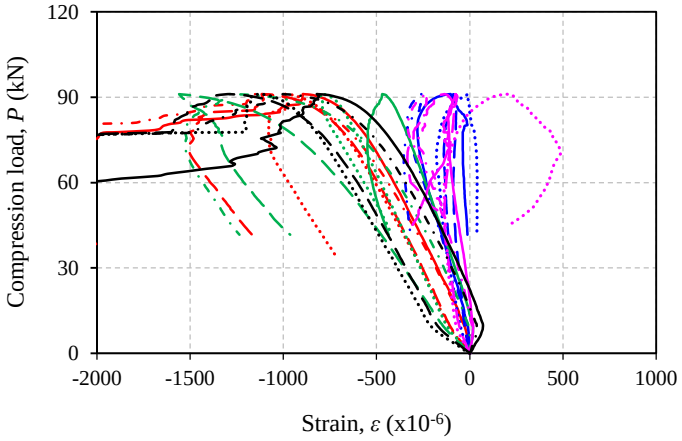

(f) Specimen A16S05L25

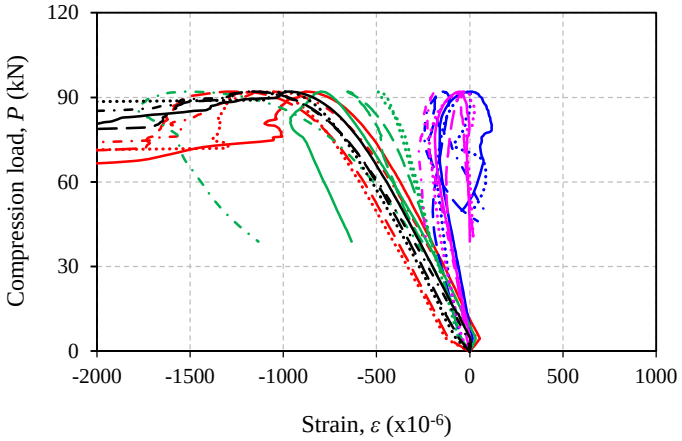

(g) Specimen A16S05L30

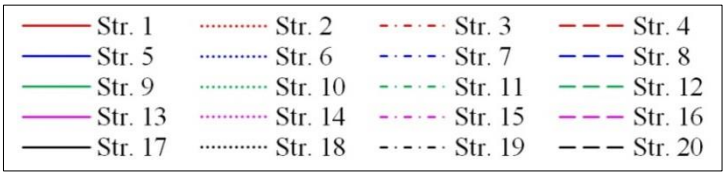

Figure 5.12 Strain responses for specimens of Group A (Continued.)

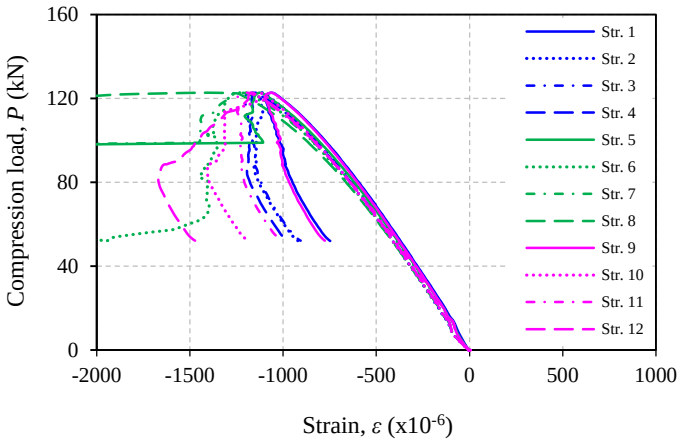

Figure 5.13 Strain responses for specimens A12S00L00

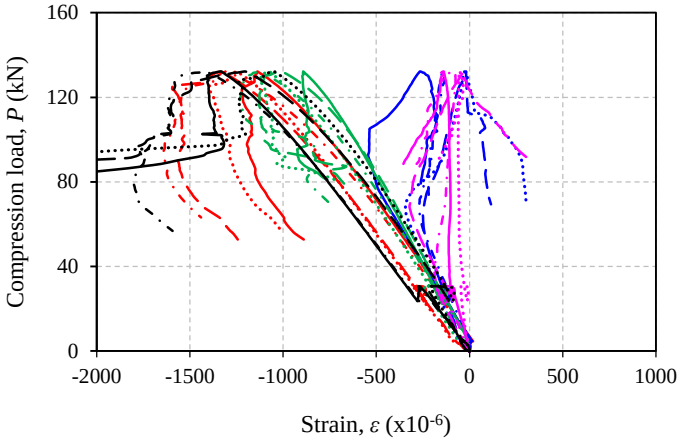

(a) Specimen A12S05L10

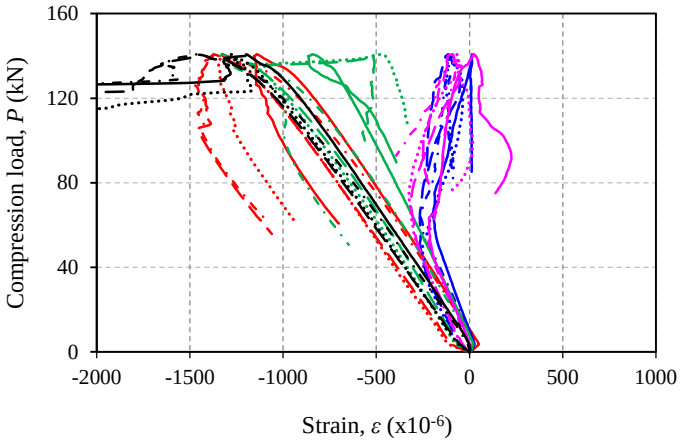

(b) Specimen A12S05L18

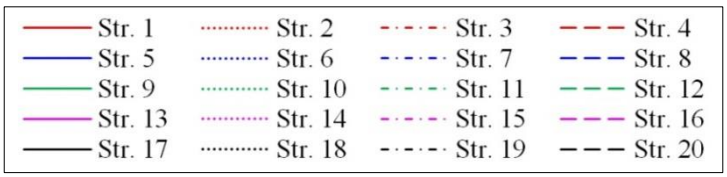

Figure 5.14 Strain responses for specimens of Group B

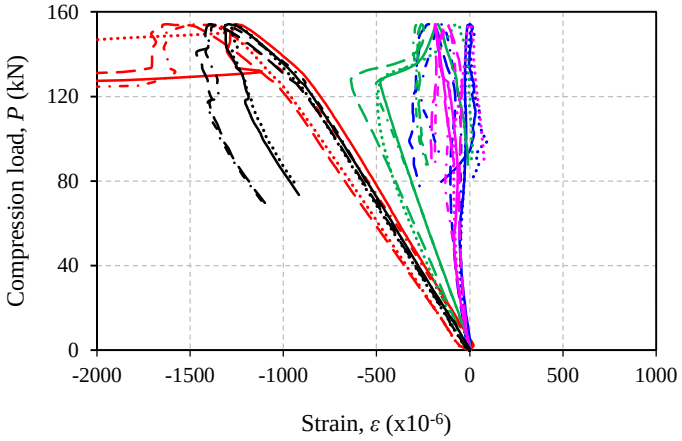

(c) Specimen A12S05L25

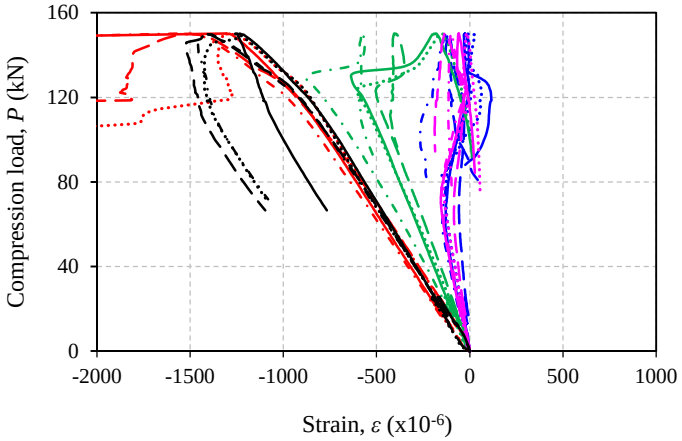

(d) Specimen A12S05L30

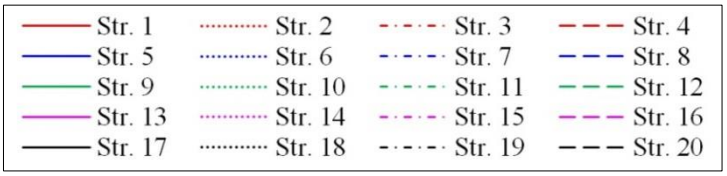

Figure 5.14 Strain responses for specimens of Group B (Continued.)

CHAPTER 6
SUMMARY AND CONCLUSIONS

6.1 Summary

The use of CFRP laminates for strengthening of steel structures has attracted a great deal of attention recent years replacing conventional methods of bolting or welding additional steel plates. The CFRP material is preferred due to its excellent nature of light weight, high strength, and excellent in fatigue and corrosion resistance. It is also easy to assemble so that it holds a great promise for on-site application. Most of the research conducted in the area of strengthening steel with CFRP has focused on strengthening by adhesively-bonding technique where the CFRP is attached to steel using adhesive material. A number of published literatures are reviewed in this dissertation regarding this strengthening method and the factors affecting the bonding performance of CFRP to steel substrate.

A research program is conducted to investigate a new and promising method for strengthening steel structures with CFRP, namely unbonded CFRP strengthening. This strengthening method does not exploit the bonding approach between CFRP and steel so that no steel surface treatment is required at all. Strength contribution is expected to be obtained only from rigidity of CFRP. The research study, in particular, investigated the use of unbonded CFRP to improve the buckling performance of axial compression steel members. Effect of several parameters, such as number of CFRP layers, CFRP length, and steel slenderness ratio, on the improvement of structural performance is explored.

An experimental, analytical, and finite element study is conducted to investigate the buckling performance of compression steel bars. As the first phase of investigation, steel bars (small scale members) are used for easy and simplicity of implementation. The strengthening requirements for the unbonded CFRP are derived from analytical models. In experimental work, the unbonded CFRP is fabricated by Vacuum-assisted Resin Transfer Molding process. A total of eight compression steel bar specimens, including control un-strengthened specimens, with pinned-end conditions are prepared and tested under monotonic loading. The load-deflection behavior of each specimen is recorded along with failure modes and longitudinal strain responses. A finite element

model of the test specimens is developed and validated with the experimental results. The validated model is then used in parametric study to further investigate the influential identified variables in the experimental program. Additional analytical work is carried out to determine strength recommendation values for the unbonded CFRP strengthened members. In this stage, an equivalent slenderness ratio is proposed. The validity of the equivalent slenderness ratio method in determining strength recommendations for the unbonded CFRP strengthened steel bars is verified by three different provisions: AIJ 2005, CAN/CSA S16-9, and ANSI/AISC 360-16.

The potential use of the unbonded CFRP strengthening technique to strengthen real-scale structural steel member is investigated through buckling test of angle steel. The unbonded CFRP are designed based on analytical model of stiffening requirements developed from the axial steel bars study. The unbonded CFRP is also fabricated by the VaRTM technique. None of the steel surface treatments are applied. The advantage of the VaRTM technique in creating CFRP with higher fiber content is demonstrated in this study. The buckling performance of all specimens strengthened with the proposed strengthening method is compared to the responses of the angle steel specimen without strengthening to evaluate the improvement in performance obtained. In addition, the effectiveness of the proposed method of equivalent slenderness ratio for determining strength recommendation values for the unbonded CFRP strengthened angle steel is also validated.

Additional experimental test to explore another alternative strengthening scheme for angle steel is also carried out. In this study, the unbonded CFRP is not applied to cover entire cross section of the angle steel but only on both legs. This allows the use of less amount of CFRP. The response of the unbonded CFRP strengthened specimens is then compared to the control unstrengthened specimens. The strengthening effect of the CFRP is scrutinized for a different number of CFRP layers, CFRP lengths, and the angle steel's slenderness ratios. Failure modes and strain responses of the specimens are also discussed.

6.2 Conclusions

Based on experimental, analytical, and finite element studies conducted in this dissertation, the following conclusions can be drawn:

1. The proposed unbonded CFRP strengthening method can successfully increase the buckling capacity of axial compression steel members. Therefore, it can be exploited to improve an overall behavior of steel structures.
2. Analytical model derived for stiffening requirements can be used to effectively determine the amount of CFRP required for strengthening.
3. The developed finite element model for axial steel members provides a good comparison to the experimental test results.
4. Improvement in buckling capacity of axial steel members can be affected by number of CFRP layers, CFRP length, and steel's slenderness ratio.
5. The method of equivalent slenderness ratio is also proposed in this study and can be used effectively to determine the strength recommendation values for the axial compression steel members strengthened with unbonded CFRP.
6. The effectiveness of the proposed unbonded CFRP strengthening method for application to real-scale structural steel members is proven through its success in increasing the buckling capacity of angle steel members.
7. VaRTM technique utilized in this study is proven to be able to produce CFRP laminates with higher fiber contents (>50%).

6.3 Recommendations for Future Research

The following are recommended research topics for future investigation in order to better understand about the behavior of the proposed method of unbonded CFRP for strengthening steel:

1. The characteristic interaction between CFRP laminates and steel substrate were not investigated in this study. An experimental program could be carried out to investigate the interaction behavior remembering that a minor bonding might be occurred between these two materials as the peel ply would also be impregnated by resin during the VaRTM process.
2. The current study only focused on the behavior of axial steel members under static loading. The cyclic behavior of the unbonded CFRP strengthened steel members need to be explored because the proposed strengthening is highly potential to be applied for steel building structures in high seismic area.

REFERENCES

Abu-sena, A.B.B., Said M., Zaki M.A., Dokmak M. (2019) "Behavior of hollow steel sections strengthened with CFRP", *Construction and Building Materials*, Vol. 205, pp.306-320.

Abusrea, M.R., Han S.W., Arakawa K., Choi N.S. (2019) "Bending strength of CFRP laminated adhesive joints fabricated by vacuum-assisted resin transfer molding", *Composites: Part B*, Vol. 156, pp.8-16.

Agarwal, A., Foster S.J., Hamed E., Ng T.S. (2014) "Influence of freeze–thaw cycling on the bond strength of steel–FRP lap joints", *Composites: Part B*, Vol. 60, pp.178-185.

Architectural Institute of Japan (AIJ). (2017) "AIJ Design standard for steel structures – based on allowable stress concept – (2005 Edition)", AIJ 2005, Tokyo, Japan.

Al-Shawaf, A., Zhao X.L. (2013) "Adhesive rheology impact on wet lay-up CFRP/steel joints' behaviour under infrastructural subzero exposures", *Composites: Part B*, Vol. 47, pp.207-219.

Altaee, M.J., Cunningham L.S., Gillie M. (2017) "Experimental investigation of CFRP-strengthened steel beams with web openings", *Journal of Constructional Steel Research*, Vol. 138, pp.750-760.

American Institute of Steel Construction (AISC). (2016) "Specification for structural steel buildings", ANSI/AISC 360-16, Chicago, USA.

Bambach, M.R., Elchalakani M. (2007) "Plastic mechanism analysis of steel SHS strengthened with CFRP under large axial deformation", *Thin-Walled Structures*, Vol. 45, pp.159-170.

Bambach, M.R., Jama H.H., Elchalakani M. (2009) "Axial capacity and design of thin-walled steel SHS strengthened with CFRP", *Thin-Walled Structures*, Vol. 47, pp.1112-1121.

Canadian Standards Association (CSA). (2009) "Design of steel structures", CAN/CSA S16-09, Mississauga, Canada.

Chahkand, N.A., Jumaat M.Z., Sulong N.H.R., Zhao X.L., Mohammadizadeh M.R. (2013) "Experimental and theoretical investigation on torsional behaviour of CFRP strengthened square hollow steel section", *Thin-Walled Structures*, Vol. 68, pp.135-140.

Chen, T., Qi M., Gu X.L., Yu Q.Q. (2015) "Flexural strength of carbon fiber reinforced polymer repaired cracked rectangular hollow section steel beams", *International Journal of Polymer Science*, Vol. 2015, Article ID 204861.

Chen, Y., Wan J., He K. (2018) “Experimental investigation on axial compressive strength of lateral impact damaged short steel columns repaired with CFRP sheets”, *Thin-Walled Structures*, Vol. 131, pp.531-546.

Colombi, P., Poggi C. (2006a) “An experimental, analytical and numerical study of the static behavior of steel beams reinforced by pultruded CFRP strips”, *Composites: Part B*, Vol. 37, pp.64-73.

Colombi, P., Poggi C. (2006b) “Strengthening of tensile steel members and bolted joints using adhesively bonded CFRP plates”, *Construction and Building Materials*, Vol. 20, pp.22-33.

Crisfield, M.A. (1981) “A fast incremental/iterative solution procedure that handles “snap-through”, *Computers and Structures*, Vol. 13, pp.55-62.

El-Kholi, A.M., Mourad, S.A., Shaheen, A.A., Mohamed, Y.A. (2019) “Finite element simulation for steel tubular members strengthened with FRP under compression”, Structural Engineering and Mechanics, Vol. 72, pp.569-583.

Fernando, D., Teng J.G., Yu T., Zhao X.L. (2013) “Preparation and characterization of steel surfaces for adhesive bonding”, *Journal of Composites for Construction*, Vol. 17.

Gao, X.Y., Balendra T., Koh C.G. (2013) “Buckling strength of slender circular tubular steel braces strengthened by CFRP”, *Engineering Structures*, Vol. 46, pp.547-556.

Ghaemdoust, M.R., Narmashiri K., Yousefi O. (2016) “Structural behaviors of deficient steel SHS short columns strengthened using CFRP”, *Construction and Building Materials*, Vol. 126, pp.1002-1011.

Haedir, J., Bambach M.R., Zhao X.L., Grzebieta R.H. (2009) “Strength of circular hollow sections (CHS) tubular beams externally reinforced by carbon FRP sheets in pure bending”, *Thin-Walled Structures*, Vol. 47, pp.1136-1147.

Haedir, J., Zhao X.L. (2011) “Design of short CFRP-reinforced steel tubular columns”, *Journal of Construction Steel Research*, Vol. 67, pp.497-509.

Hatami, F., Ghamari A., Rahai A. (2012) “Investigating the properties of steel shear walls reinforced with Carbon Fiber Polymers (CFRP)”, *Journal of Constructional Steel Research*, Vol. 70, pp.36-42.

Haydaroglu, C., Celik O.C. (2012) “Experimental investigation of partially CFRP wrapped steel HSS braces for seismic performance improvement”, *Proceedings of the 15th World Conference on Earthquake Engineering (WCEE)*, Lisbon, Portugal.

Hiroshi, S. (Editor). (2009) “Mechanics of composite materials: Introduction to engineering beginners”, Baifukan. (In Japanese).

Hmidan, A., Kim Y.J., Yazdani S. (2011) "CFRP repair of steel beams with various initial crack configurations", *Journal of Composites for Construction,* Vol. 15, pp.952-962.

Jones, R.M. (1999) "Mechanics of composite materials", 2nd Edition, Taylor & Francis.

Karimian, M., Narmashiri K., Shahraki M., Yousefi O. (2017) "Structural behaviors of deficient steel CHS short columns strengthened using CFRP", *Journal of Constructional Steel Research,* Vol. 138, pp.555-564.

Kazem, H., Rizkalla S., Kobayashi A. (2018) "Shear strengthening of steel plates using small-diameter CFRP strands", *Composite Structures,* Vol. 184, pp.78-91.

Keykha, A.H., Nekooei M., Rahgozar R. (2015) "Experimental and theoretical analysis of hollow steel columns strengthening by CFRP", *Civil Engineering Dimension,* Vol. 17, pp.101-107.

Kim, Y.H., Son J.H., Choi B.K., Jo Y.D., Kim K.J., Han J.W. (2006) "Evaluation of mechanical properties of CFRP by VARTM and its application", *International Journal of Modern Physics,* Vol. 20, pp.3896-3901.

Kumar, A.P., Senthil R. (2016) "Axial behaviour of CFRP-strengthened circular steel hollow sections", *Arabian Journal for Science and Engineering,* Vol. 41, pp.3841-3850.

Lenwari, A., Thepchatri T., Albrecht P. (2005) "Flexural response of steel beams strengthened with partial-length CFRP plates", *Journal of Composites for Construction,* Vol. 9, pp.296-303.

Li, S., Zhu T., Lu Y., Li X. (2016) "Effect of temperature variation on bond characteristics between CFRP and steel plate", *International Journal of Polymer Science,* Vol. 2016, Article ID 5674572.

Lu, Y., Li W., Li S., Li X., Zhu T. (2015) "Study of the tensile properties of CFRP strengthened steel plates", *Polymers,* Vol. 7, pp.2595-2610.

LUSAS. (2011) "Theory Manual Volume 1", LUSAS Version 14.7, Surrey, UK.

Mieda, G., Nakamura H., Matsui T., Ochi Y., Matsumoto Y. (2019) "Mechanical behavior of CFRP on steel surface molded and bonded by vacuum-assisted resin transfer molding technology", *SN Applied Sciences,* Vol. 1, 601.

Narmashiri, K., Jumaat M.Z., Sulong N.H.R. (2012) "Strengthening of steel I-beams using CFRP strips: An investigation on CFRP bond length", *Advances in Structural Engineering,* Vol. 15, pp.2191-2204.

Nguyen, T.C., Bai Y., Zhao X.L., Al-Mahaidi R. (2011) "Mechanical characterization of steel/CFRP double strap joints at elevated temperatures", *Composite Structures,* Vol. 93, pp.1604-1612.

Nguyen, T.C., Bay Y., Zhao X.L., Al-Mahaidi R. (2012) "Effects of ultraviolet radiation and associated elevated temperature on mechanical performance of steel/CFRP double strap joints", *Composite Structures*, Vol. 94, pp.3563-3573.

Peiris, A., Harik I. (2021) "Steel beam strengthening with UHM CFRP strip panels", *Engineering Structures*, Vol. 226.

Poul, M.K., Alahi F.N., Zhao X.L. (2016) "Experimental testing on CFRP strengthened thin steel plates under shear loading", *Thin–Walled Structures*, Vol. 109, pp.217-226.

Ritchie, A., Fam A., MacDougall C. (2015) "Strengthening long steel columns of S-sections against global buckling around weak axis using CFRP plates of various moduli", *Journal of Composites for Construction*, Vol. 19.

Sayed-Ahmed, E.Y., Shaat A.A., Abdallah E.E. (2018) "CFRP-strengthened HSS columns subject to eccentric loading", *Journal of Composites for Construction*, Vol. 22.

Shadan, P., Kabir M.Z. (2018) "Enhancing local buckling behavior of SHS braces using GFRP and CFRP wrap", *Journal of Composites for Construction*, Vol. 22.

Shaat, A., Fam A. (2006) "Axial loading tests on short and long hollow structural steel columns retrofitted using carbon fibre reinforced polymers", *Canadian Journal of Civil Engineering*, Vol. 33, pp.458-470.

Shaat, A., Fam A.Z. (2009) "Slender steel columns strengthened using high-modulus CFRP plates for buckling control", *Journal of Composites for Construction*, Vol. 13, pp.2-12.

Sharrock, J., Wu C., Zhao X.L. (2015) "CFRP strengthened square hollow section subject to pure torsion", *Proceeding of the 15th International Symposium on Tubular Structures*, Rio De Janeiro, Brazil.

Siwowski, T.W., Siwowska P. (2018) "Experimental study on CFRP-strengthened steel beams", *Composites Part B*, Vol. 149, pp.12-21.

Tamai, H., Hattori A., Ozawa Y., Haitani T., Takamatsu T. (2012) "Design Formula for Rehabilitated Angle Steel Member Using Carbon Fiber Reinforced Plastic Plates", *Proceedings of the 15th World Conference on Earthquake Engineering (WCEE)*, Lisbon, Portugal.

Teng, J.G., Yu T., Fernando D. (2012) "Strengthening of steel structures with fiber-reinforced polymer composites", *Journal of Constructional Steel Research*, Vol. 78, pp.131-143.

Uddin, N., Vaidya U., Shohel M., Serrano-Perez J.C. (2004) "Cost-effective bridge girder strengthening using vacuum-assisted resin transfer molding (VARTM)", *Advanced Composite Materials*, Vol. 13, pp.255-281.

Yalcinkaya, M.A., Sozer E.M., Altan M.C. (2017) “Fabrication of high quality composite laminates by pressurized and heated-VARTM”, *Composites: Part A*, Vol. 102, pp.336-346.

Yu, T., Fernando D., Teng J.G., Zhao X.L. “Experimental study on CFRP-to-steel bonded interfaces”, *Composites: Part B*, Vol. 43, pp.2279-2289.

Wang, Z.Y., Zhang N., Wang Q.Y. (2016) “Tensile behaviour of open-hole and bolted steel plates reinforced by CFRP strips”, *Composites Part B*, Vol. 100, pp.101-113.

Wu, C., He L., Ghafoori E., Zhao X.L. (2018) “Torsional strengthening of steel circular hollow sections (CHS) using CFRP composites”, *Engineering Structures*, Vol. 171, pp.806-816.

Zhao, X.L., Bai Y., Al-Mahaidi R., Rizkalla S. (2014) “Effect of dynamic loading and environmental conditions on the bond between CFRP and steel: State-of-the-art review”, *Journal of Composites for Construction*, Vol. 18.